TECHNICAL REPORT No. 23

COMPARISON OF MEDIUM RANGE FORECASTS MADE WITH MODELS USING SPECTRAL OR FINITE DIFFERENCE TECHNIQUES IN THE HORIZONTAL

by

M. Jarraud, C. Girard and U. Cubasch

February 1981

C O N T E N T S

		PAGE
ABSTRACT		1
1.	INTRODUCTION	1
2.	DESCRIPTION OF THE MODELS	2
2.1	The horizontal schemes	2
2.2	The vertical scheme and the hydrostatic equation	3
2.3	The time discretisation scheme	4
2.4	The parameterization of subgrid scale processes	4
2.5	Efficiency of the models	5
3.	THE DATA AND THE EXPERIMENTS	5
3.1	Initial and verification data sources	5
3.2	Initialisation of the grid point model	5
3.3	Initialisation of the spectral model	5
3.4	Verification procedures for the experiments	6
4.	SYNOPTIC EVALUATION	7
4.1	Presentation	7
4.2	Case 1. Forecasts from 15.2.76	8
4.2.1	Days 0 to 5	8
4.2.2	Days 5 to 10	15
4.2.3	Days 5 to 10 mean maps	15
4.2.4	Precipitation forecasts	24
4.3	Case 2. Forecasts from 6.2.76	27
4.3.1	Days 0 to 5	27
4.3.2	Days 5 to 10	33
4.4	Case 3. Forecasts from 18.2.76	35
4.4.1	Days 0 to 5	35
4.5	Summary of the synoptic evaluation	41
5.	OBJECTIVE COMPARISONS (Northern Hemisphere)	42
5.1	Introduction	42
5.2	Comparative performance of T63 and N48	44
5.3	Comparative performance of T63 and T40	50
5.4	Intercomparison of T63, T40 and N48	54
5.5	Mean rms differences and correlations between models	64
6.	GEOGRAPHICAL DISTRIBUTION OF THE SYSTEMATIC ERRORS	68
7.	ENERGETICS	80
7.1	Time evolution of the total energetics	80
7.2	Spectra of KE	86
7.3	Zonally averaged energetics	86
8.	SUMMARY AND CONCLUSION	91
Acknowledgements		93
REFERENCES		94

ABSTRACT

We present the results of seven forecasts based on data selected from February 1976 made with two models using different techniques for the numerical treatment of the equations in the horizontal (constant σ surfaces) but almost identical in their other aspects. The grid point model (N48 - 15 levels) with minor modifications is the ECMWF's operational model. The spectral model has been developed as a possible alternative operational model and a longer comparison including cases regularly chosen over a whole year has been performed since then. The experiments with the spectral model were carried out with two different horizontal resolutions (triangular truncations T40 and T63). Therefore this report includes resolution comparisons in addition to model comparisons.

It is shown that the grid point model and the two spectral models are similar. However the T63 spectral model is found to give better results than the grid point model and to improve significantly those of the spectral model with a coarser resolution (T40).

1. INTRODUCTION

As pointed out by Hollingsworth et al (1979) - we shall refer to their report as TR.13 in what follows - many factors can influence the quality of numerical forecasts. Amongst them the type of numerical method used for handling the horizontal part of the equations seemed of sufficient importance to justify a thorough comparison between two possible techniques, spectral and grid point. But since a high resolution grid point model is likely to provide more accurate forecasts than a low resolution spectral model - and vice versa - it was also decided to perform a parallel resolution experiment which could also give some insight into the problem of finding the spectral resolution equivalent to a given grid point model.

Spectral-grid-point-model comparisons have already been performed by several groups, either in idealised cases (Simmons and Hoskins,1975 or Doron et al, 1974) or for short range forecasts (Daley et al, 1976) or even for medium range forecasts (Baede and W. Hansen, 1977 and Walløe-Hansen, 1980). The idealised studies were not conclusively in favour of any of the models. In particular, Simmons and Hoskins stressed that the nature of the errors in the two kinds of models were of different type: the spectral method dealing better with large scale phase and amplitude and the finite difference method dealing better with small scale features such as fronts.

Daley et al concluded that up to 36 hours a spectral model was at least as efficient as a grid point model giving equivalent results.

Wallø-Hansen described a single 10-day forecast. He arrived at the same conclusion, namely, a spectral model can be at least as efficient as a grid point model for a given accuracy. Furthermore he points out the similarity of results obtained with a spectral model using a triangular T40 truncation and a N48 grid point model.

Spectral resolution experiments have also been previously reported in the literature, for barotropic integrations (Rasmussen, 1974; Puri and Bourke, 1974) and for short-range baroclinic integrations (Leblanc, 1977). For medium-range forecasts, the influence of horizontal resolution has only been so far investigated with grid point models (e.g. Miyakoda et al, 1971).

This report aims at presenting a further insight into both problems, but with emphasis on comparison of techniques, by performing experiments at medium range on a larger number of cases and with higher resolutions than the ones found so far in the literature. We shall first describe the models involved and the conditions of this comparison. Then a synoptic evaluation will be done on 3 cases selected out of the 7 and objective verifications will be presented to evaluate the individual and mean performances of the models. Some attention will be paid to the geographical distribution of mean errors and to the energetics.

This study must be considered as preliminary, since a comparison involving more cases regularly spread over a whole year has been performed in ECMWF and will be the subject of another report where we shall discuss the differences in more detail and also try to explain them.

2. DESCRIPTION OF THE MODELS

2.1 The horizontal schemes

There lies the main difference between the two models. For a complete description of the schemes used, we shall refer to Burridge and Haseler (1977) for the grid point model and to Baede et al (1979) for the spectral model.

The grid point model uses the "C" grid (Arakawa's classification) with a regular spacing of 1.875^{o} in both latitude and longitude, i.e. a N48 grid. Therefore, in the following we shall refer to it as N48. There are 97 latitude lines - including the North and the South Poles, and 192 equally spaced points on each line. The scheme is designed to conserve enstrophy but not energy and its accuracy with respect to the horizontal derivatives is second order.

The spectral model uses a spherical harmonic expansion triangularly truncated. The choice of truncation was made after preliminary experiments involving several kinds of truncation, in particular rhomboidal and trapezoidal. The experiments will be described in another report. It is sufficient to say here that this choice has been taken for quality and not for efficiency reasons. The use of triangularly truncated spherical harmonic expansions provides for a truly uniform and isotropic representation of spectral model variables on the sphere. In N48, resolution is uniform in latitude-longitude with true distance between grid points on the same latitude increasing from pole to equator and the poles are special points.

In order to carry out resolution experiments in parallel with model comparisons we selected two triangular truncations, one retaining 40 zonal wave numbers and the other 63. We shall refer to them in the following as T40 and T63 respectively.

The nonlinear computations in the horizontal are performed on the so-called Gaussian transform grid (Eliassen et al, 1970 and Orszag, 1970). It is worth noting that for triangular truncations the equivalent Gaussian grid is an almost regular latitude-longitude grid with no staggering of variables. The size of the Gaussian grid is chosen to avoid aliasing in all quadratic, but not cubic terms, whereas the grid point model allows aliasing in all non-linear terms. For T40 the equivalent grid is close to an N32 grid: 64 latitude lines with 128 points on each of them. For T63 it is almost an N48 grid: 96 latitude lines with 192 points on each of them.

The basic theoretical differences between spectral and grid point techniques are described in detail elsewhere (for example, Bass and Orszag, 1976) and will not be discussed here. One relevant point not already mentioned above refers to the calculations of horizontal derivatives. These are computed exactly in the spectral models, i.e. for all the scales retained by the truncation (T40 or T63), with an infinite order of accuracy compared with only second order for N48.

2.2 The vertical scheme and the hydrostatic equation

They are the same in both models (see Baede et al - 1979 - for a complete description). Let us just say here that the $\sigma = p/ps$ coordinates (Phillips, 1957) are used with 15 unequally spaced levels defined by

$$\sigma_k = 0.75s + 1.75s^3 - 1.5s^4 \qquad \left(s = \frac{2k+1}{30}\ k = 1,2.....15\right)$$

2.3 The time discretisation scheme

It is also identical for both models: it is a semi-implicit leap-frog scheme using a time step of 15 minutes for N48, 18 minutes for T63 and 26 minutes 40 seconds for T40. N48 used a Fourier filtering of tendencies of p_*, T, u, v, q in the polar region in order to avoid too small time steps. A weak time filter (Asselin, 1971) of the form

$$\bar{X}_t = X_t + \alpha(\bar{X}_{t-\Delta t} - 2X_t + X_{t+\Delta t}) \text{ and } \alpha = 0.06$$

was found to be necessary to carry out 10-day integrations.

2.4 The parameterization of subgrid scale processes

Except for horizontal diffusion both models have the same parameterization developed at ECMWF and described in Tiedtke et al (1979). It includes radiation, large scale condensation, dry and moist convection, boundary layer and vertical turbulent fluxes. We give details of the horizontal diffusion schemes only. N48 used a nonlinear 4th order diffusion scheme:

$$\frac{\partial X}{\partial t} = -\alpha(\Delta\delta)^6 \sqrt{(\nabla^2\xi)^2 + (\nabla^2 D)^2}\ \nabla^2(\nabla^2 X)$$

$\Delta\delta$ = grid length at the equator

∇^2 = Laplacian operator

ξ = vorticity

D = divergence

X = any of the variables, T, u, v or q (mixing ratio)

α had the value 0.01

This is different from the linear 4th order diffusion scheme used by the operational version of the model.

T63 and T40 use a linear 4th order diffusion of the type :

$$\frac{\partial X}{\partial t} = -k\nabla^4 X \text{ with X = any of the variables T, } \xi\text{, D, q.}$$

and $k = 7.10^{14}$ for both T40 and T63. The choice of the value for k derives from previous tests.

The nonlinear diffusion scheme in N48 is more local and more selective than the linear scheme used by T40 and T63. It can be verified that the effective diffusion (at high wavenumbers) is larger for N48, with the coefficients chosen.

2.5 Efficiency of the models

Although it should no longer be necessary to prove that the spectral method can be at least as efficient as grid point techniques, we give in Table 1 details of the comparative efficiency of the models on the ECMWF Cray 1 computer. The following figures are likely to be improved for all models but should remain representative.

Table 1. Comparative efficiency of the models (valid in Spring 1980) (CRAY 1 - times)

	N48	T63	T40
CPU time	2h40	2h45	0h45
CPU spent in the system*	0h20	0h20	0h05
Waiting for I/O (I/O not covered)	0h20	0h25	0h15
Post-processing of forecast data	0h30	0h30	0h25
TOTAL	3h50	4h	1h30

* This time, mainly spent to initiate I/O is fairly large and due to operating system overheads.

In particular one can see that T63 and N48 are presently very close to each other from an efficiency point of view, while T40 is much cheaper.

3. THE DATA AND THE EXPERIMENTS

3.1 Initial and verification data sources

Seven cases from the NMC Data System Test for February 1976 were selected, i.e: 00Z on 3rd, 6th, 9th, 12th, 15th, 18th, 22nd February. All the data and the corresponding verifying analyses were prepared on an N48 grid in the way described in TR13.

3.2 Initialisation of the grid point model

The data sets were initialised using the nonlinear normal mode procedure described in Temperton and Williamson (1979).

3.3 Initialisation of the spectral model

The files interpolated and initialised for the grid point model consist of data on the N48 grid and are not directly usable by the spectral model. Therefore an extra step is necessary: spectral coefficients for T63 or T40 are computed from the regular N48 grid, in the way described by Machenhauer and Daley (1972).

for all variables including orography and many surface fields. Then grid point values for all these fields are calculated on the required Gaussian grid using Legendre and Fourier transforms. Special care is taken of some surface fields: albedo, surface wetness, snow - to avoid negative values, for example. We are however fully aware, that performing a spectral analysis on the surface fields is unnecessary and perhaps not the best interpolation procedure.

3.4 Verification procedures for the experiments

The processing of forecast data at 12h intervals was performed exactly in the same way for both models. One has to note however that the vertical interpolation from σ to pressure surfaces needs the orography of the models which is different for all models because of the spectral truncation.

In the following, the results are studied both from a synoptic and from an objective point of view. For the synoptic evaluation it was not possible to show results from all the experiments. Since the models in the mean are very close, the choice of particular cases was not easy. We decided to select and discuss the cases showing the largest differences in the objective scores. Most of the maps shown are 500 or 1000 mb height maps. In addition, we present a few maps of precipitation plus some mean maps for the last 5 days of the forecasts.

For the objective evaluation we proceeded as in TR13: we mainly made use of standard deviations and anomaly correlations. The latter especially was found to be more sensitive to the small differences that were being investigated. A clear definition of these scores and of the associated confidence limit is given in Arpe (1980).

We also found it useful to introduce the concept of predictability as a continuous variable allowing for the calculations of mean predictability of a model (with respect to a given threshold) and mean predictability difference between the models.

4. SYNOPTIC EVALUATION

4.1 Presentation

As mentioned in Section 3.4 we selected for synoptic evaluation the cases showing the largest differences in the objective scores. The first case is February 15th, by far the best medium range forecast of the series (in terms of scores) for both T63 and N48, while T40 is much worse. The second case is February 6th where T63 performs better than N48 and the third is February 18th, the only case out of the seven where N48 performs better than T63. The first two cases are also evaluated in TR13. We shall concentrate our attention to the northern hemisphere middle latitudes, mostly showing maps for the 1000 and 500 mb height field.

The synoptic evaluation for days 0 to 5 will be presented first, with emphasis on the 1000 mb height field on days 2,3,4,5. Whenever sufficient skill remains in the forecast the synoptic discussion will be extended to days 5 to 10. Mean charts for the extended period will sometimes be shown. All figures with height maps will have the following presentation:

NMC analysis	N48 forecast
T63 forecast	T40 forecast

TR13 describes the difficulties encountered when making a synoptic assessment of medium range forecasts and we shall try to make use of their experience.

The choice of a non chronological order for the presentation of these selected cases is of course deliberate. The first case warrants more discussion and will allow many conclusions that need not be repeated for the two others. Accordingly a more detailed description of the first case will be given, while many figures and details will be omitted for the two others.

We do not give a complete review of the 6 - 28 February period: the interested reader can find one in TR13. We would only like to mention three major events over Europe during this period: an intense gale on February 10th over the North Sea and two major changes of circulation over Western Europe around February 19th and between February 23rd and 24th. In all three situations significant differences of particular interest to the present comparison were found in the behaviour of the models.

4.2 Case 1. Forecasts from 15.2.76

4.2.1 Days 0 to 5

At *1000 mb*, in the first 3 days the forecasts are good but not everywhere excellent. On day 2 (Fig. 4.1) for example the low in the Arctic and the associated trough over the Atlantic are too deep in all models with very little to choose between them.

On day 3 (Fig. 4.2) differences become noticeable. All models maintain the Arctic system too deep, but T63 is somewhat more successful in simulating its decay. Furthermore, while T40 and N48 develop a spurious secondary low in the Barents Sea, T63 gives some indication of the observed ridge. Another distinction between T63 and the two other models can be found in the structure of the north east Pacific depression. T63 correctly forecasts the position of its centre on 130°W while T40 and N48 have it centred on 150°W. Over the rest of the Pacific all models have already lost much skill. As a whole, on day 3, T40 and N48 are of similar skill while T63 is slightly better in many small scale features.

On day 4 (Fig. 4.3) a noticeable change of weather occurs over the North Atlantic and Western Europe. In connection with the intensification of the Icelandic low, the European high is pushed eastwards. A southerly flow establishes itself from Morocco to the North Sea. Both T63 and N48 capture this change relatively well although T63 is slightly more correct over Scandinavia. T40 however does not deepen the Icelandic low enough and moves it slightly too fast failing to raise the heights over the North Atlantic. On the other hand T63 maintains the advantage acquired earlier over T40 and N48 in the handling of the Artic system. In the Pacific all models fail to develop the intense Aleutian low. They forecast a ridge instead.

On day 5 (Fig. 4.4) N48 and T63 appear closer to each other than on day 4 and different from T40 which has lost much skill at the surface. The southerly circulation over Europe associated with the blocking high over Russia is missed and the pattern over the Pacific has little to do with reality. On the other hand T63 and N48 do quite well over Europe even if the eastern Atlantic trough is not extended enough towards the South. At that stage it would be difficult to choose between them: the double low structure of the Atlantic and the associated trough are better represented by N48 and the North Siberian low by T63.

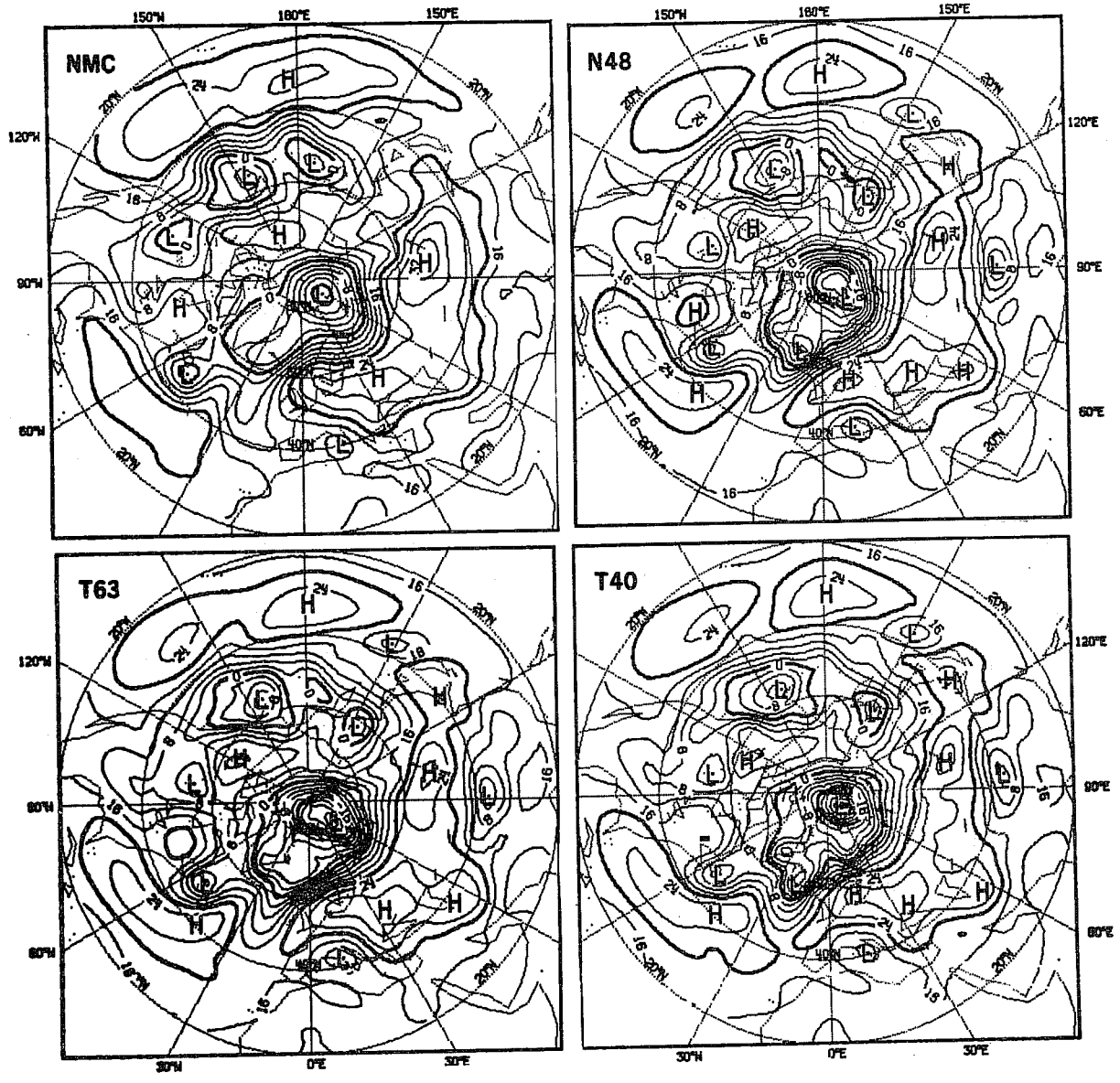

Fig. 4.1 Day 2, 1000 mb height forecasts from February 15, 1976

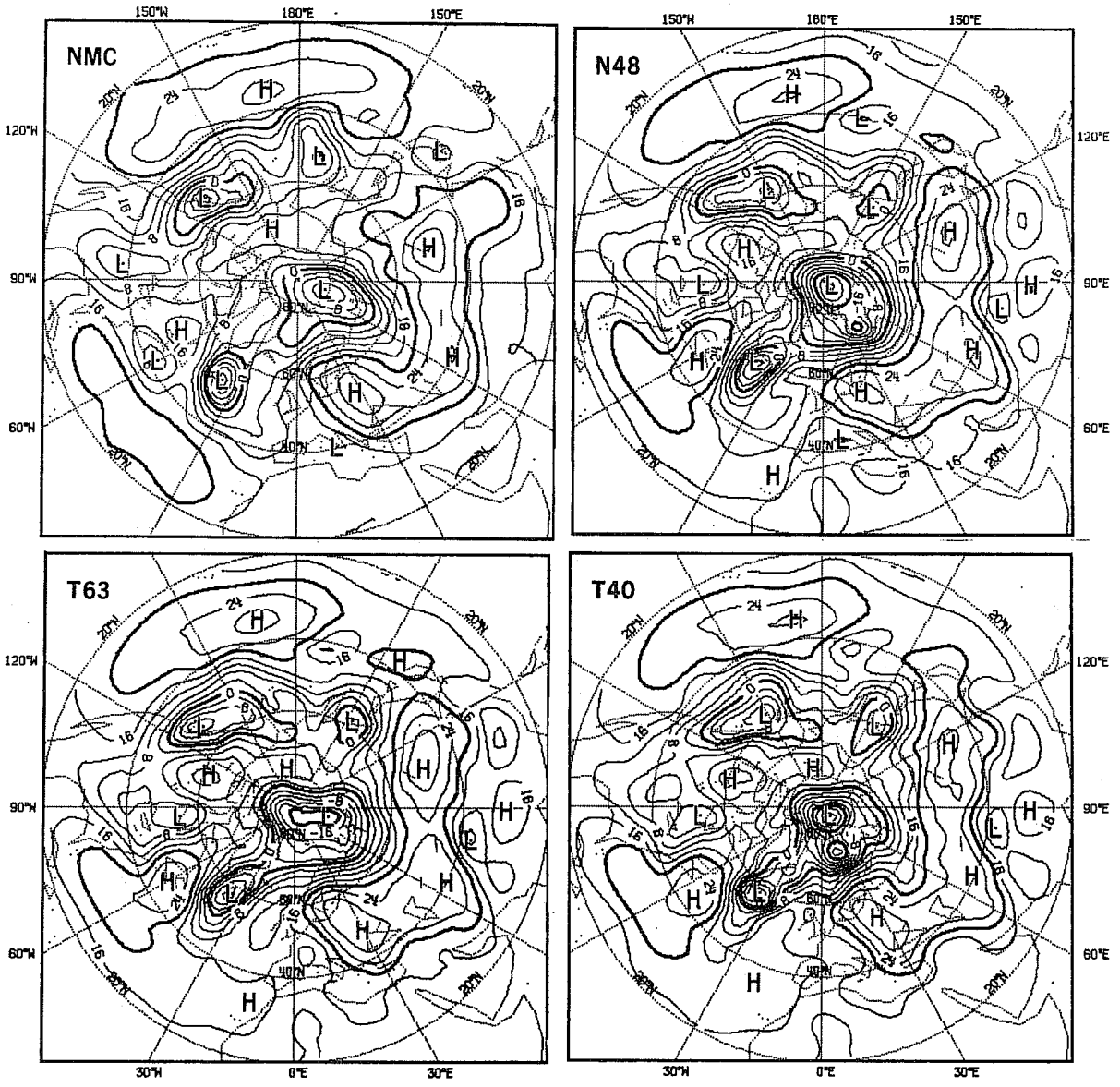

Fig. 4.2 Day 3, 1000 mb height forecasts from February 15, 1976

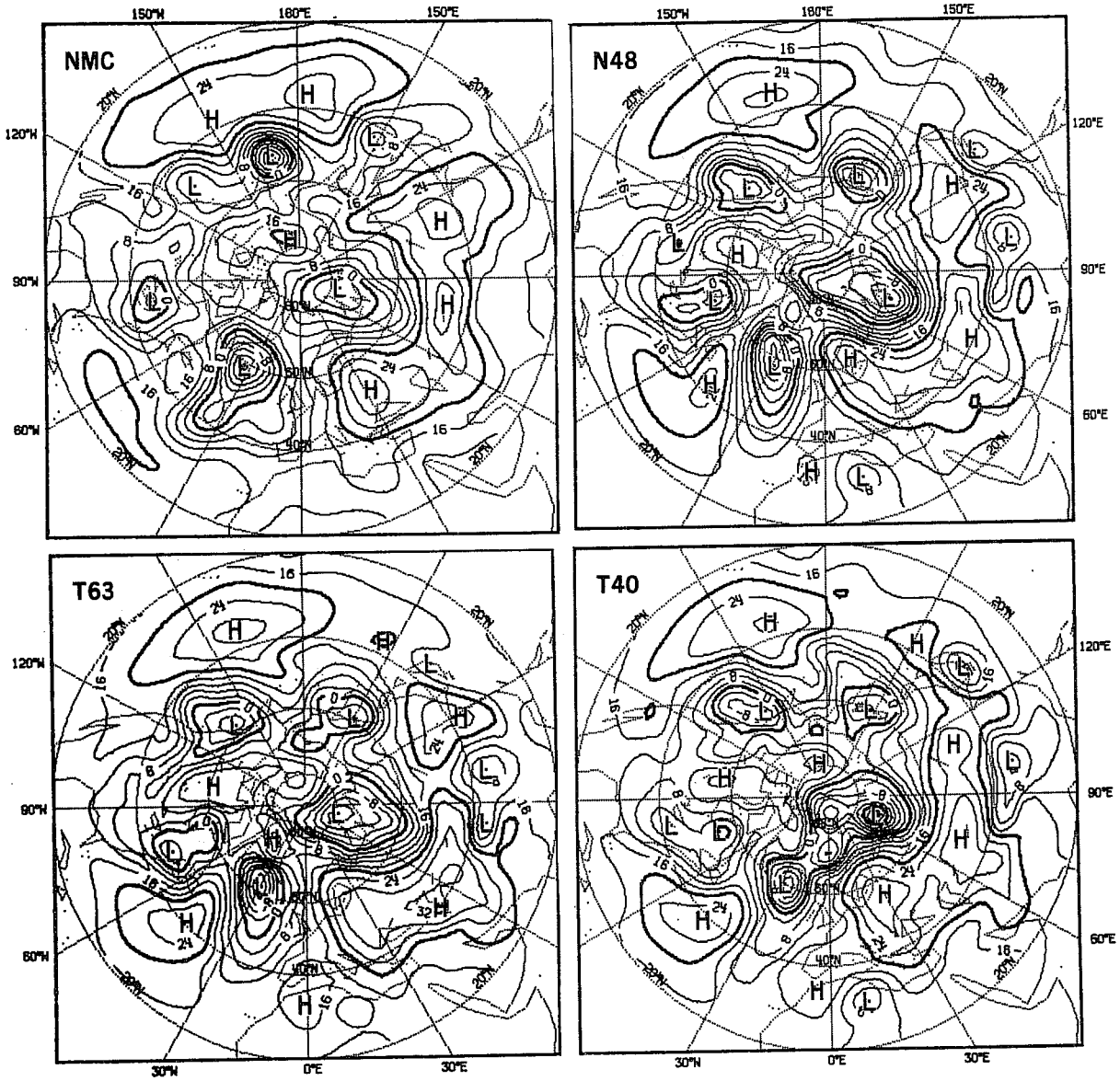

Fig. 4.3 Day 4, 1000 mb height forecasts from February 15, 1976

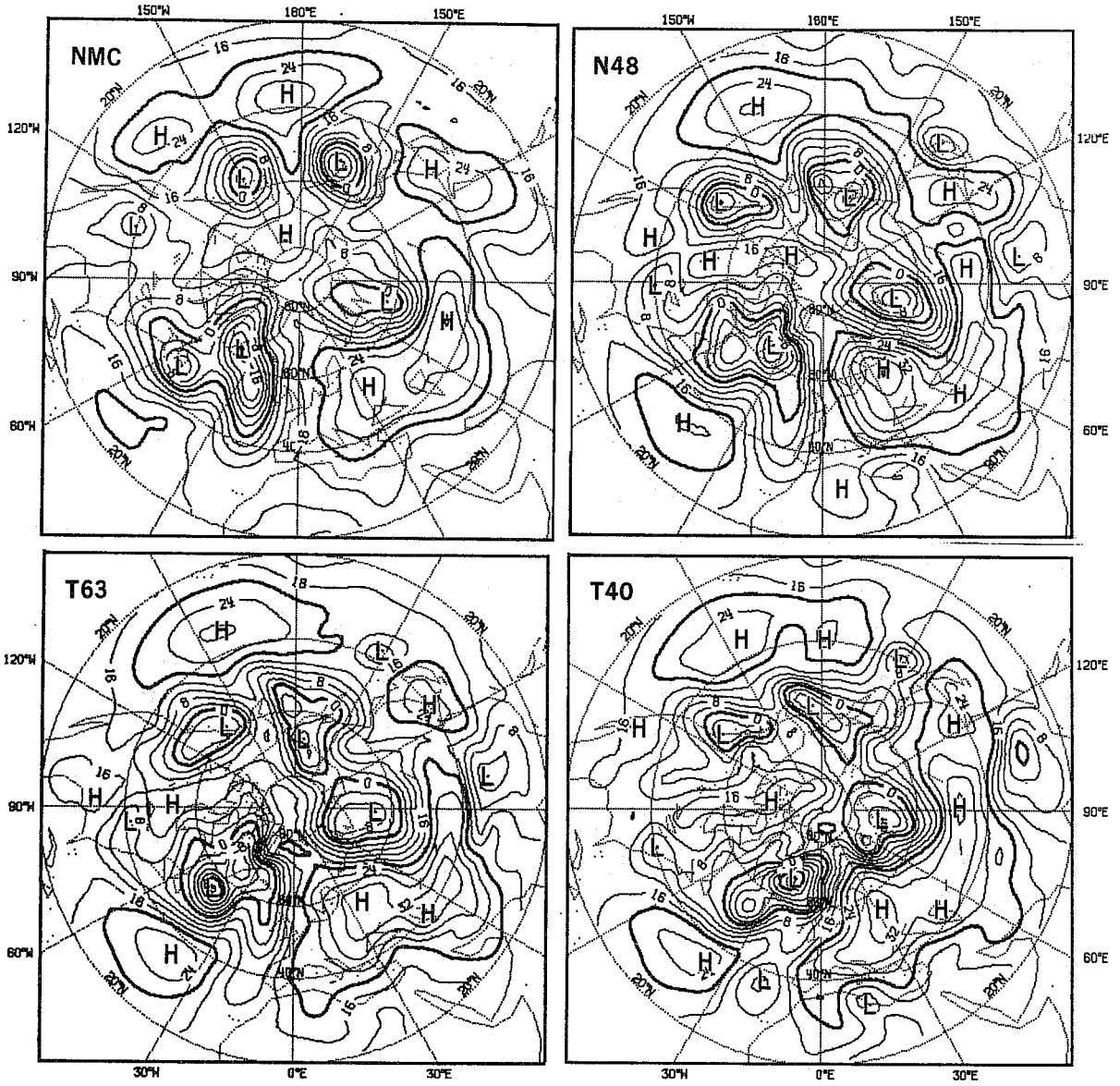

Fig. 4.4 Day 5, 1000 mb height forecasts from February 15, 1976

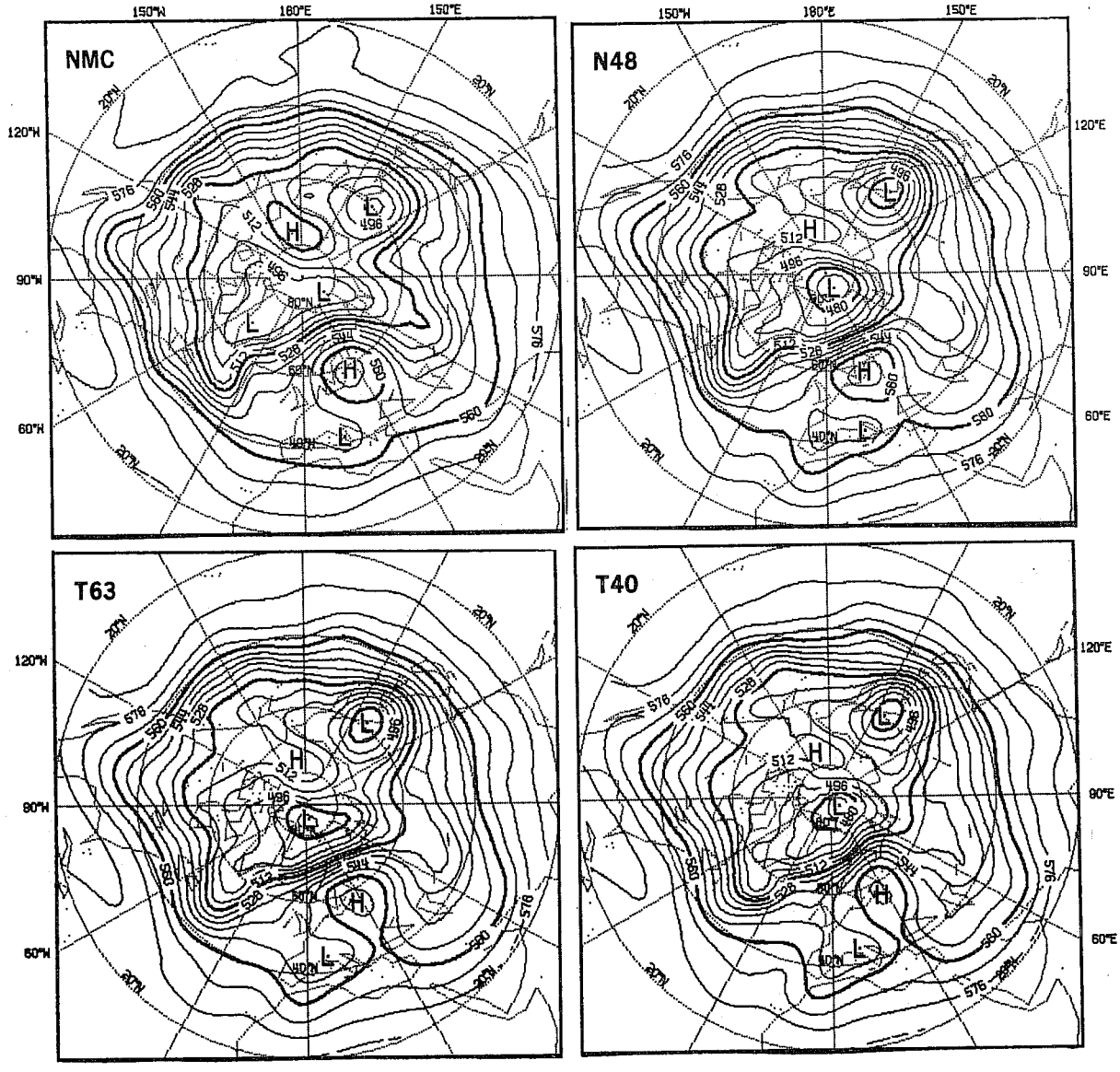

Fig. 4.5 Day 3, 500 mb height forecasts from February 15, 1976

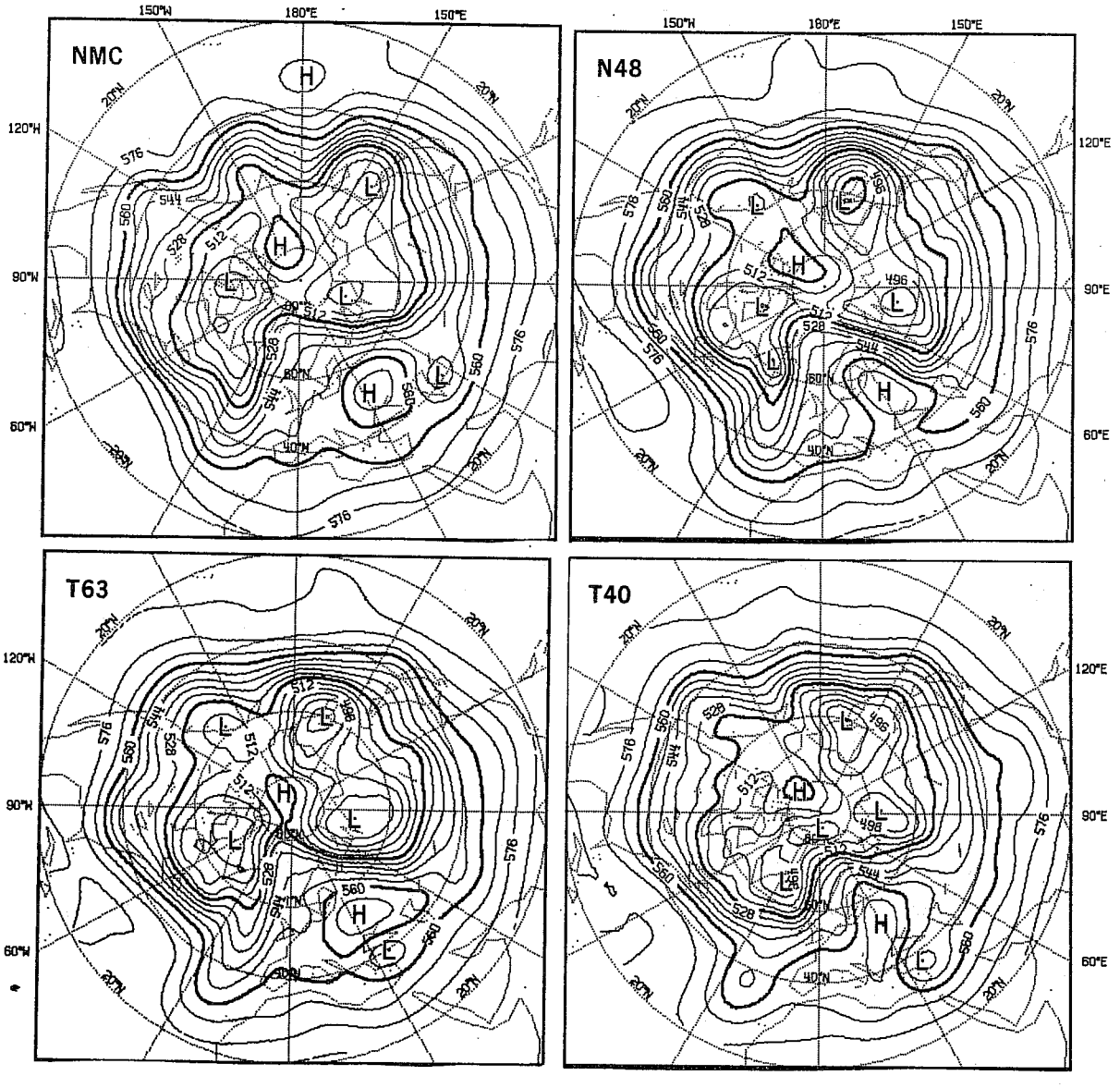

Fig. 4.6 Day 5, 500 mb height forecasts from February 15, 1976

At *500 mb* on day 3 (Fig.4.5) all forecasts are very good: T63 and N48 are extremely close while T40 presents a slightly different flow over Northern Scandinavia. On day 5 (Fig. 4.6) T63 and N48 remain very similar and better than T40, specially over eastern Atlantic and Europe. These results are consistent with the conclusions made at 1000 mb.

4.2.2 Days 5 to 10

For this period we shall no longer comment on the T40 1000 mb forecasts since already on day 5 there was little skill left. For the same reason we shall mainly concentrate our attention on the European area where skill remains and where a major change occurs. At 1000 mb the blocking high over Russia merges with an Atlantic anticyclone to form a high pressure band over all central and southern Europe. The flow over western Europe changes direction dramatically from southerly to westerly (Fig. 4.7 to 4.9). N48 fails in forecasting that change and on day 9 the pattern stays remarkably similar to the one on day 5. On the other hand T63 is more successful in breaking up the blocking. Although on day 6 (Fig. 4.7) some details are in favour of N48, T63 produces a more correct tendency from day 7 (Fig. 4.8) to 9 (Fig. 4.9).

The 500 mb maps on day 7 (Fig. 4.10) and on day 9 (Fig. 4.11) tell a similar story over the European area. T63 shows more skill than N48 in forecasting the change in circulation. The lack of skill of T40 compared to the two others is also quite obvious over this region. Over the rest of the hemisphere all forecasts are equally lacking in skill.

4.2.3 Days 5 to 10 mean maps

The mean (day 5 to 10) geopotential maps at 1000 mb (Fig. 4.12) reflect the comments made above: the mean N48 map resembles very much any of the individual ones on days 5, 7, 9, that is with the southerly flow over western Europe and a too deep trough from Siberia to the Aral Sea. T63 is significantly better over the same region. The small features being smoothed by the averaging process, the mean map is close to the analysed one: the European high extends correctly towards the Atlantic and the flow over Russia is fairly accurately represented. On the other hand the low south of Greenland is too deep.

At 500 mb the mean N48 map (Fig. 4.13) shows a too intense trough over the eastern Atlantic. The mean T63 map has a more correct intensity for that trough and also a good simulation of the cut off low over Turkey. Over the Pacific both models miss the ridge on 180°W.

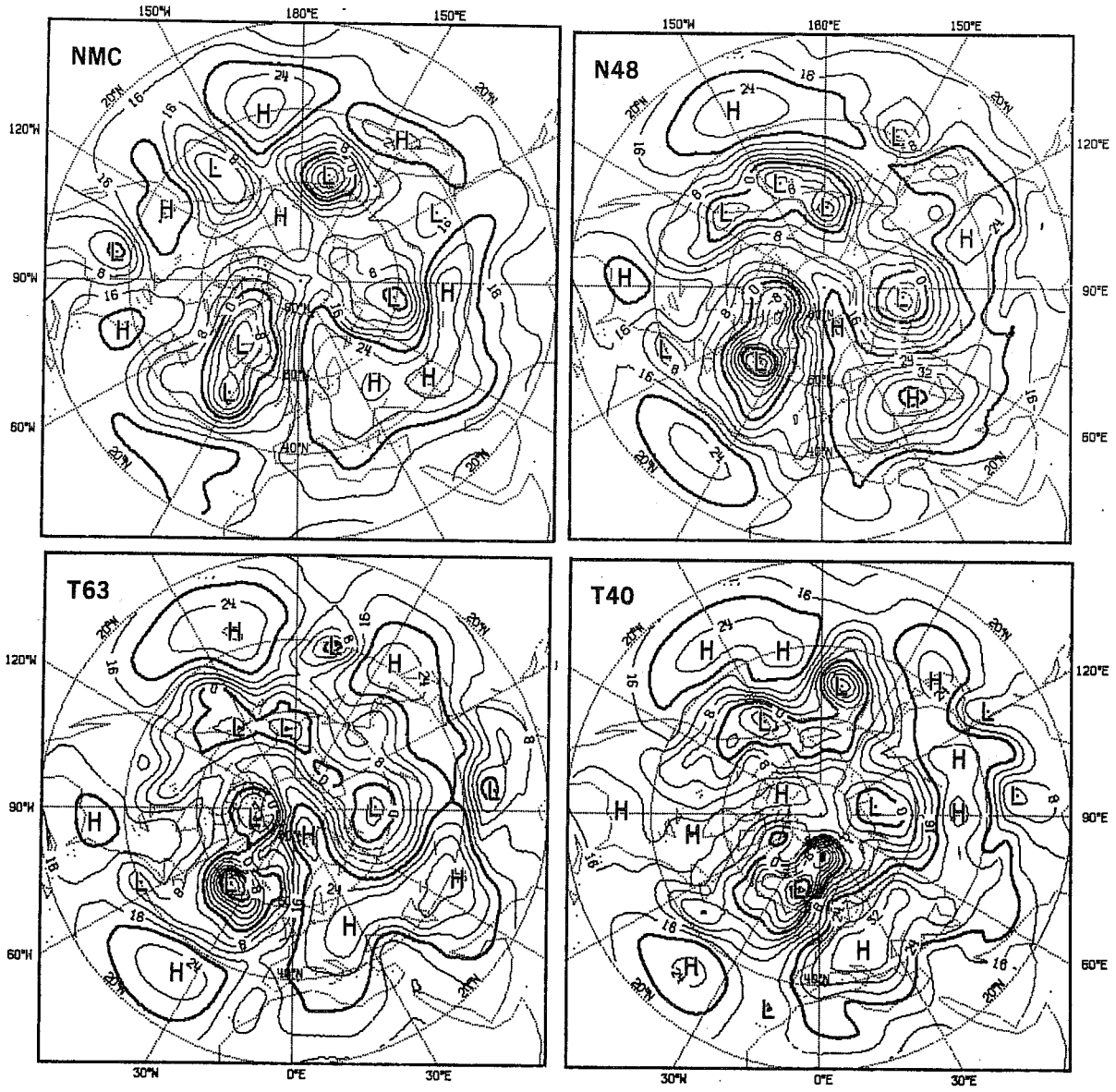

Fig. 4.7 Day 6, 1000 mb height forecasts from February 15, 1976

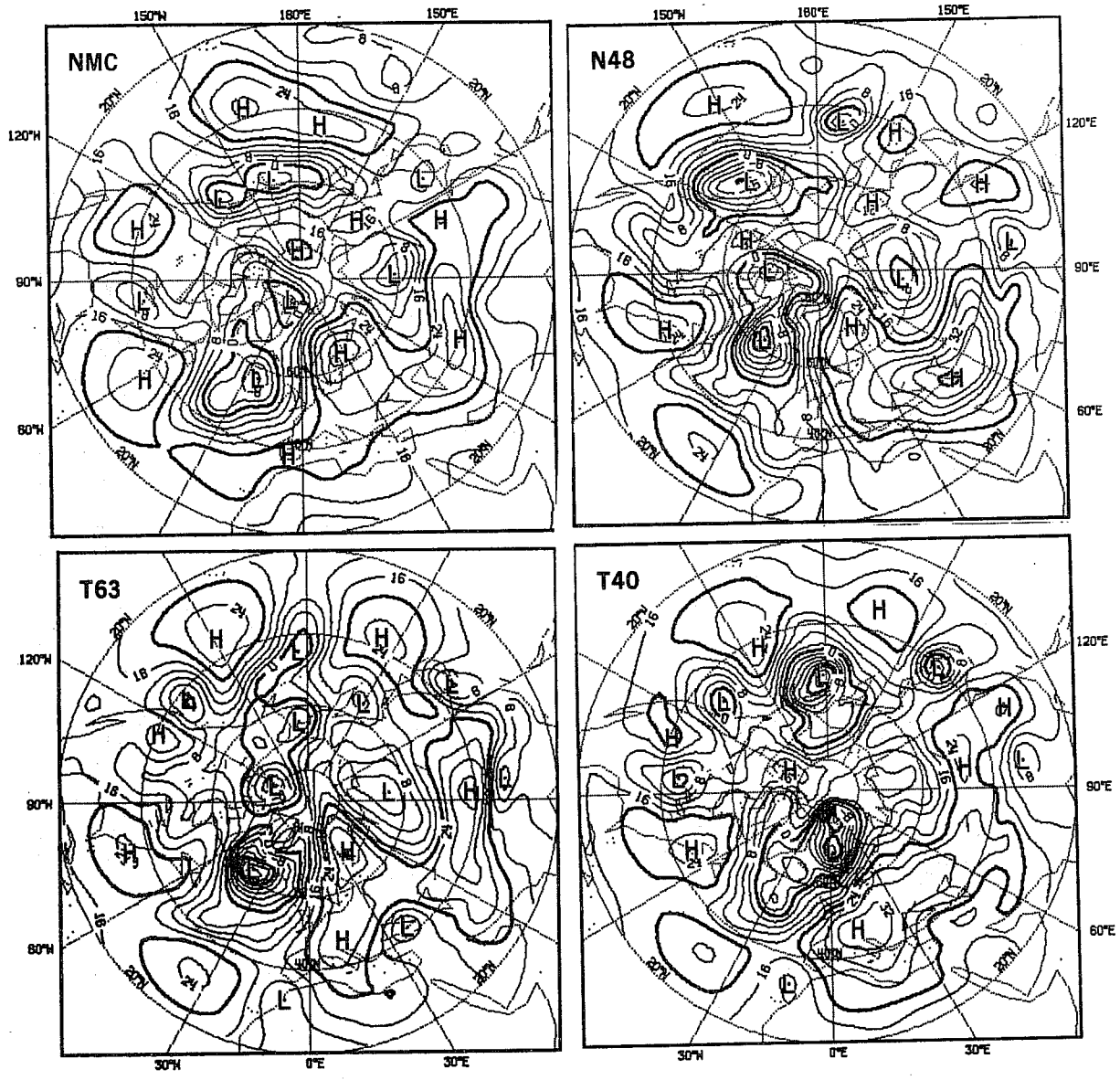

Fig. 4.8 Day 7, 1000 mb height forecasts from February 15, 1976

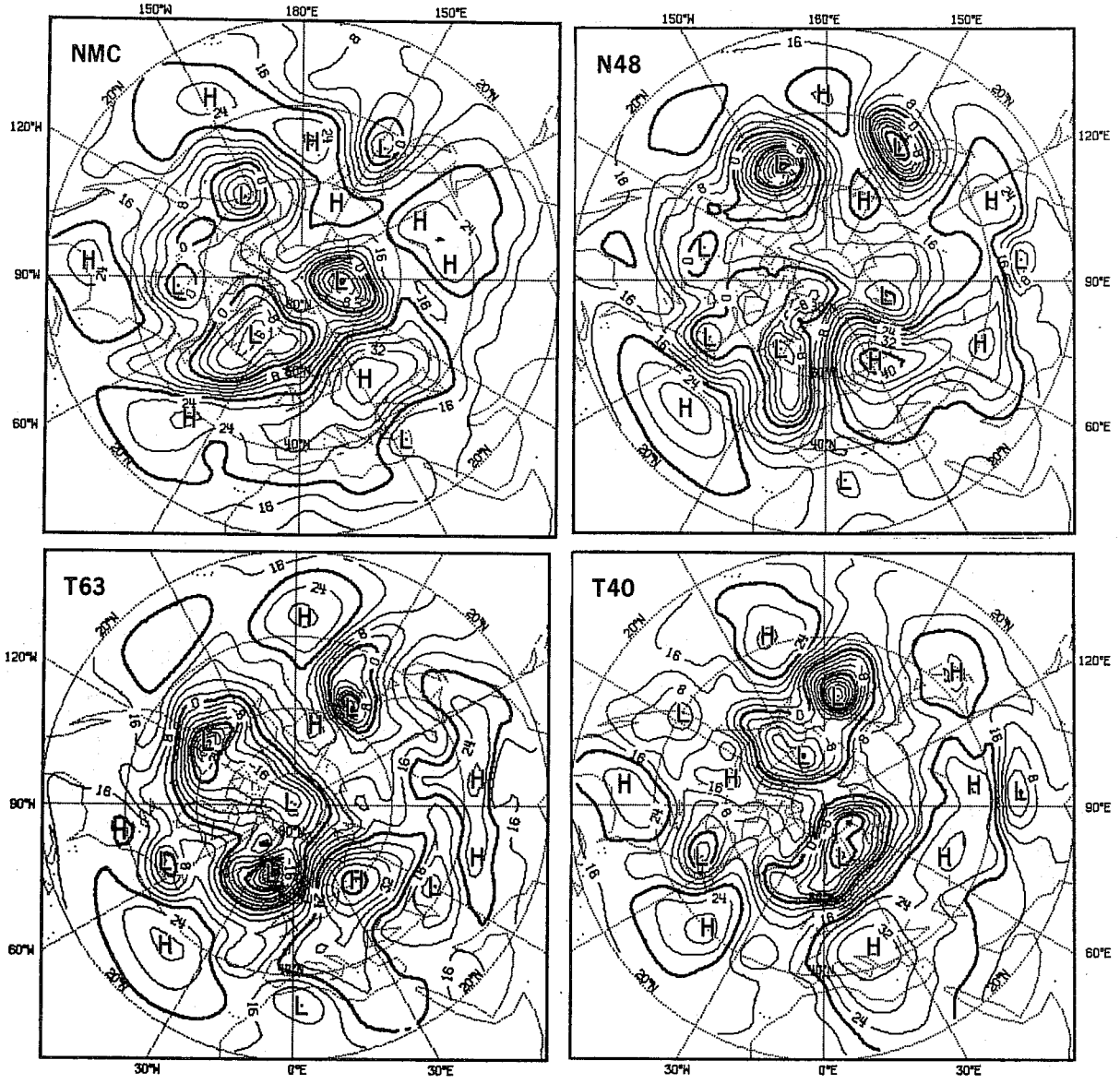

Fig. 4.9 Day 9, 1000 mb height forecasts from February 15, 1976

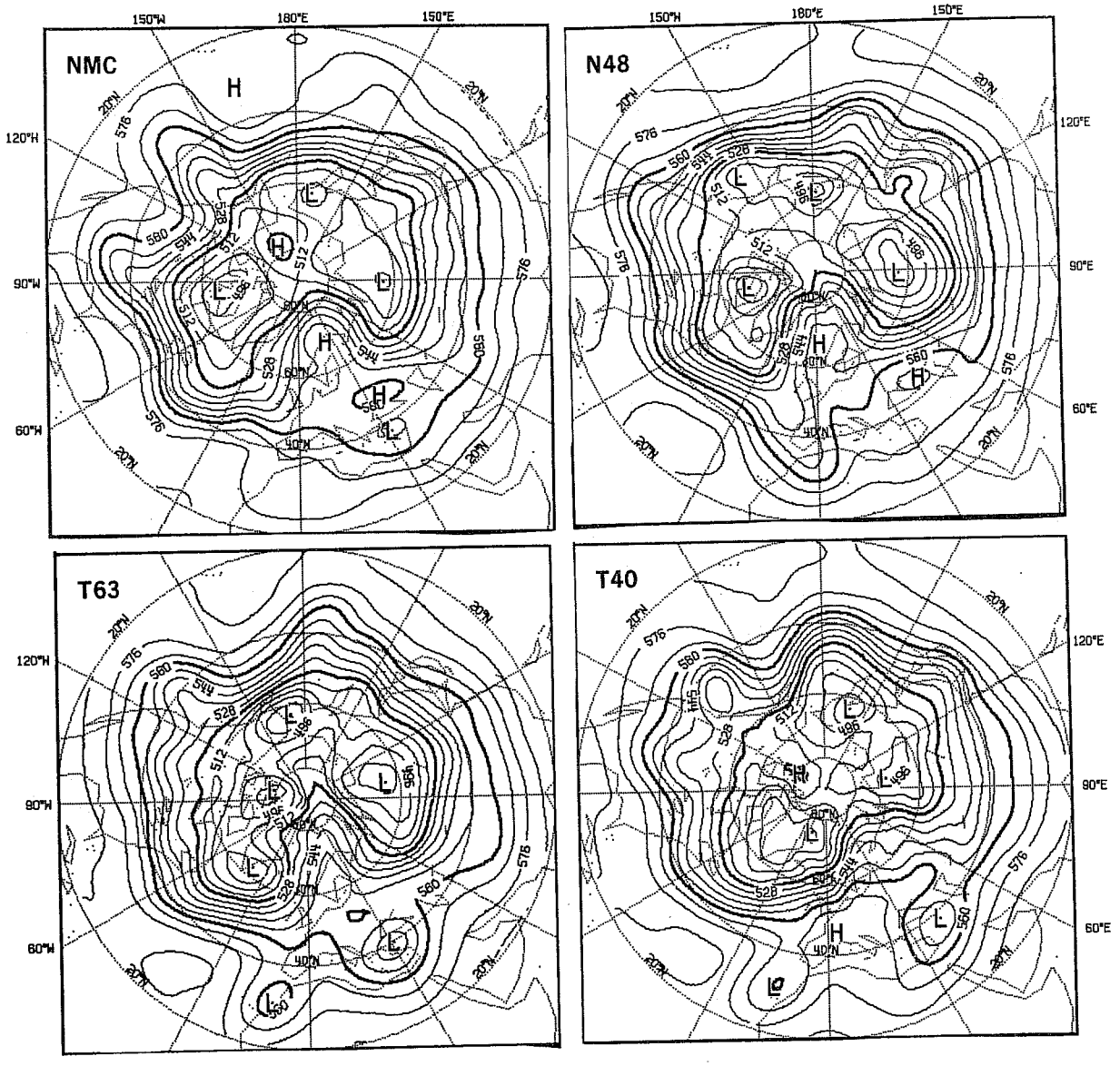

Fig. 4.10 Day 7, 500 mb height forecasts from February 15, 1976

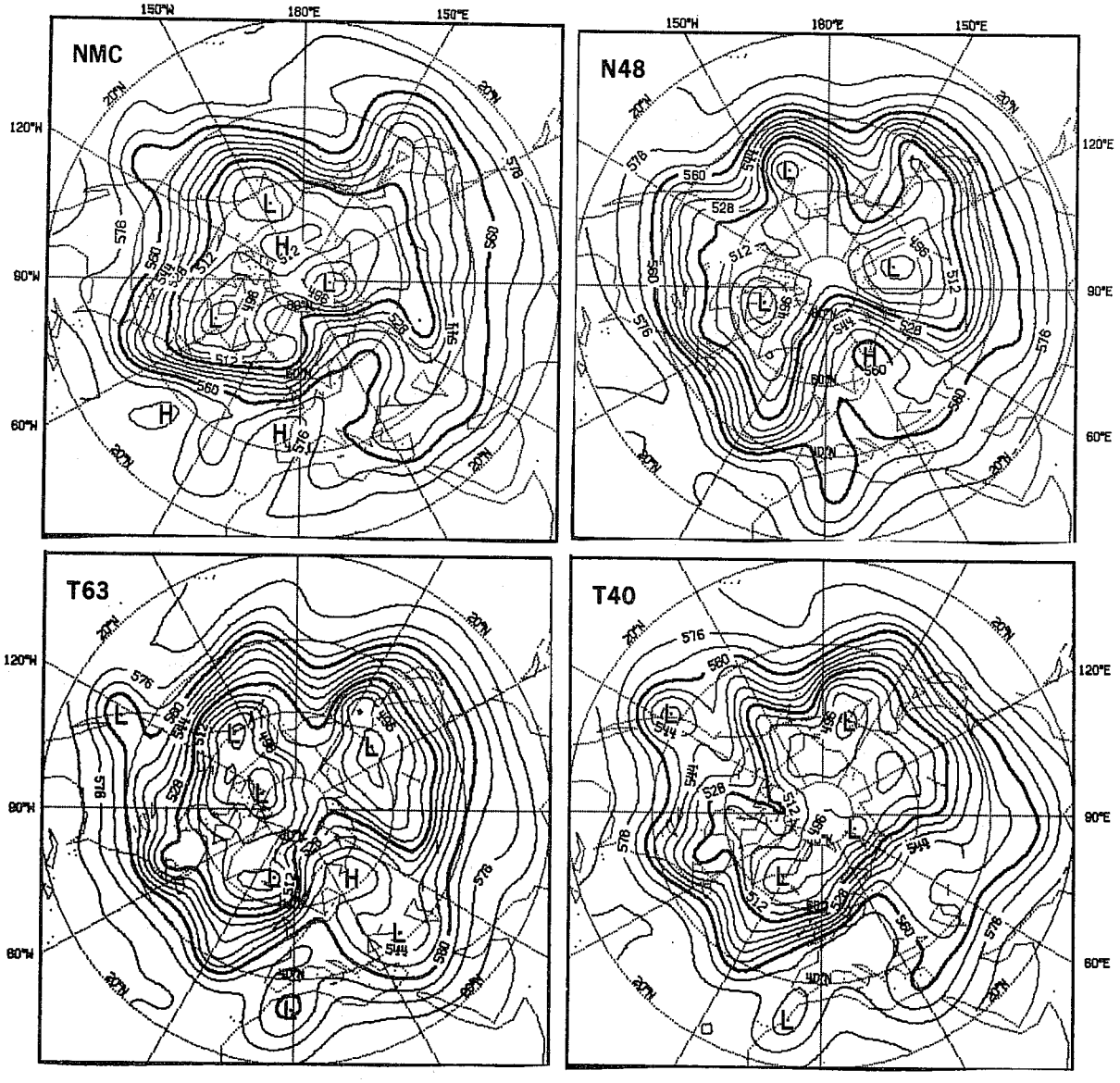

Fig. 4.11 Day 9, 500 mb height forecasts from February 15, 1976

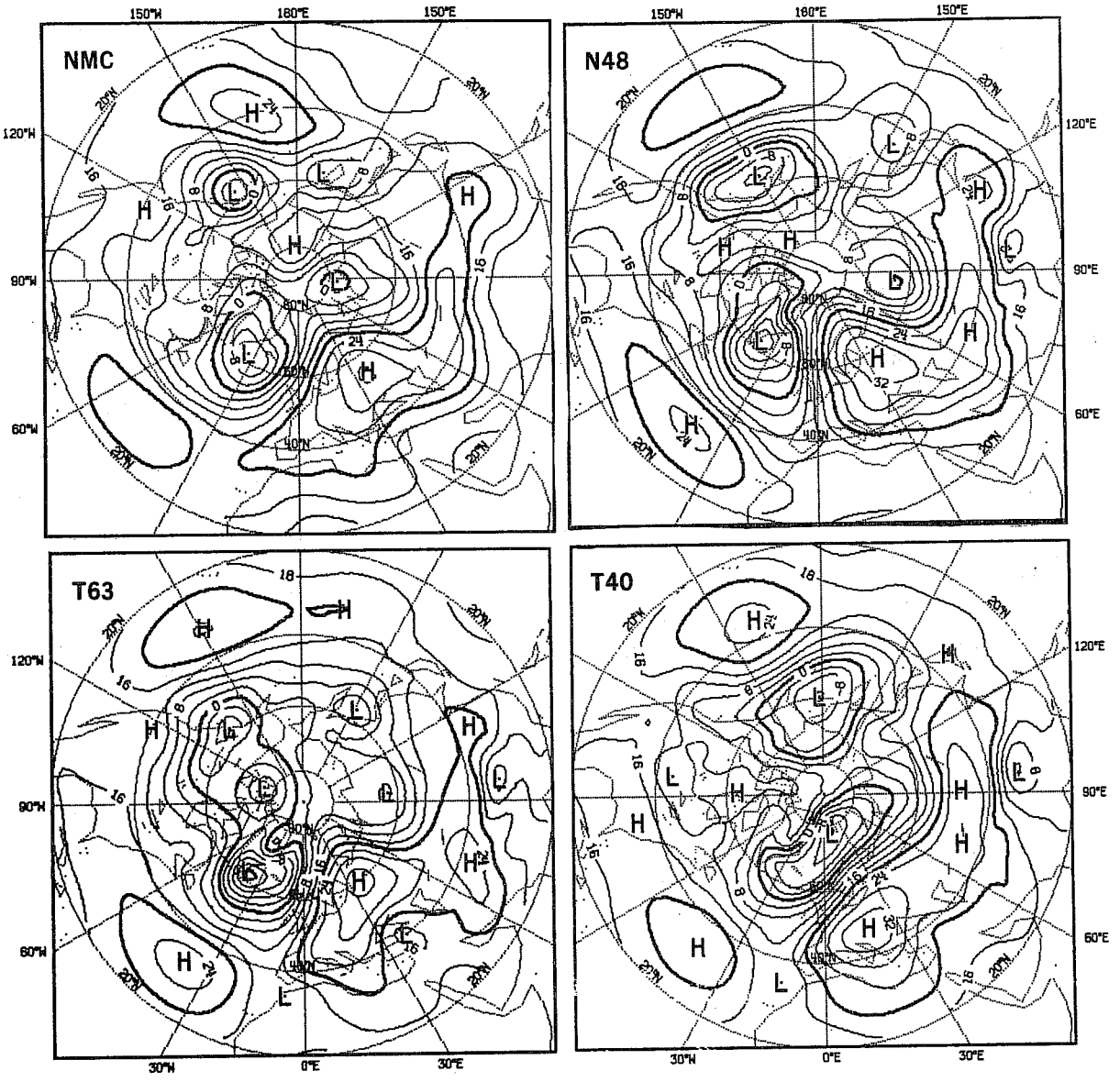

Fig. 4.12 Mean of day 5 to 10, 1000 mb height forecasts from February 15, 1976

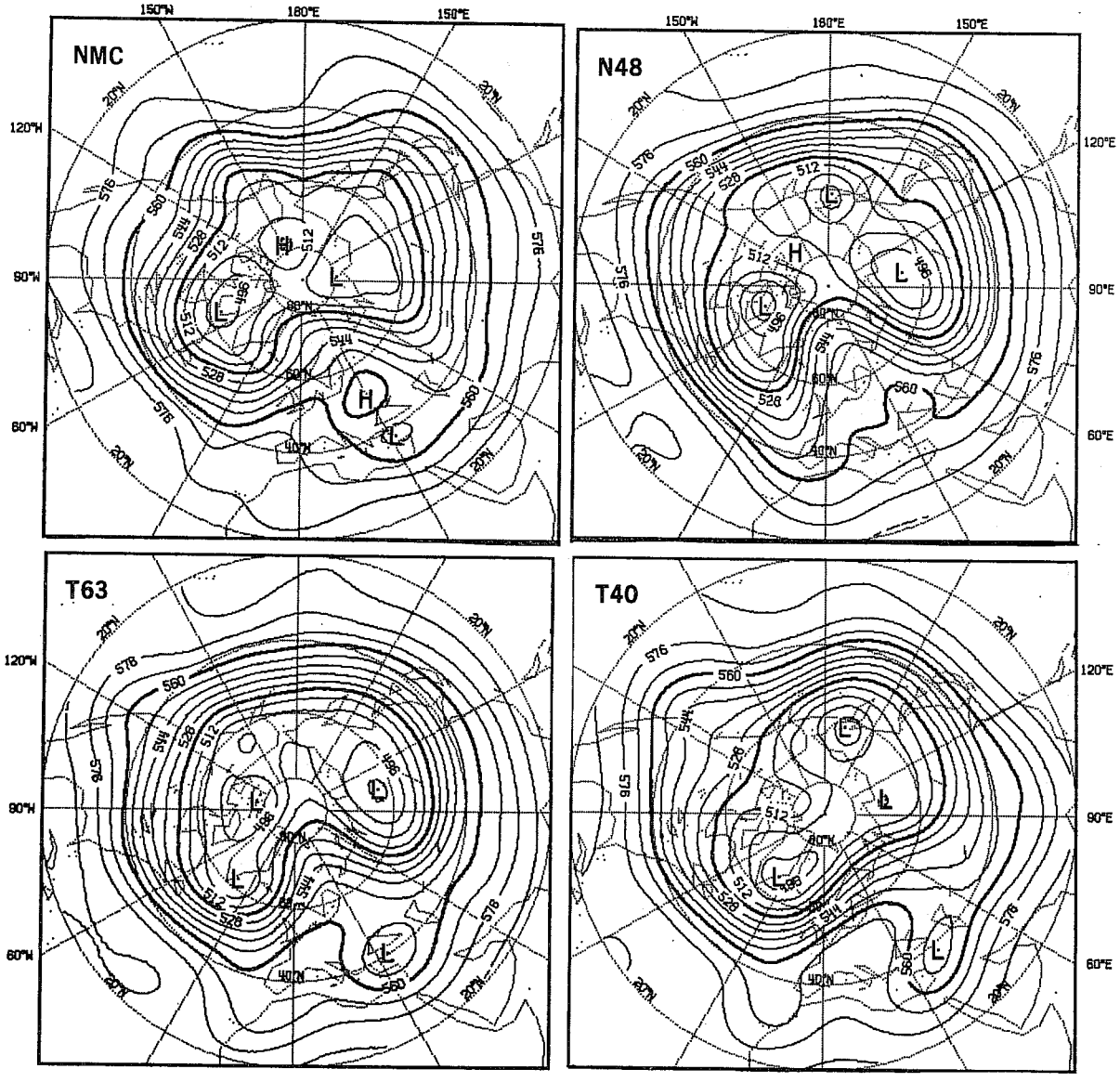

Fig. 4.13 Mean of day 5 to 10, 500 mb height forecasts from February 15, 1976

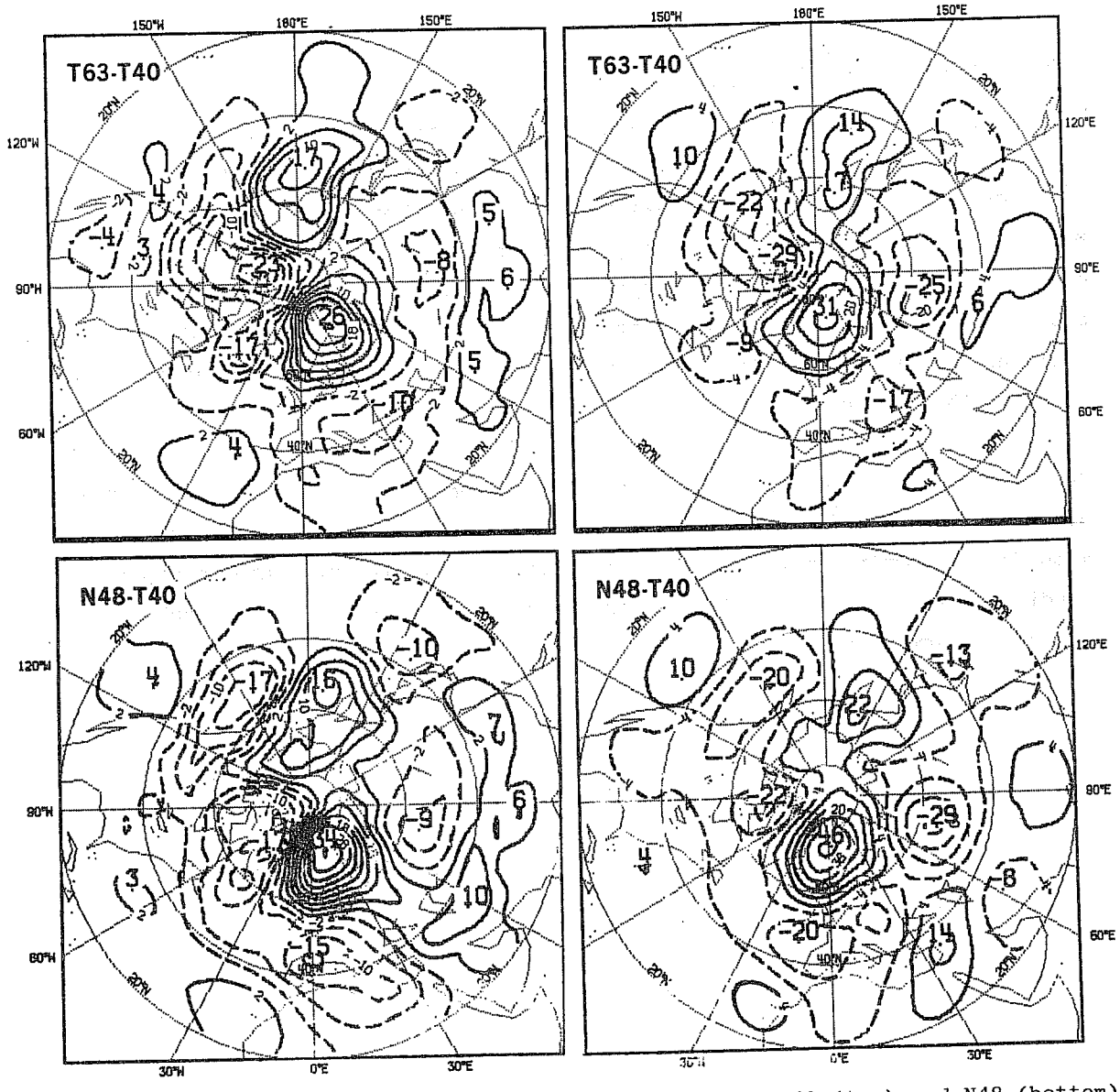

Fig. 4.14 Mean of day 5 to 10, height differences of T40 (top) and N48 (bottom) to T63 at 1000 mb (left) and 500 mb (right)

Fig. 4.14 presents the differences between T63 and T40 on one hand and N48 and T40 on the other hand at both 500 and 1000 mb, averaged over the last 5 days of the 10-day period. These differences are considerable. They are bigger than those between reality and T63 for example. Thus it is not always true to say that models are closer to each other than any one of them is to reality.

4.2.4 Precipitation forecasts

Figs. 4.15 and 4.16 present, on a Mercator projection covering the globe minus the south polar cap, the total accumulated precipitation after the first day and for the entire 10-day period, respectively. The maps for N48 and T63 show very similar precipitation forecasts by the models. T40, however, generates on day 1 small precipitation areas over northern USSR and Canada which are not seen in either the T63 or N48 maps. Accumulated over the 10-day period, the precipitation forecast of T40 is also much smoother than the others.

On the whole, precipitations which are overestimated by N48 (according to TR13) appear as intense in the spectral forecasts. The size and scale of the present maps do not permit a more detailed comparison and in the two other synoptic studies we shall no longer display precipitation forecasts as they would not add any information.

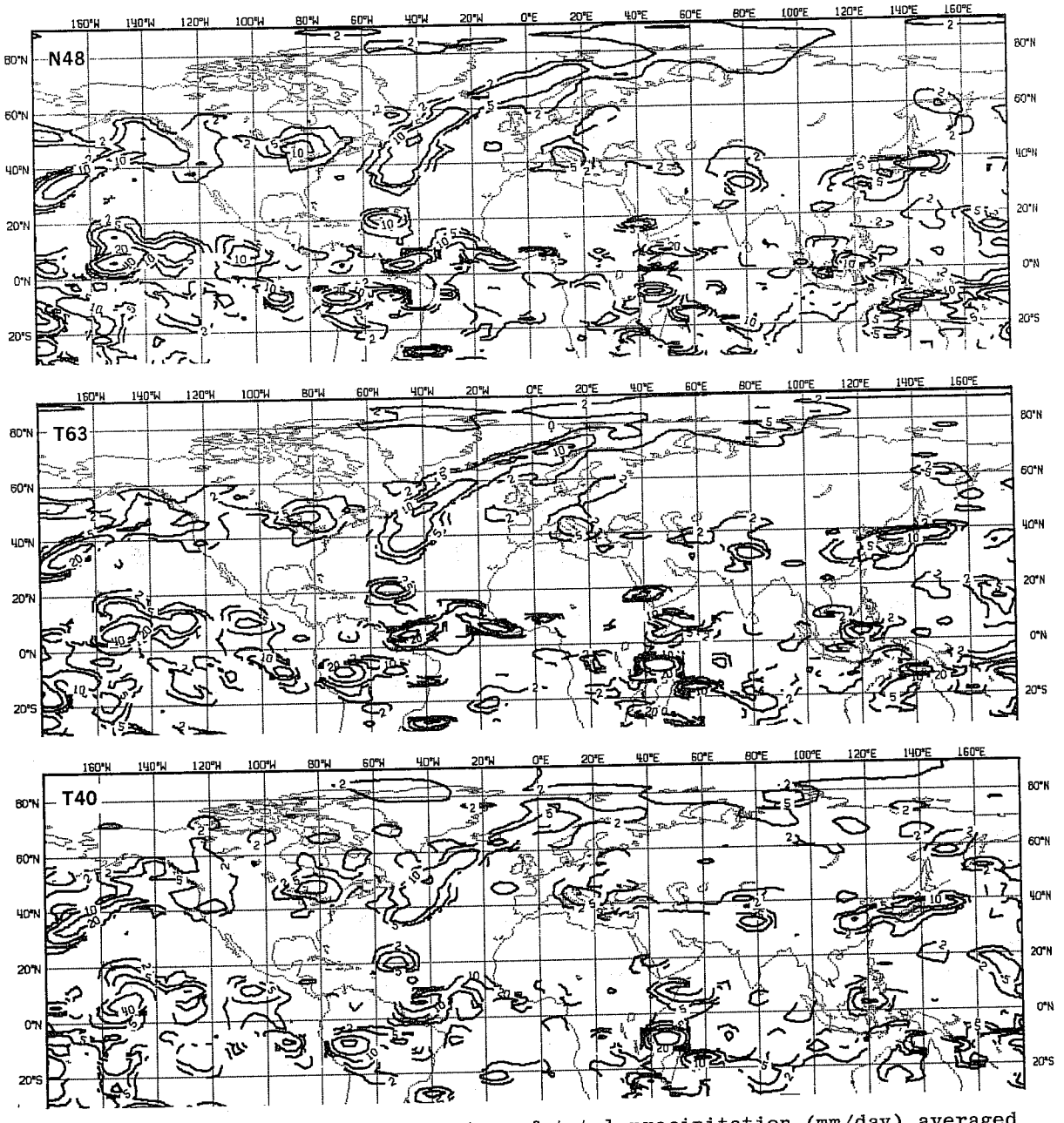

Fig. 4.15 Global maps for the rates of total precipitation (mm/day) averaged for the first day of the forecast from February 15, 1976 by N48 (top), T63 (middle) and T40 (bottom)

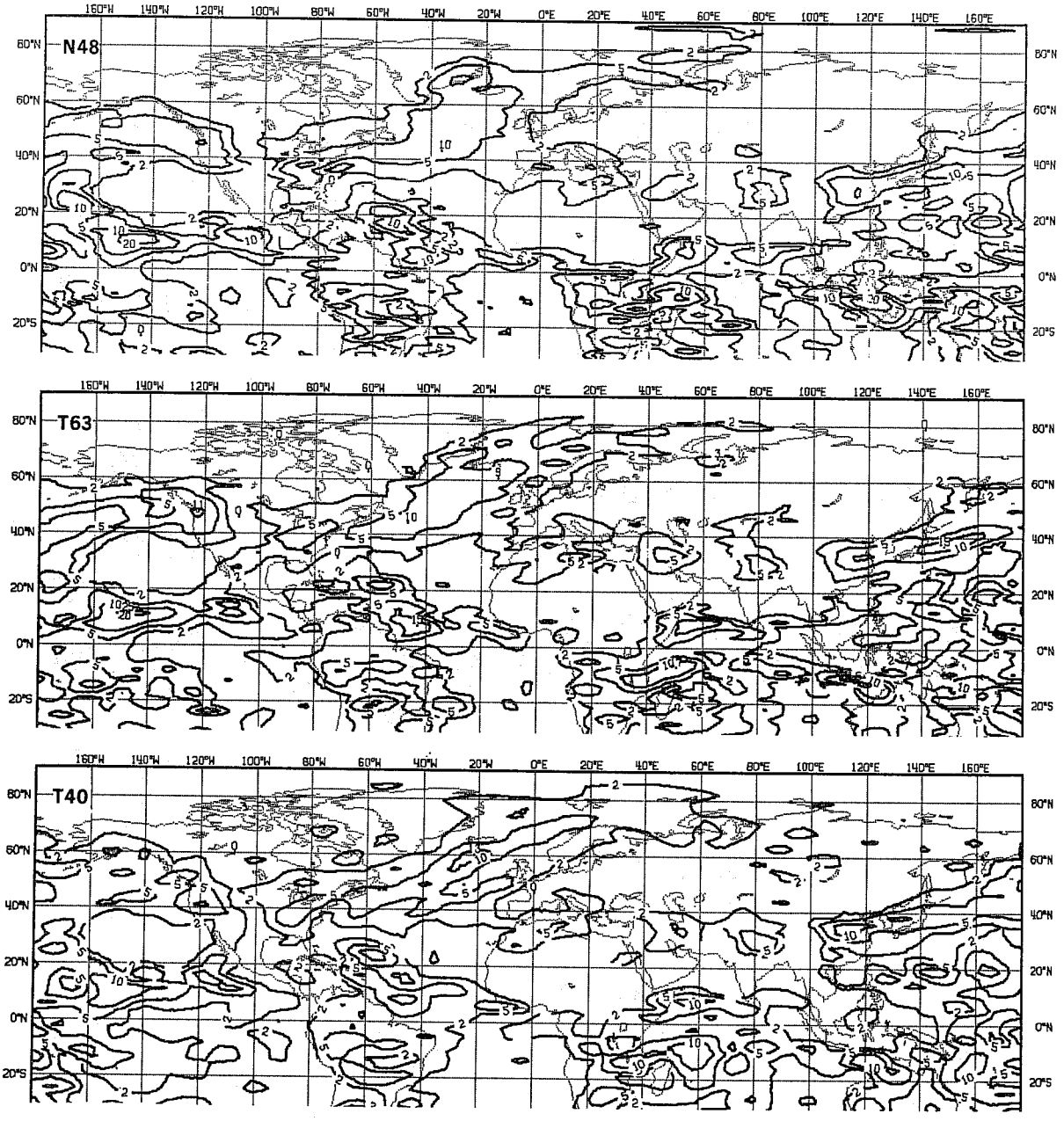

Fig. 4.16 Same as 4.15, but averaged for the whole (10-day) period of the forecast

4.3 Case 2. Forecasts from 6.2.76

4.3.1 Days 0 to 5

Already on day 2 of this forecast some differences can be observed between the models at 1000 mb (Fig. 4.17). N48 has moved the low south of Greenland too far eastwards by about 5^{o}. T63 and T40 have it slightly better positioned. It is too deep in all models, but more in T40 and N48. The north eastern Pacific low is also too deep and has moved too far eastwards in all forecasts. But in this case T63 shows the largest error and T40 the smallest one.

On day 3 (Fig. 4.18) the same low has moved inland. It remains too deep in all forecasts with the best position and depth still given by T40. The formation of a high pressure belt over central and southern Europe is correctly predicted by all models, but the high over the Balkans is too intense. All models show too deep a low system over the north Atlantic with a spurious cut off north west of the British Isles. However the flow over north eastern Atlantic and the trough along 30^{o}W are better captured by T63 than by either T40 or N48.

On day 4 (Fig. 4.19) the high pressure belt remains well forecast except for its northward extension over central Europe. A major feature at this time is the intense low over Iceland associated with gales in the North Sea and over Scandinavia. It is best represented by T63. Both the position of the low centre and the direction of the flow over the North Sea are good. Taking into account the given systematic tendency of the models to overdeepen lows in this area, it is interesting to note that only T63 has succeeded in forecasting intensification between day 3 and 4. Another feature, the ridge and low system over North America is relatively well represented in all models, although the low is again typically too deep.

On day 5 (Fig. 4.20) the Icelandic low started to fill. The trend is seen in all models. But in general over north eastern Atlantic T63 maintains a superiority over T40 and N48 in defining the position and shape of the complete system. For example the trough over the British Isles is forecast by T63. N48 shows a weak ridge in its place. The flow there and over Scandinavia, as produced by T63 is certainly more qualitatively correct than in the two other models. Over the Pacific all models have lost most of their skill.

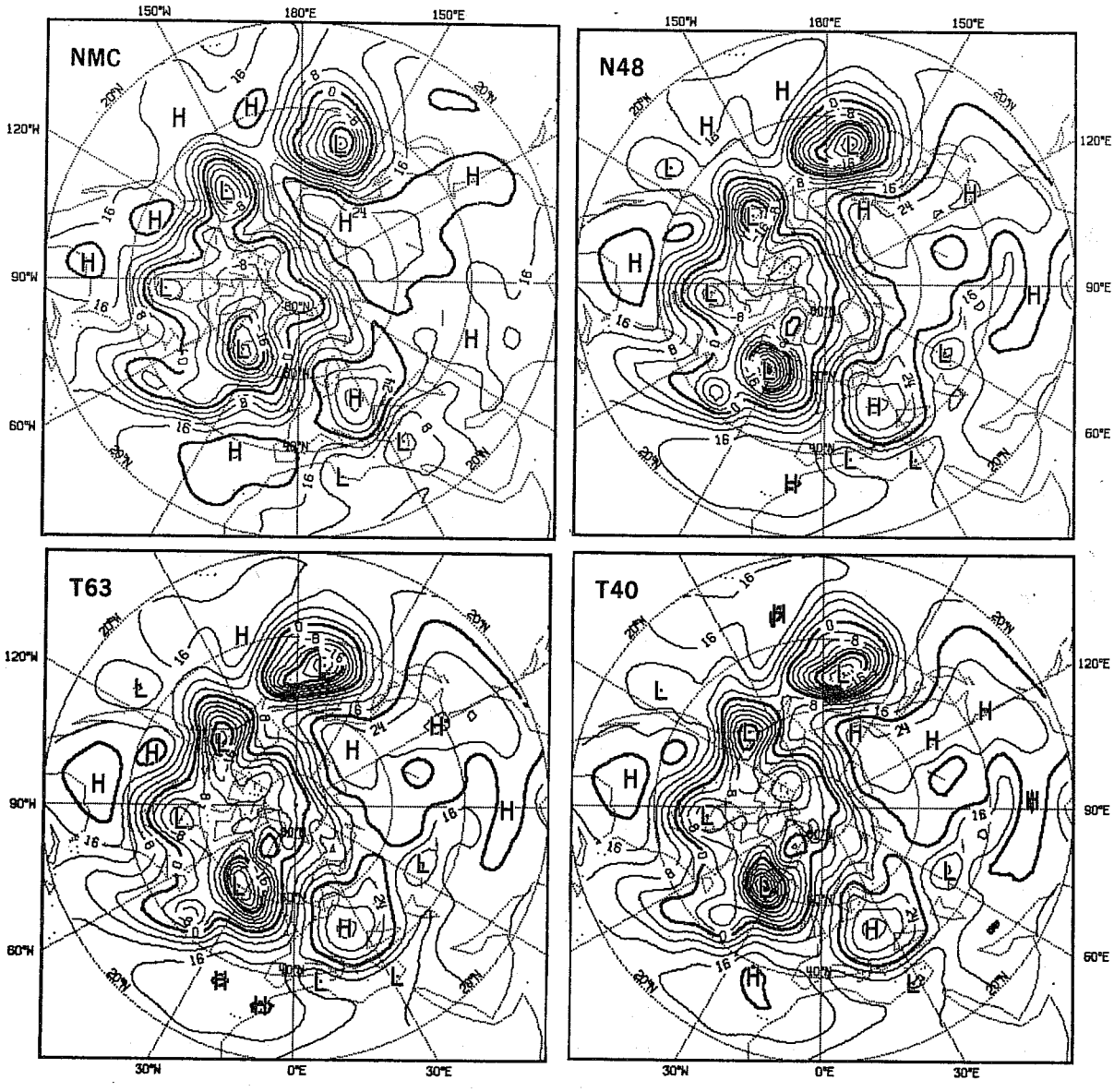

Fig. 4.17 Day 2, 1000 mb height forecasts from February 6, 1976

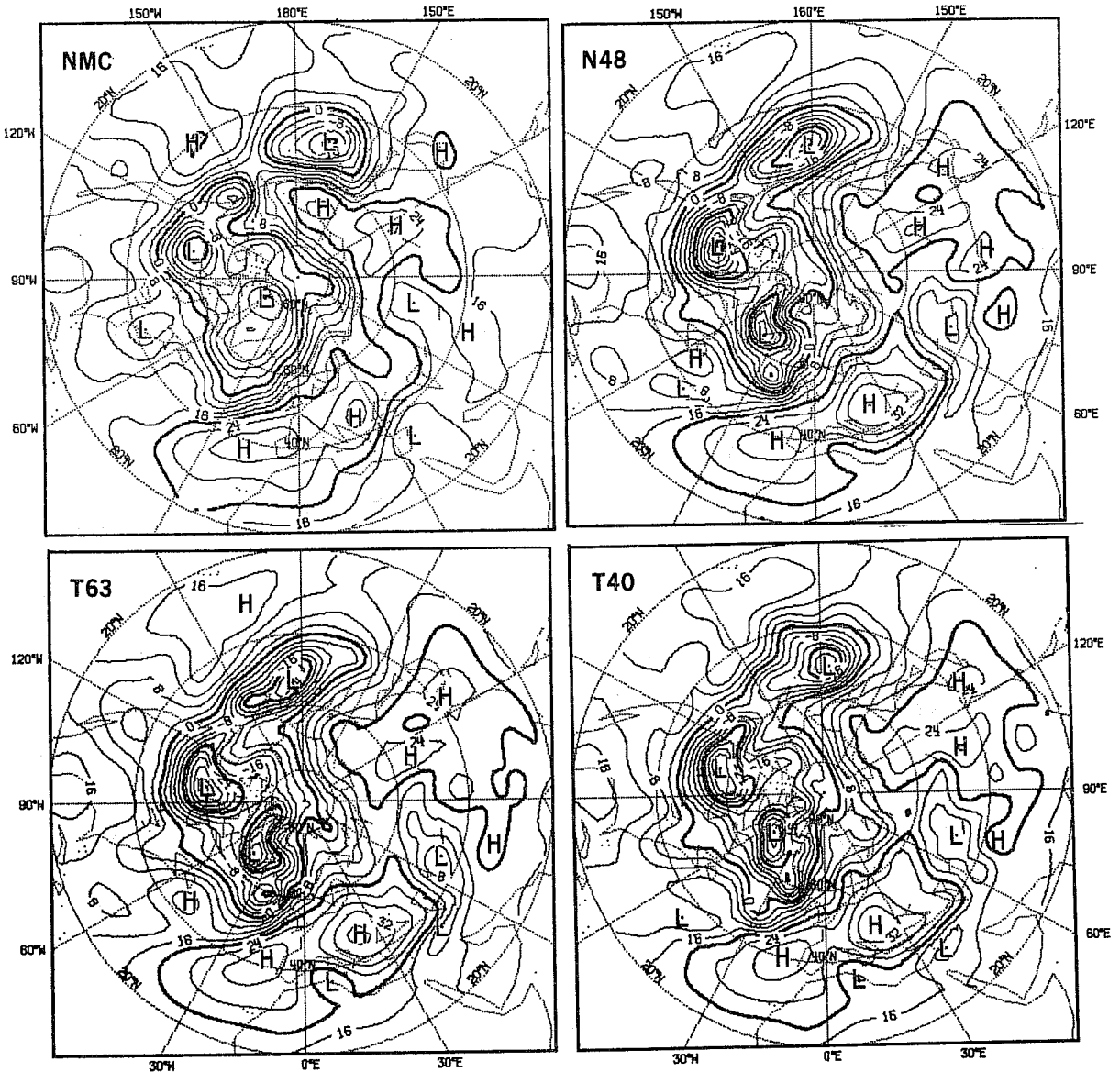

Fig. 4.18 Day 3, 1000 mb height forecasts from February 6, 1976

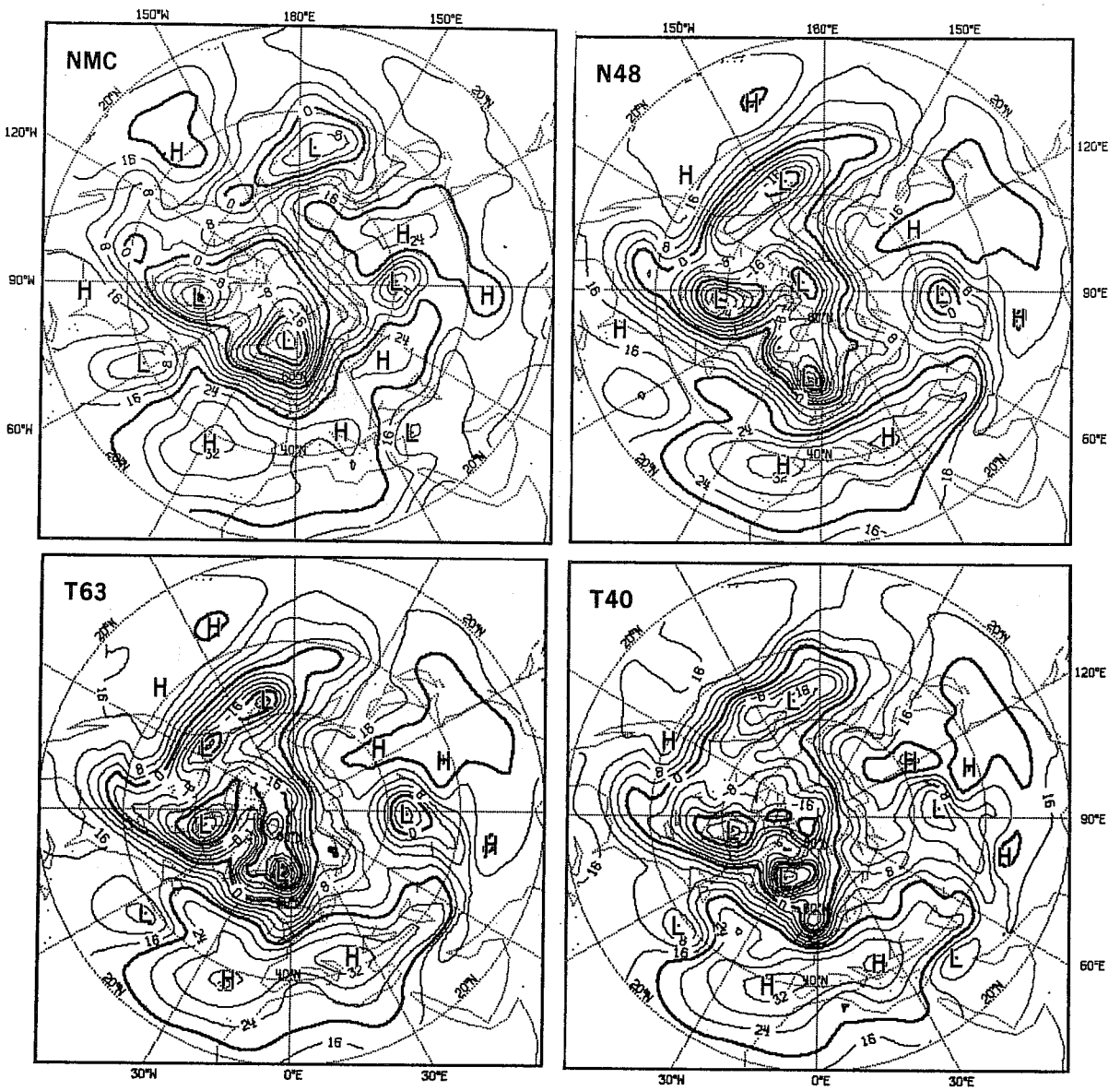

Fig. 4.19 Day 4, 1000 mb height forecasts from February 6, 1976

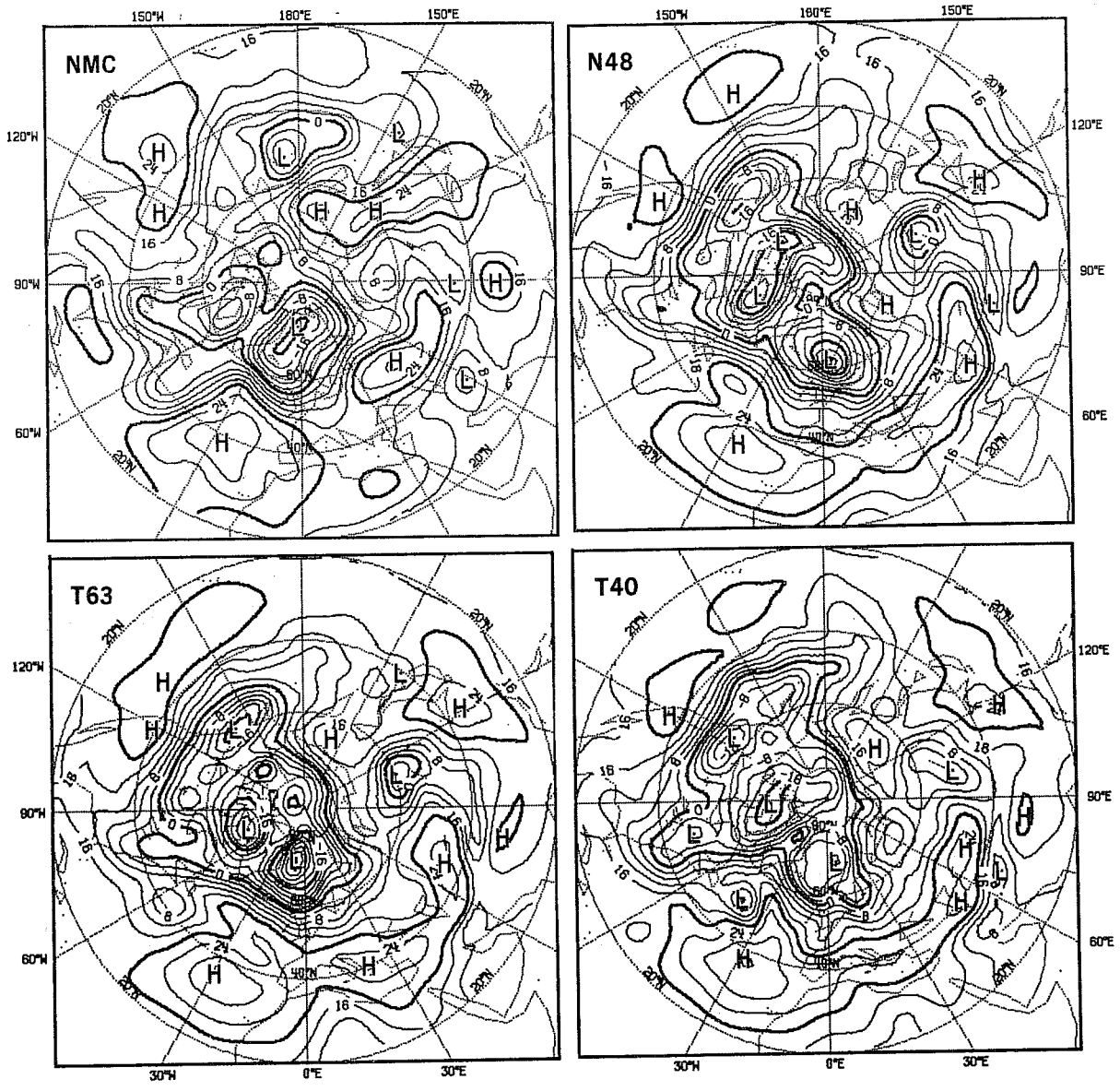

Fig. 4.20 Day 5, 1000 mb height forecasts from February 6, 1976

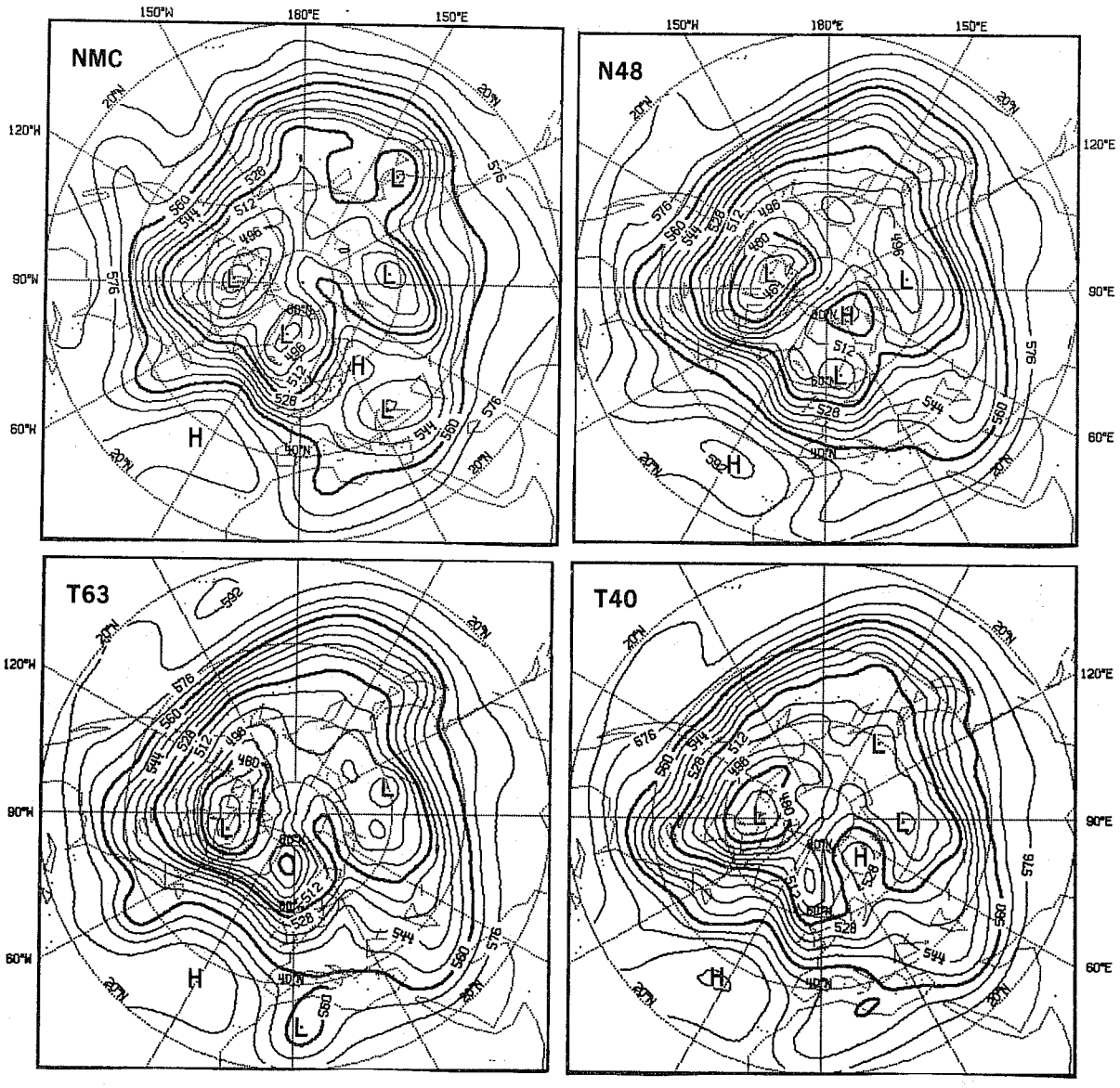

Fig. 4.21 Day 5, 500 mb height forecasts from February 6, 1976

From the day 5 500 mb maps (Fig. 4.21) one can draw similar conclusions about the performances of the models over north eastern Atlantic and western Europe: the low east of Greenland and the associated trough over the British Isles and ridge from Italy to Finland are satisfactorily forecast by T63. T40 could be described as slightly less useful. N48 has developed a circulation largely erroneous in its details over most of western Europe in spite of the fact that the very large scale components of the flow remain acceptable. Over the Pacific all models perform poorly.

4.3.2 Days 5 to 10

On day 6 at 500 mb (Fig. 4.22) N48 has too deep a trough over western Europe with the northern stream of the separated flow too far south over the continent. T63 retains more skill in this area.

After day 6 all models have lost most skill and we do not display any maps for this period.

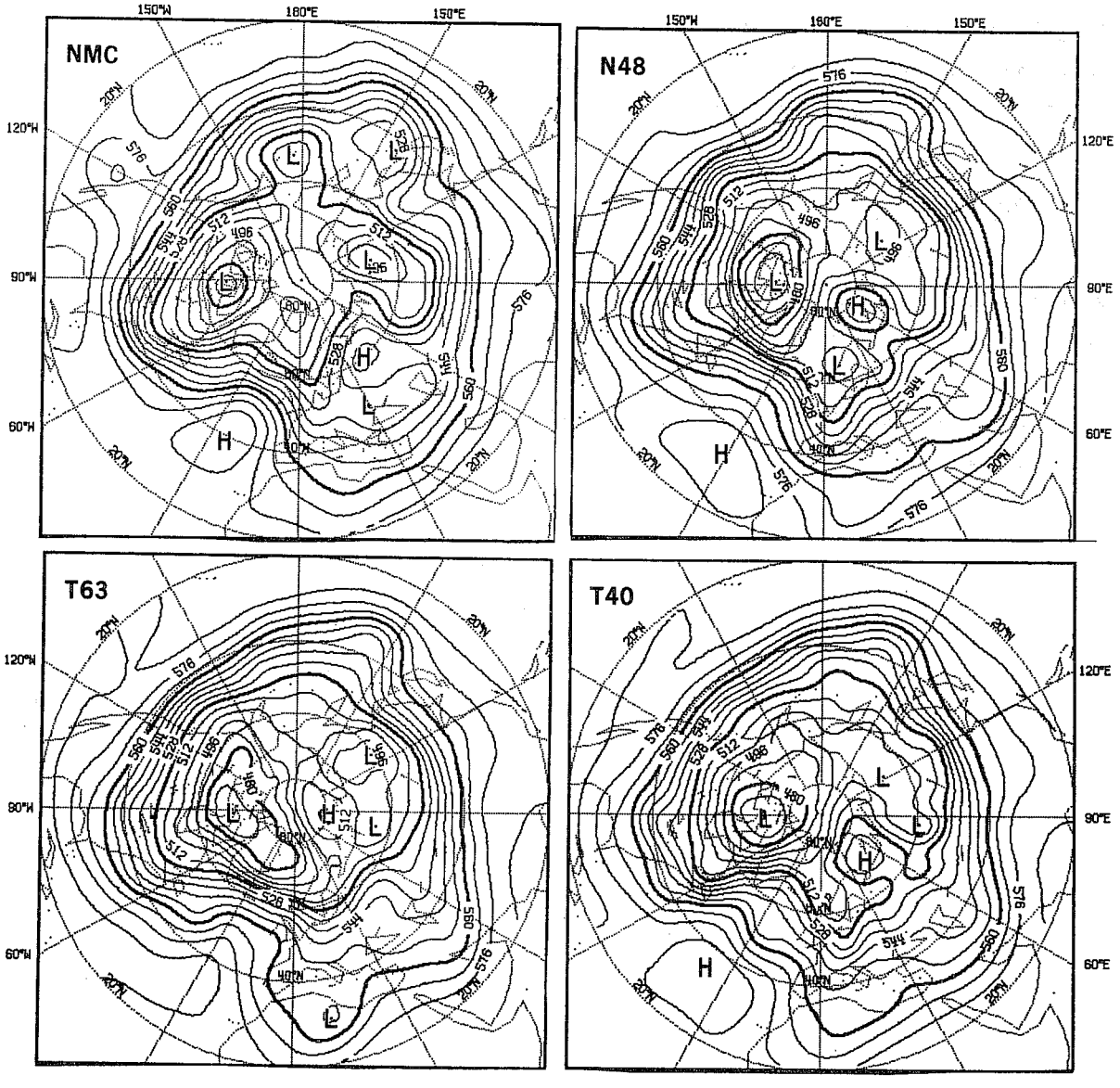

Fig. 4.22 Day 6, 500 mb height forecasts from February 6, 1976

4.4 Case 3. Forecasts from 18.2.76

4.4.1 Days 0 to 5

This case is different from cases 1 and 2 since already on day 2 at 1000 mb (Fig. 4.23) considerable errors can be found in the forecasts: none of the models has succeeded in moving the Atlantic trough eastwards quickly enough. All the major lows are already noticeably too deep. The forecast over western Europe presents many deficiencies.

On day 3 (Fig. 4.24) these deficiencies are accentuated. The southerly flow from Spain to Great Britain is missed by all models which develop a trough over the British Isles and a ridge over Greenland. N48 is slightly more successful than T63 and T40 in particular with respect to the ridge over Scandinavia. The forecast over the Pacific is however quite acceptable.

On day 4 (Fig. 4.25) the usefulness of the forecasts already becomes doubtful over Northern Europe: T63 and T40 show a cut off low over Scandinavia where there should be a ridge; N48 does slightly better there. The trough from Siberia to the Caspian Sea and the other one on 40^{o}W are also better captured by N48.

On day 5, at 1000 mb (Fig. 4.26) none of the low systems is correctly positioned and all models behave similarly and wrongly. N48 having only a ridge north of Russia instead of a deep low is less incorrect than T63 and T40 which both produce a pronounced high.

At 500 mb (Fig. 4.27) the quality of the forecasts is not much better and from day 6 onwards no skill remains. Therefore we do not display any maps for the second half of the period.

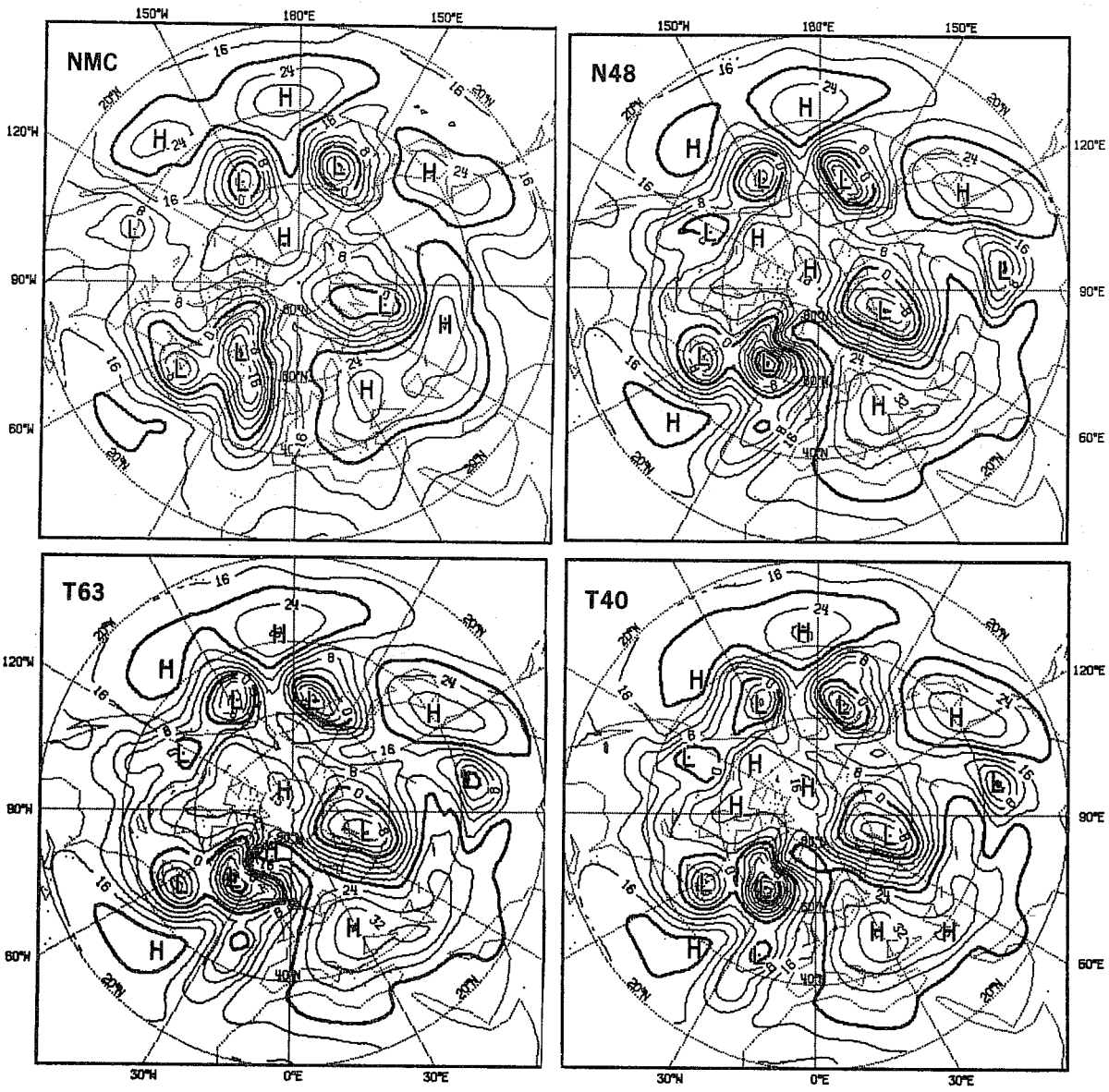

Fig. 4.23 Day 2, 1000 mb height forecasts from February 18, 1976

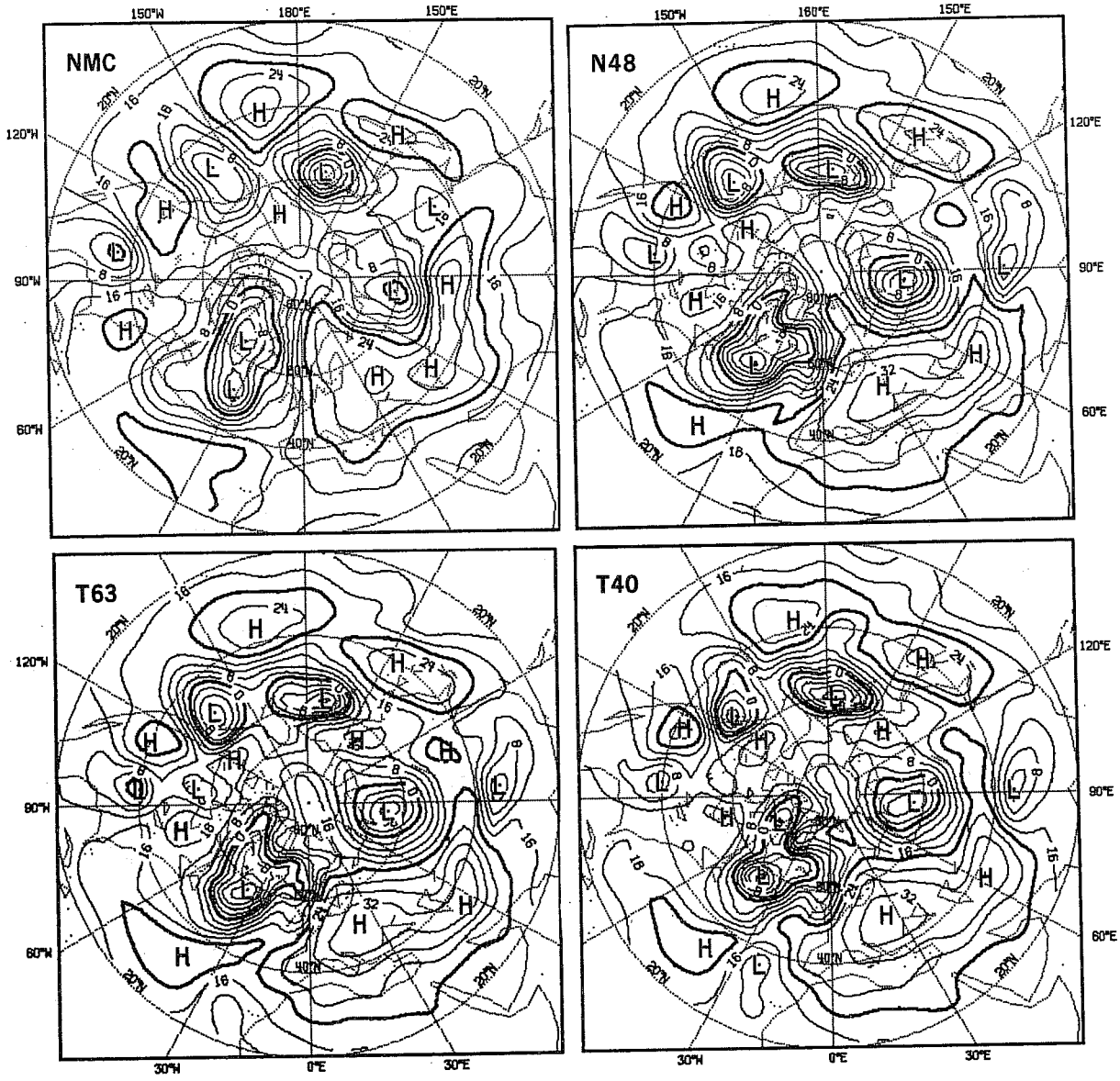

Fig. 4.24 Day 3, 1000 mb height forecasts from February 18, 1976

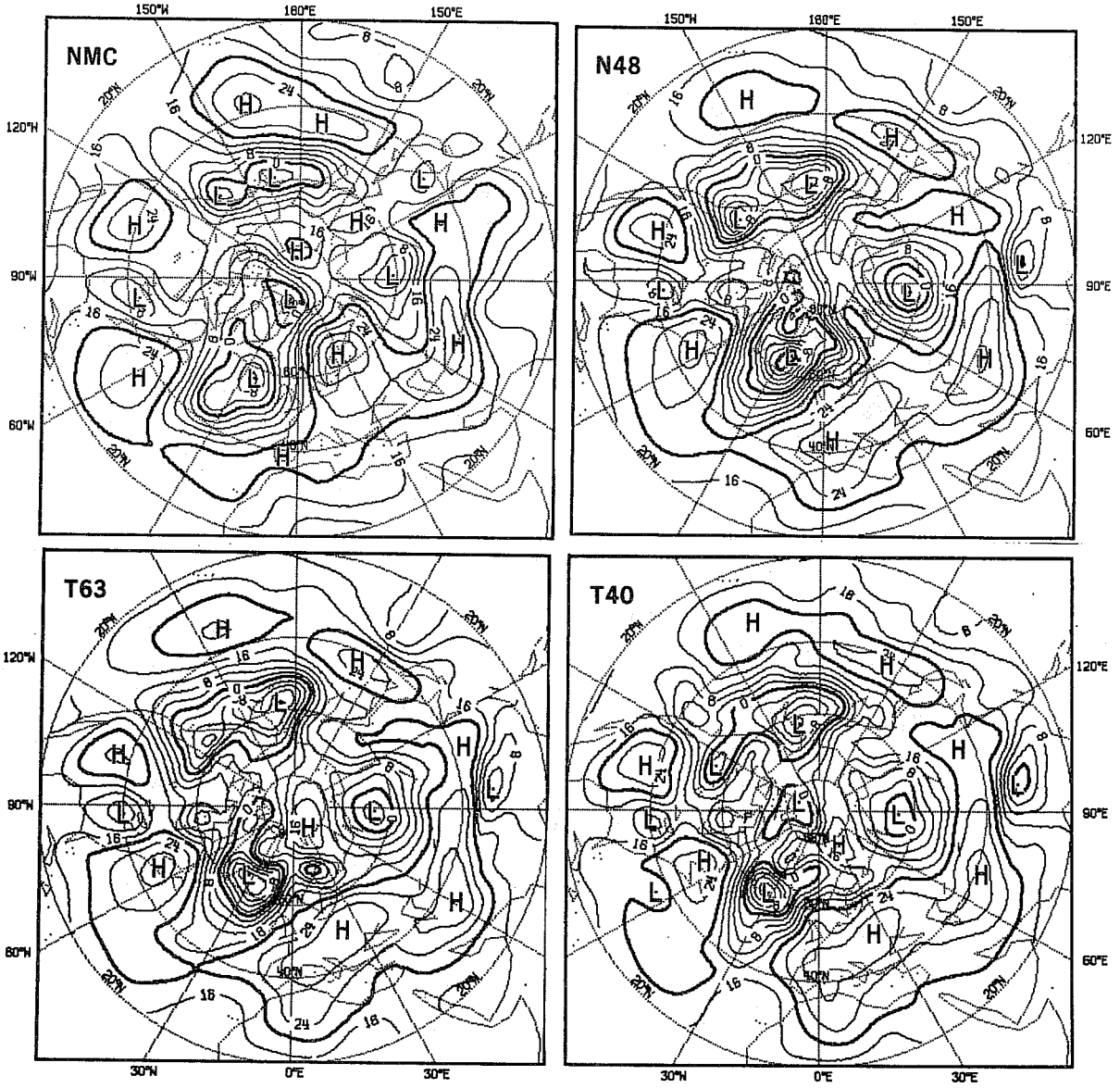

Fig. 4.25 Day 4, 1000 mb height forecasts from February 18, 1976

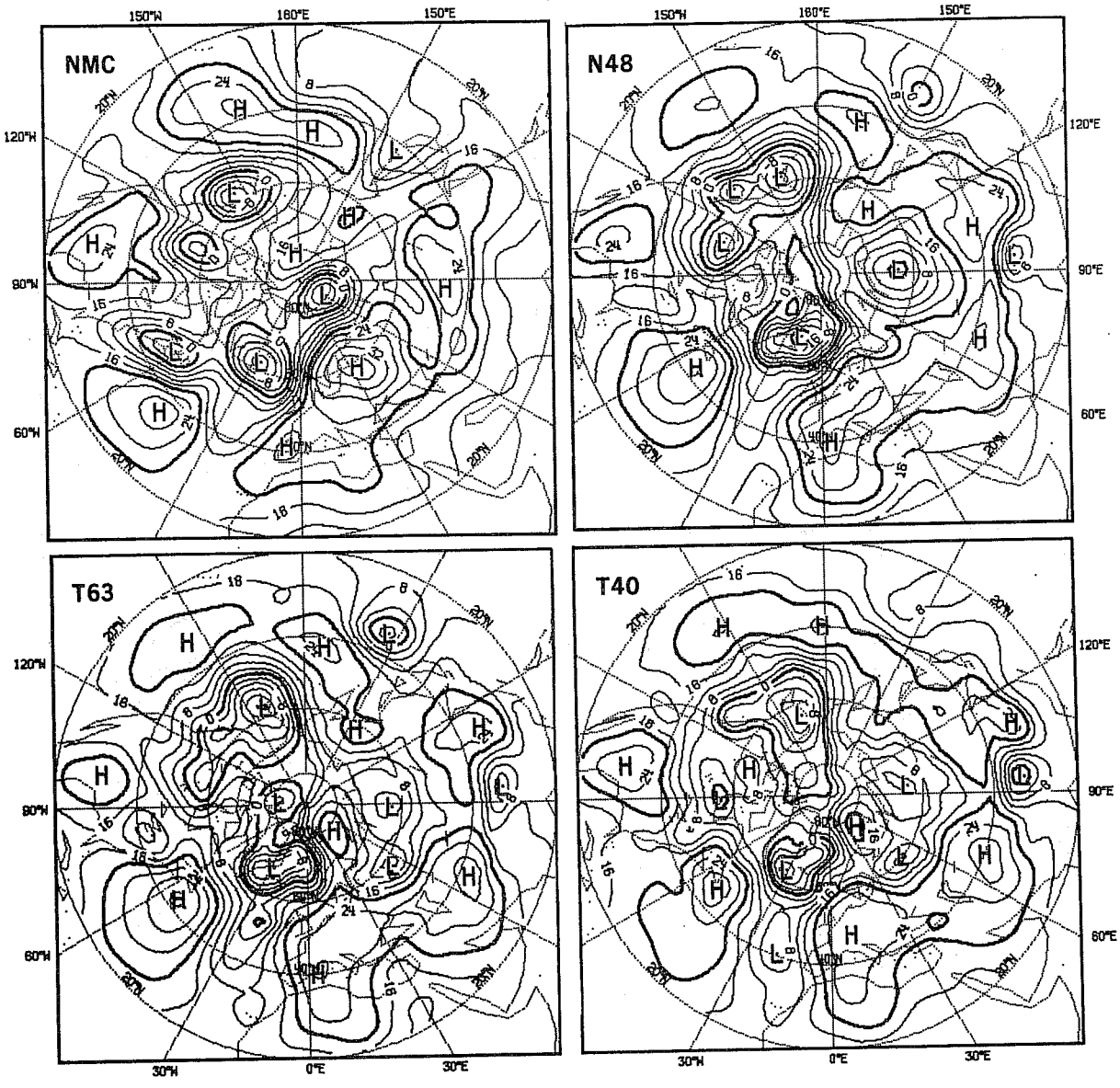

Fig. 4.26 Day 5, 1000 mb height forecasts from February 18, 1976

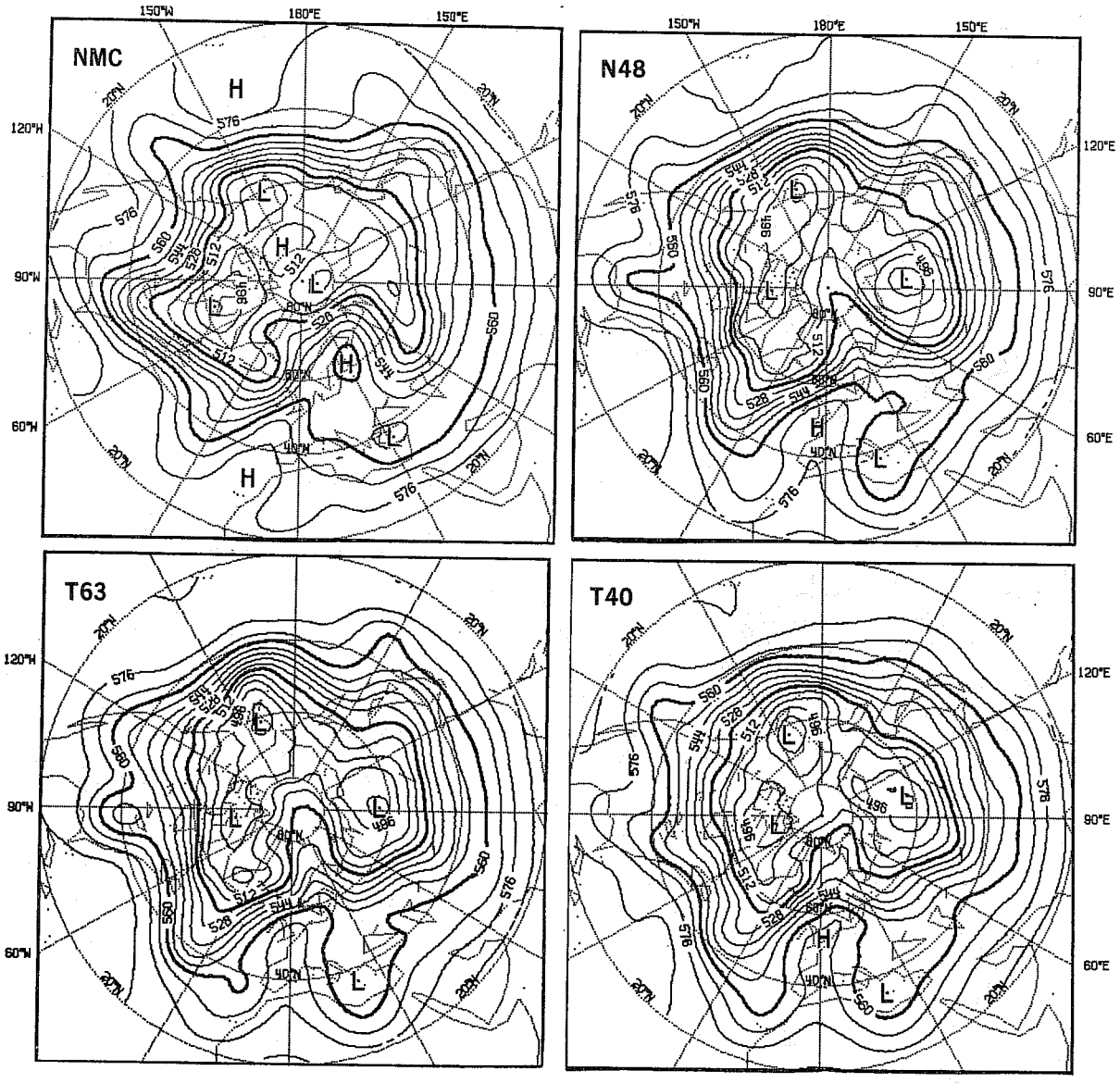

Fig. 4.27 Day 5, 500 mb height forecasts from February 18, 1976

4.5 Summary of the synoptic evaluation

We have made a synoptic assessment of three selected cases with special attention being paid to the European and north Atlantic area.

The forecasts made from February 15th were very successful for T63 and N48 which both retained skill almost until the end of the period. The forecast made with the lower resolution spectral model - T40 - deteriorated much more quickly after having failed to generate the blocking situation over north western Europe on day 4. During the second half of the forecast period T63 predicted a second change of circulation over western Europe while N48 did not.

The forecast made from February 6th was also rather successful for T63 which retained useful skill over Europe up to day 6. The forecast made by T40 was less skillful but remained useful, while many details of the one made by N48 were misleading in this area by day 4.

The forecasts made from February 18th were very unsuccessful for all models, with major deficiencies over Europe already apparent by day 3 and hardly any skill was left on day 5. As mentioned earlier this is the only case where N48 objectively did better than T63.

The first case resembles what could be described as a textbook example of the effect of increase resolution on forecast skill. All models have relatively high horizontal resolution and are therefore very successful and almost indistinguishable at short-range (up to 3 days). However, during the latter part of the forecast, out of the two major circulation changes observed, T40 already failed on the first at around day 4-5, N48 failed on the second one at around day 7-8 and T63 was relatively successful on both situations. The second case could be taken as an example of the effect of using a better computational technique since both the spectral models outperformed N48 over Europe. The third case may be regarded as a good example also, but of the difficulties to which may be subjected experiments of the type reported here. Not only is it a case where all models are rather unsuccessful, it is also a case where the lower resolution T40 performs as well as, if not better than, the higher resolution T63. Furthermore, the initial conditions for this case (February 18th) happen to fall three days only after the initial conditions for the good case (February 15th). Indeed, comparing over Europe

forecasts obtained for February 22nd (4-day forecasts from February 18th, Fig. 4.25, and 7-day forecasts from February 15th, Fig. 4.8) it is apparent that the earlier 7-day forecasts of both T63 and N48 are more correct than the later 4-day forecasts.

In addition, in all cases shown and also not shown, all models suffer from the same systematic tendencies, already noticeable on day 2, of overdeveloping the main depressions as well as failing to fill them quickly enough. Usually the depressions move eastwards too fast, penetrating too far into the American and European land masses. These errors, unfortunately, very often dominate model differences. Their full impact is even more apparent when looking at the large scale geographical error patterns that remain after averaging over the ensemble of cases (see Section 6).

In spite of the effort made to emphasize model differences in the above three synoptic evaluations, it must be admitted that it is their similarities which stand out and this is true in all the aspects considered, including precipitation as well as height forecasts, hits as well as misses. Horizontal truncation errors remaining in these forecasts and differences attributable to the horizontal discretization techniques must be much smaller than the rest of the errors.

Nevertheless, we have demonstrated that such model differences are not so small as to be considered meteorologically insignificant, especially after day 3 of the forecasts. The expectation that T63 should perform better than T40 has been shown to be reasonably fulfilled and evidence has been brought up to strengthen the implicit assumption that N48 would show an average performance in between T63 and T40.

5. OBJECTIVE COMPARISONS (Northern Hemisphere)

5.1 Introduction

In order to evaluate the quality of the forecasts from an objective point of view we chose the scores commonly used in ECMWF as mentioned in Section 3.4: the standard deviation of the errors and the anomaly correlation coefficients. In TR13 an attempt was made at defining the concept of range or period of predictability which is related to the limit of skill of a given forecast with respect to any one of these scores. Accordingly a forecast was considered to have some skill as long as the corresponding standard deviation is lower than a climatological forecast (NORM). One could of course argue that this might not be the most restrictive definition since there are other

"no skill forecasts" which could be taken as references. Alternatively one can consider that the limit of skill is reached when the anomaly correlation coefficients drop under 60%.

Here we would like to give a more quantitative definition of predictability (with regard to anomaly correlations) and not only to the range of predictability. For more details see Girard and Jarraud (1980). We define predictability, as a function of the anomaly correlations coefficient ($P = f(A_c)$) to be the time at which a given value of the anomaly correlation between a forecast and an analysis is reached for the first time. As a consequence $P = f(100\%)$ should be 0, and $P = f(A_c)$ is a decreasing monotonous function of A_c. Thus it is also possible to calculate correctly and unambiguously the mean predictability as the ensemble average of individual predictabilities.

i.e. $$P_M(A_c) = \frac{1}{N} \sum_{i=1}^{N} P_i(A_c)$$ for a ensemble of N cases.

In TR13 a mean range of predictability was estimated from a fictitious forecast having the same objective scores as the mean of the individual scores in association with a synoptic assessment. This estimation from a fictitious run, as defined above, can only give an approximation of the range of usefulness of a model, but it should in no way be used to evaluate differences between models. Another advantage of our definition is that it is possible to have continuous curves of (mean) predictability without having to privilege a particular level of quality. If one is interested by high quality results (e.g. corresponding to anomaly correlations larger than 80 or 75%) one finds how longer one model can provide such forecasts compared to another model. Thus a precise definition of the range of predictability becomes unnecessary. When comparing forecasts from two models, differences in the mean predictability will be a most sensitive tool.

Of course it would have been possible and perhaps desirable to design a similar tool from the standard deviation. However, our purpose was less to accumulate as many scores as possible than to select sensitive ones for our particular purpose.

All the scores presented here have been computed over a large part of the northern hemisphere, excluding however the tropical regions in order to avoid the apparent smoothing produced by the lack of sensitivity of our scores in this area. The band studied runs from $20^{\circ}N$ to $82.5^{\circ}N$ and unless otherwise stated all scores shown will be averaged over this band.

This Chapter will be further divided into four sections:

- We first compare the objective performances of T63 and N48.
- We then compare T63 and T40 in what is basically a resolution comparison.
- In a third section we put together the main results of the 2 previous sections and present an intercomparison of the performances of the three models.
- Finally we analyse objectively the differences between the models by showing the standard deviations of model differences as well as model intercorrelations.

5.2 Comparative performance of T63 and N48

Fig. 5.1 displays the time sequence (from February 3rd to 22nd) of the anomaly correlation coefficients of the height field averaged between 1000 and 200 mb on days 3,5,7 for the 7 cases studied. The most striking feature of these curves is without doubt the closeness of the model scores for a given case relatively to their variability from case to case. One can already notice however a nearly systematic superiority of T63 over N48. It is also clear how good the 7 day forecasts from February 15th are in relation to the other cases and how poor the ones from February 18th. Furthermore recalling our choice of cases for the synoptic evaluation in Chapter 4, one notes that they very nearly correspond to the 2 best (February 6th and 15th) and to the worst (February 18th) forecasts of the ensemble.

Figs. 5.2 to 5.7 are scatter diagrams showing for various forecast lengths the performance of both T63 and N48 with respect to standard deviation as well as anomaly correlations at representative vertical levels.

Each dot corresponds to one of the 7 cases. However the dots have been replaced by special signs for the 3 cases described in the synoptic part

i.e. + (6/2/76 case), × (15/2/76 case) and * (18/2/76 case).

When a point is below the diagonal it means that N48 did better than T63 and vice versa. One can have a quick overview of the performance of the 2 models just by looking at the position of the cloud of points. When there are less than 7 points it means that the other points were out of the range of the diagram. The dashed line represents a range-of-predictability estimate: deviation from the climatological values for standard deviations and constant 60% line for the anomaly correlations. When a point is outside the inner square, one at least of the models is no longer considered to have skill.

Fig. 5.2 presents standard deviation of height at 500 mb. On day 2 the two models are extremely close, but from day 3 to 6 the mean position of the points moves above the diagonal, reflecting the superiority of T63. These diagrams show that the models behave similarly, not only as a mean, but also on individual cases, since no point up to day 4 is very far away from the diagonal. However each dot represents a mean over a large part of the northern hemisphere as stated earlier and therefore 2 models with significant local differences can give similar standard deviations.

As seen from the following figures, the anomaly correlation coefficients prove to be more sensitive to individual differences.

Fig. 5.3 and 5.4 show anomaly correlations of height at 1000 and 500 mb. The advantage of T63 over N48 is increasing from day 2 until day 6. Afterwards both models may be considered almost useless. On day 7 there is only one case left in the inner square (forecasts from February 15th).

The better performance of T63 over N48 is almost systematic: in effect there is only one case with better scores for N48 (February 18th forecast).

On day 6 at 500 mb (Fig. 5.4) there are only 3 cases in the inner square, all of them in favour of T63. Such behaviour, if verified on a larger number of cases, would suggest a tendency for T63 to be better not only on average, but also and perhaps more importantly in cases of higher predictability.

When looking separately upon these results for the long-wave (1-3) and medium-wave (4-9) components of the height field at 500 mb (Fig. 5.5 and 5.6 respectively) the improvement of T63 over N48 is seen to come mainly from the long waves where most of the energy is concentrated.

Finally, Fig. 5.7 presents anomaly correlations for the temperature field at 850 mb: up to day 3 there is a very slight advantage for N48 but on days 4 to 6 the results agree quite well with the ones obtained for the geopotential.

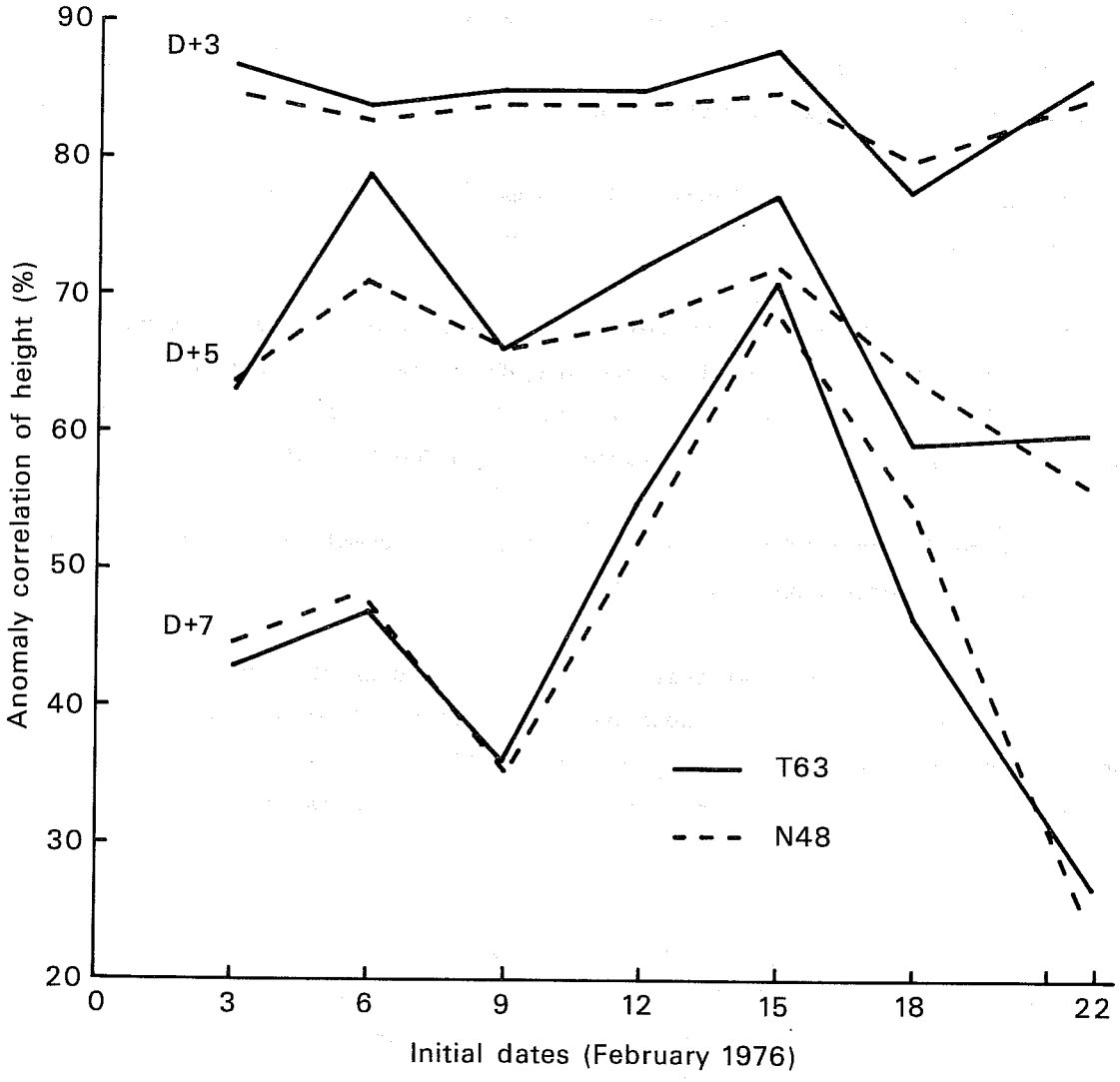

Fig. 5.1 Anomaly correlations (%) of height for forecast days 3,5 and 7 made from the seven February 1976 cases, averaged from 20°N to 82.5°N and between 1000 and 200 mb, comparing T63 and N48.

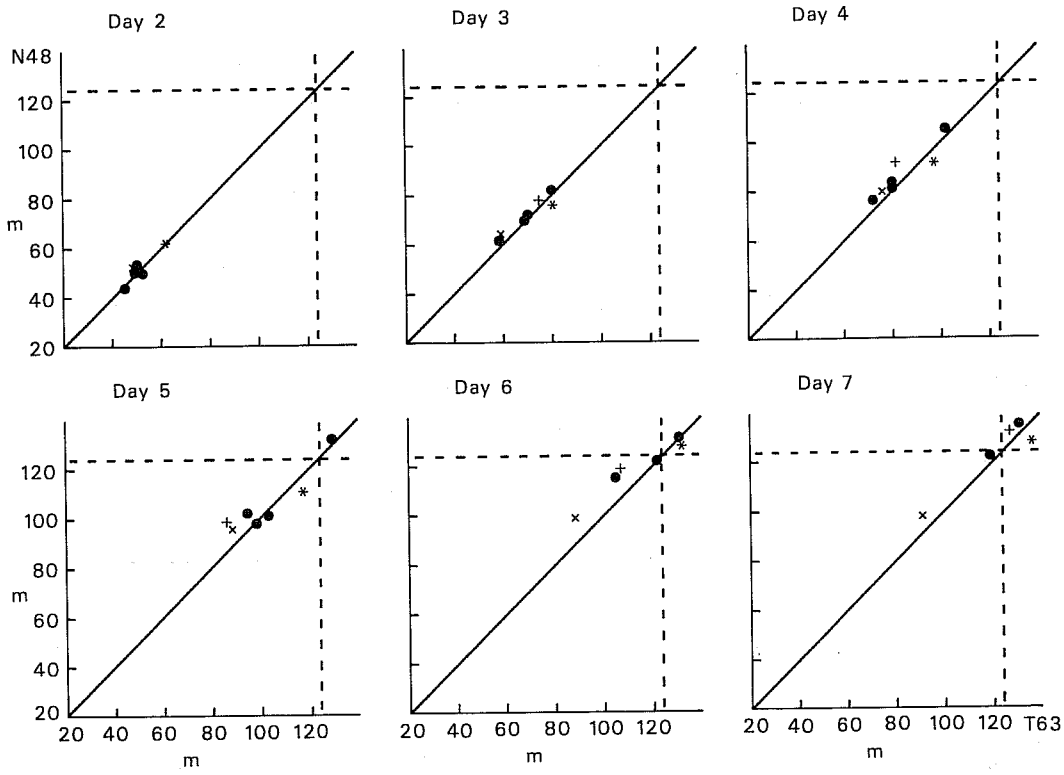

Fig. 5.2 Scatter diagram showing the standard deviation (m) of the error of height for forecast days 2, 3, 4, 5, 6 and 7 respectively averaged from 20°N to 82.5°N at 500 mb and comparing N48 to T63.

\+ 6/2/76 case × 15/2/76 case * 18/2/76 case

● all other cases

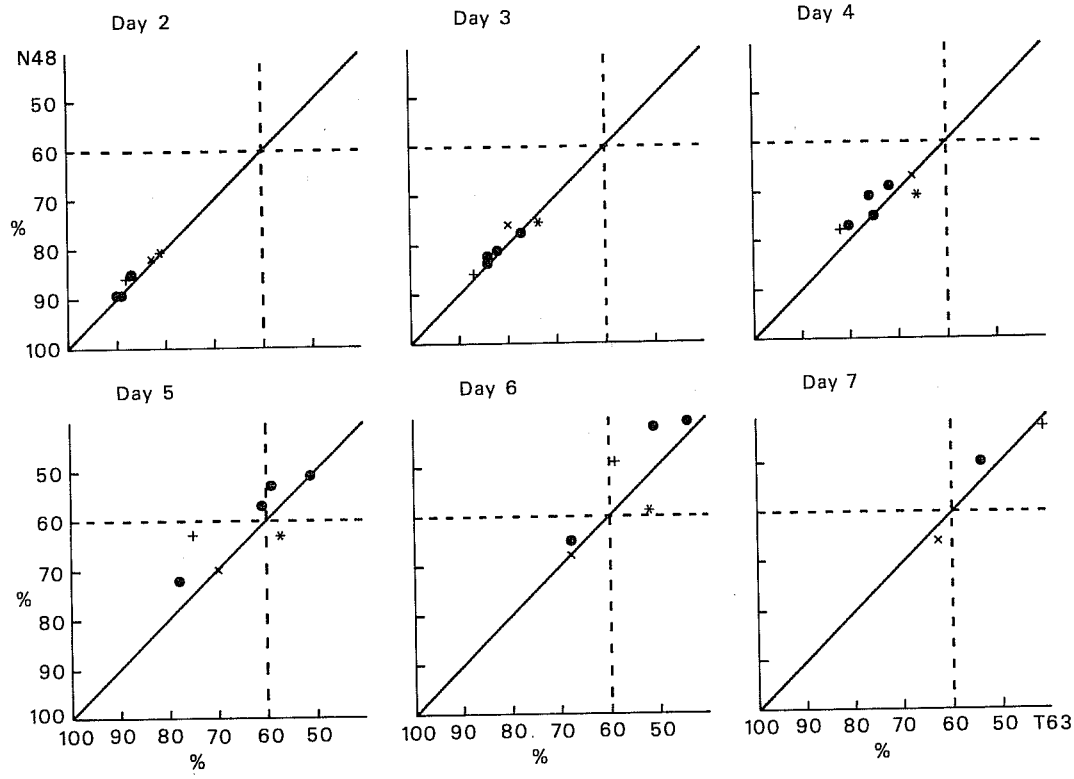

Fig. 5.3 Scatter diagram showing anomaly correlations (%) of height for forecast days 2, 3, 4, 5, 6 and 7 respectively averaged from 20°N to 82.5°N at 1000 mb and comparing N48 to T63.

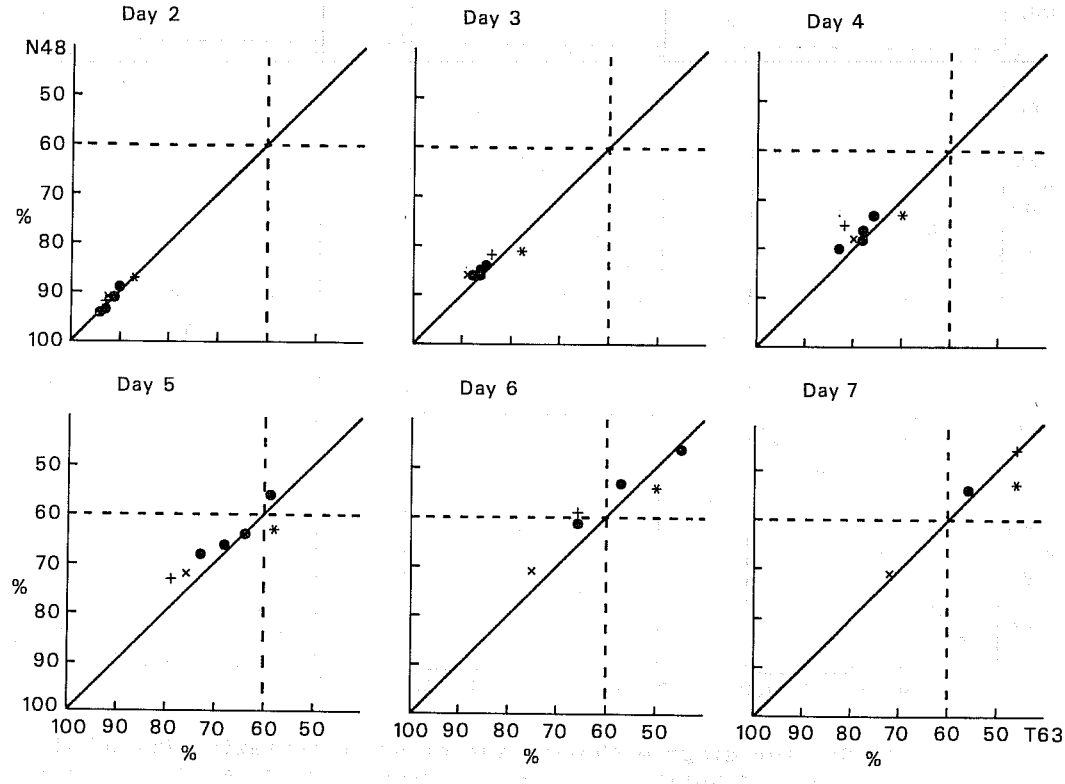

Fig. 5.4 Same as Fig. 5.3, height anomaly correlations at 500 mb comparing N48 to T63.

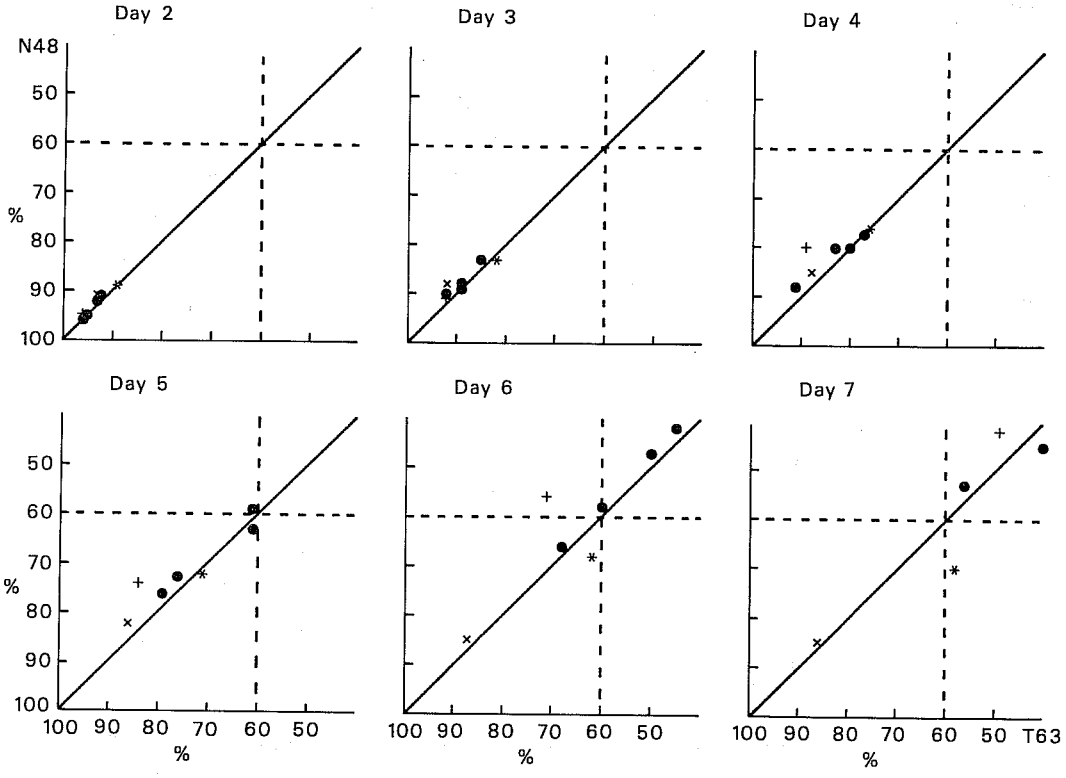

Fig. 5.5 Same as Fig. 5.3, height anomaly correlations at 500 mb comparing N48 to T63 for wavenumbers 1 to 3.

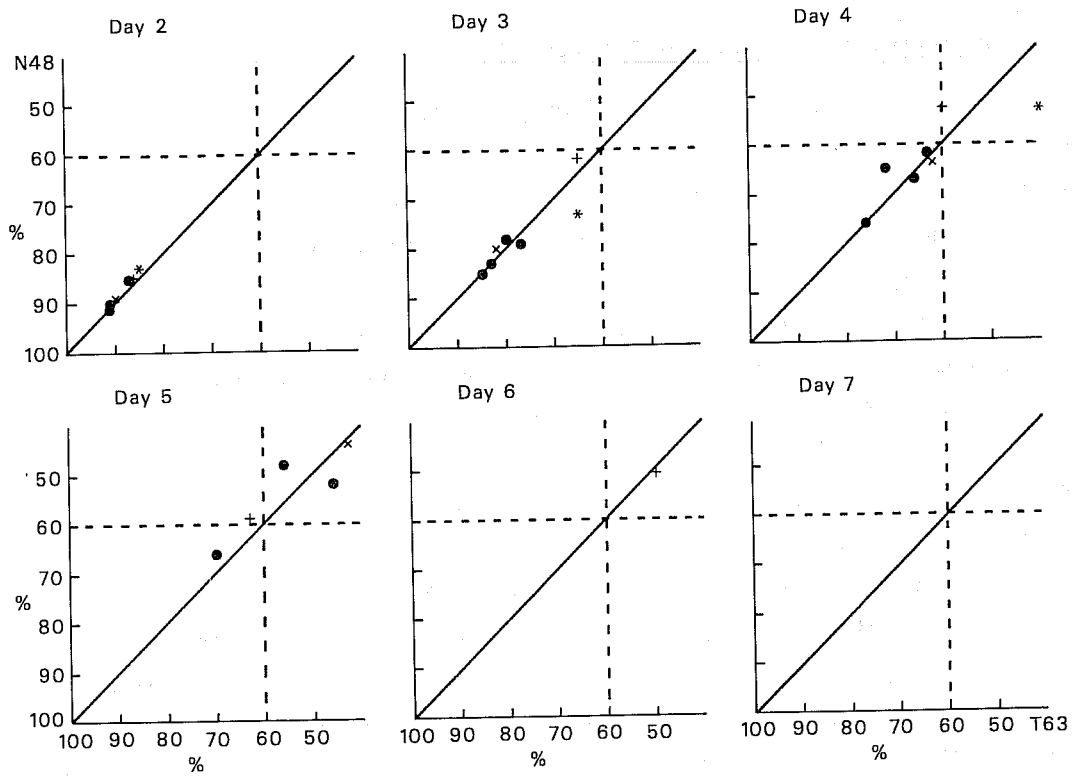

Fig. 5.6 Same as Fig. 5.3, height anomaly correlations at 500 mb comparing N48 to T63 for planetary wavenumbers 4 to 9.

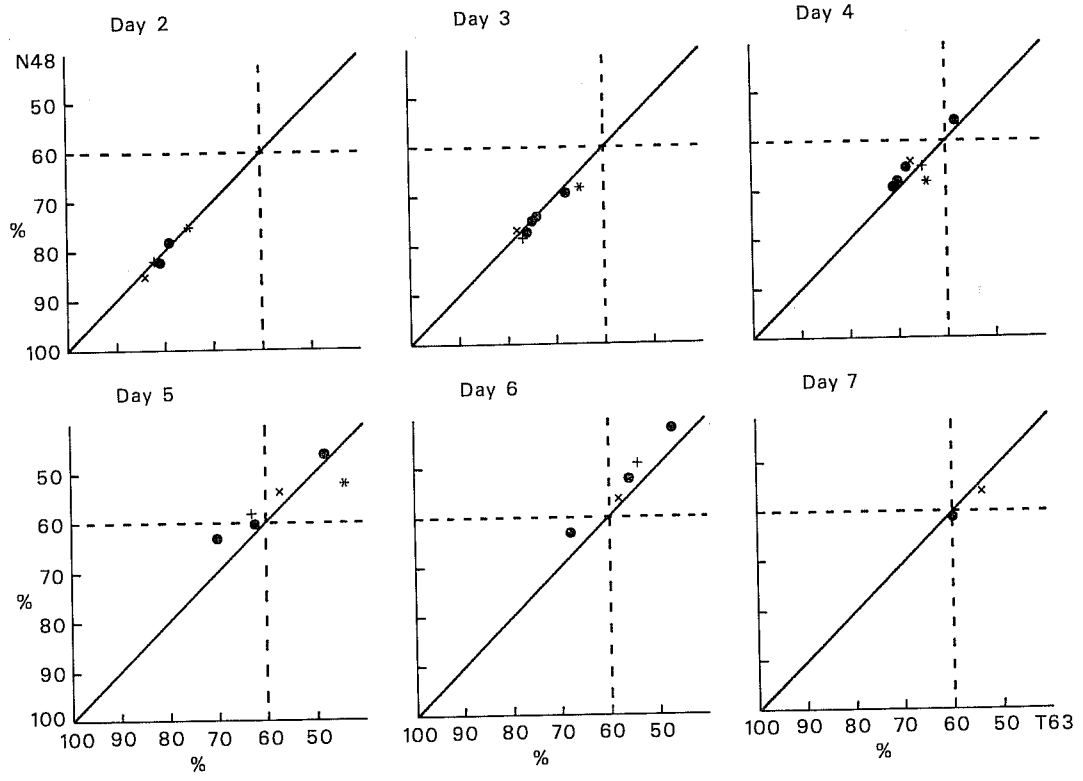

Fig. 5.7 Same as Fig. 5.3, temperature anomaly correlations at 850 mb comparing N48 to T63.

5.3 Comparative performance of T63 and T40

Fig. 5.8 in a way similar to Fig. 5.1 displays the anomaly correlation coefficients of height averaged between 1000 and 200 mb on days 3,5,7 for the 7 integrations. On day 3, the superiority of T63 over T40 is in fact less systematic than it was over N48, but it is quite clear on day 5. It is very interesting to note that on one case (forecast from February 15th) the 7-day forecast by T63 is better than the 5-day forecast by T40. This shows that a higher horizontal resolution model is sometimes retaining skill for a much longer period. Note however that the forecast made by T40 from February 18th is better on day 5 than the one by T63, and is in fact equal with respect to this score to the N48 forecast.

Figs. 5.9 and 5.10 present scatter diagrams of the anomaly correlation coefficients of height at 1000 and 500 mb. The improvement of T63 over T40, noticeable on day 3, keeps increasing up to day 5. Afterwards forecast skill decreases very quickly for both models. At 500 mb one can see that the only case where T40 does better than T63 is February 18th where N48 was also doing better than T63. In the other cases it can be noted that the improvement of T63 over T40 is often substantial. At this stage we can speak of quasi systematic improvement. We shall show later what this means in terms of predictability. The last point to be mentioned is the larger amplitude of the differences at 1000 mb than at 500 mb noticeable on days 4 and 5.

Figs. 5.11 and 5.12 show that the improvement, although larger in the long-wave (1-3) is also visible in the medium-wave (4-9) components of the height field. On day 6 it appears to be considerable in 2 cases in the long waves (Fig. 5.11).

For the temperature at 850 mb (Fig. 5.13) the improvement is less pronounced than for the height field. This is similar to what was found when comparing T63 and N48.

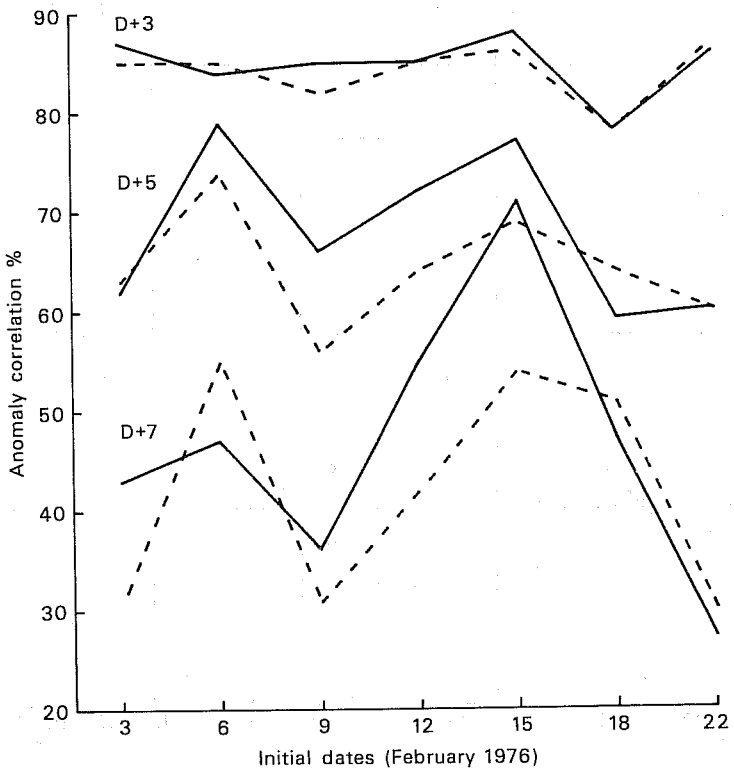

Fig. 5.8 Same as Fig. 5.1, comparing T63 to T40.

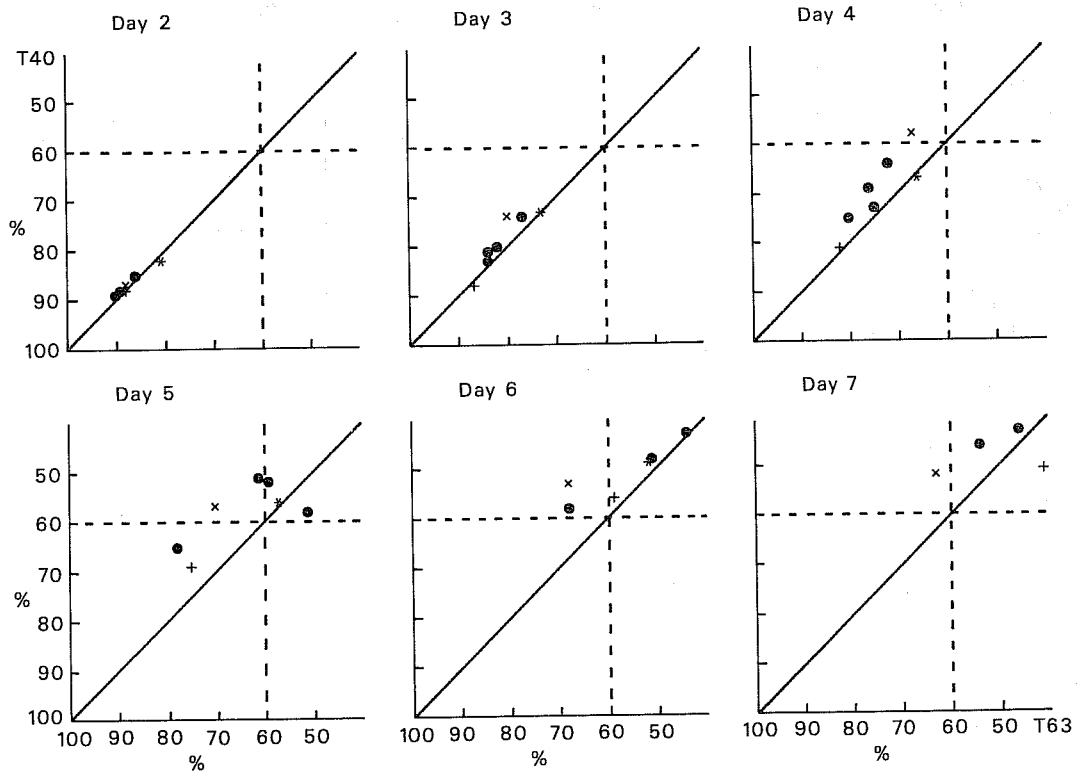

Fig. 5.9 Same as Fig. 5.3, height anomaly correlations at 1000 mb comparing T40 to T63.

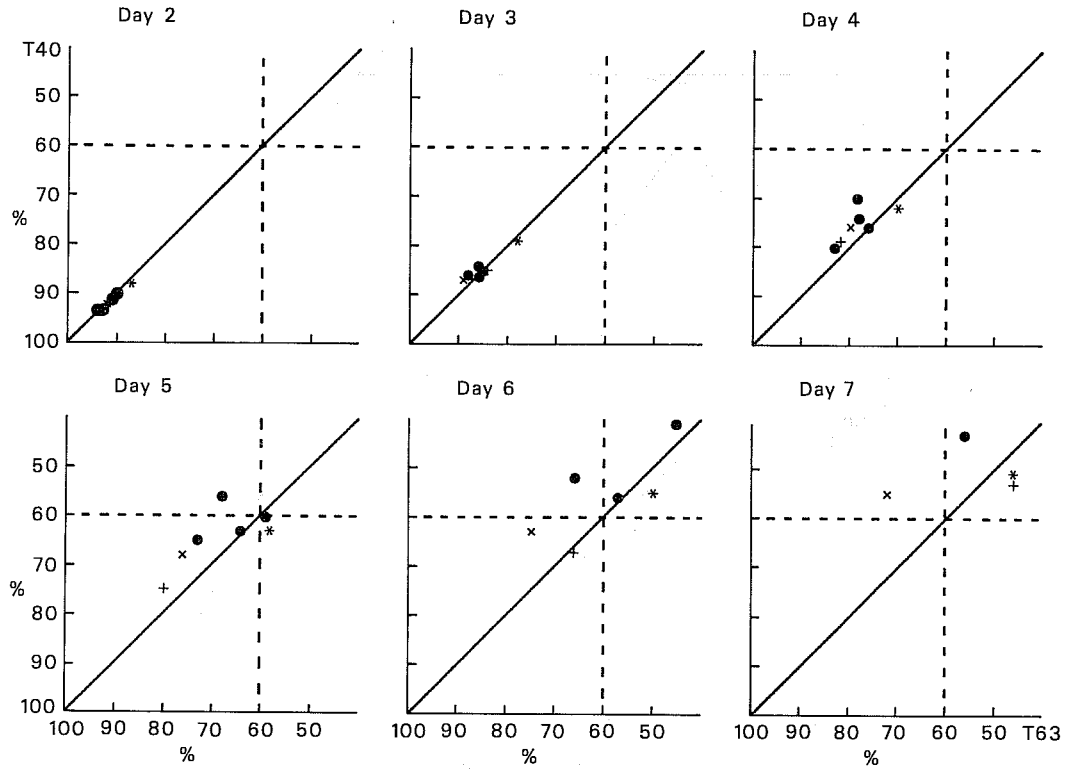

Fig. 5.10 Same as Fig. 5.3, height anomaly correlations at 500 mb comparing T40 to T63.

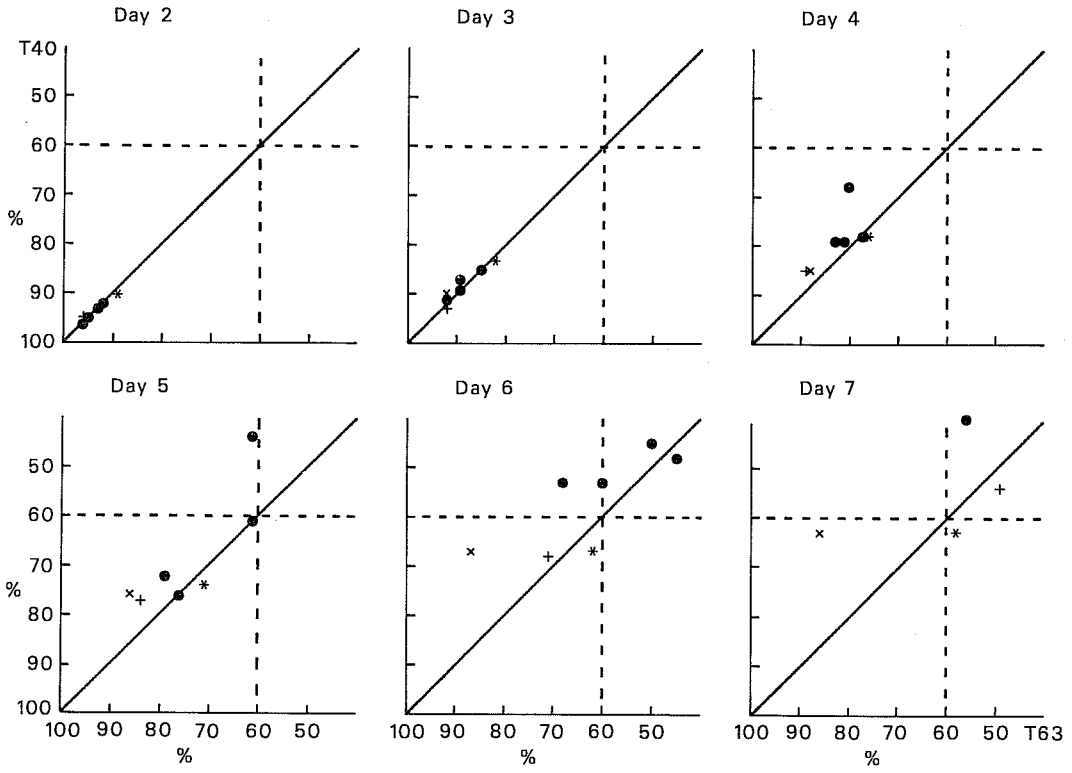

Fig. 5.11 Same as Fig. 5.3, height anomaly correlations at 500 mb comparing T40 to T63, for planetary wavenumbers 1 to 3.

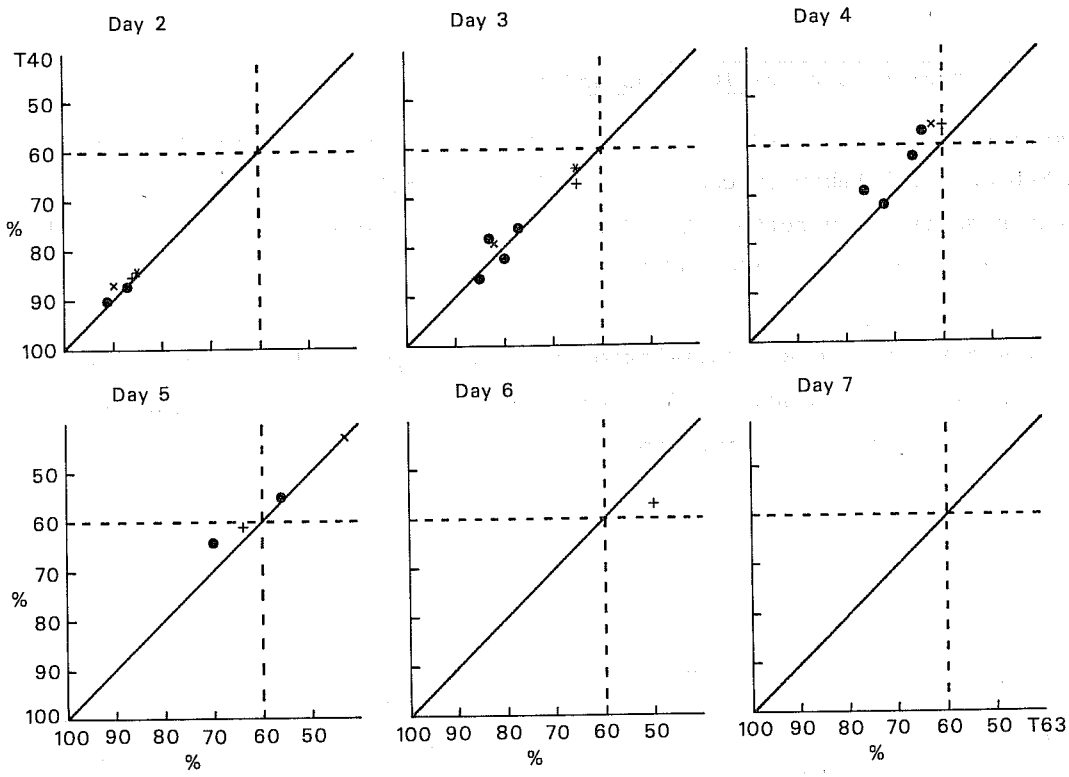

Fig. 5.12 Same as Fig. 5.3, height anomaly correlations at 500 mb comparing T40 to T63, for planetary wavenumbers 4 to 9.

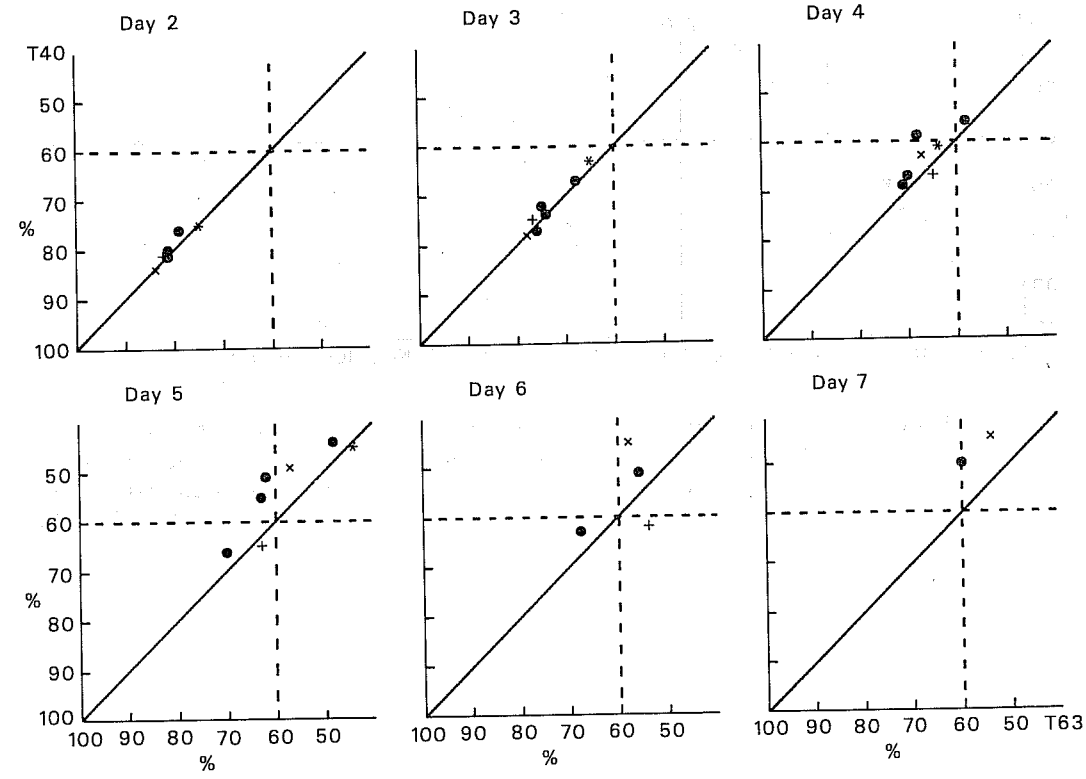

Fig. 5.13 Same as Fig. 5.3, temperature anomaly correlation at 850 mb comparing T40 to T63.

5.4 Intercomparisons of T63, T40 and N48

In Section 5.2 we presented scores suggesting that T63 was slightly better than N48 on the 7 February cases selected. In Section 5.3 we showed that T63 was significantly better than T40 but it is now important to place N48 with respect to both T40 and T63.

Fig. 5.14 presents anomaly correlation for the height field at 1000 mb on days 3 and 4. The left scatter diagrams compare T63 and N48, the middle ones N48 and T40 and the right ones T63 and T40.

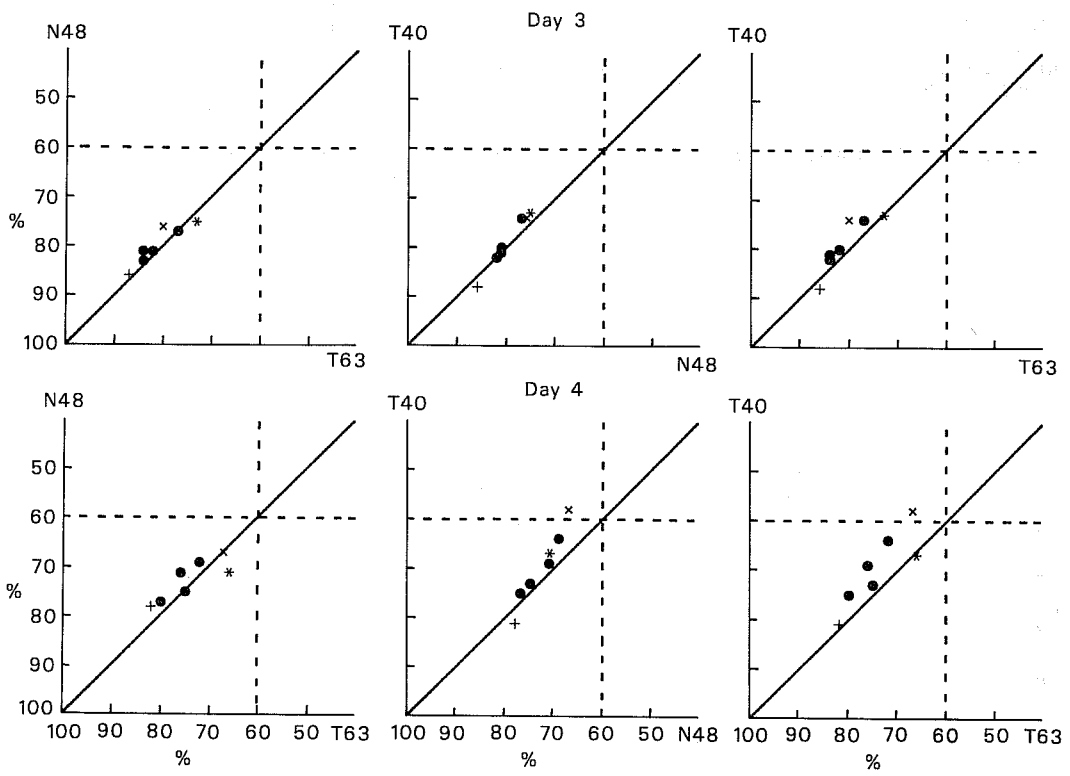

Fig. 5.14 Scatter diagram showing anomaly correlations (%) of height for forecast days 3 and 4, top and bottom, respectively averaged from 20^{o}N to 82.5^{o}N at 1000 mb and comparing N48 to T63 (left), T40 to N48 (middle) and T40 to T63 (right).

We chose days 3 and 4 since some points are already outside the predictability range on day 5 and many more on day 6. On the other hand the models are still very close on day 2.

Both on days 3 and 4 T63 appears slightly better than N48 which is in turn slightly better than T40. But T63 is significantly better than T40. The conclusion, obvious of course, is that the combination of two "small" improvements has lead to a "large" improvement. In terms of performance this means that N48 corresponds on average to a spectral model with a resolution intermediate between T40 and T63. We shall come back to this point later in Chapter 8.

Fig. 5.15 displays, from top to bottom, the ensemble averaged anomaly correlations at 500, 1000 and mean for 1000-200 mb (T63: dashed; N48: full; T40: dotted line) and their mean 1000-200 mb difference (T63-N48: full; T63-T40: dashed line) for the Northern Hemisphere from day 0 to 10. These differences when positive imply an improvement of T63 over the other models.

When comparing T63 and N48 the maximum difference occurs at about day 5 or 6 corresponding also to the time when forecasts are loosing skill in the mean. The maximum improvement is of the order of 2%. This is apparently small but it is an improvement averaged vertically throughout the atmosphere. The real meteorological significance of it has been discussed in Chapter 4. We shall also show in the following what it means in terms of increased predictability.

When comparing T63 and T40 the maximum is more pronounced and occurs later (on day 7). It is worth noting that up to and including day 3 T40 is superior to N48 but then deteriorates very quickly.

Fig. 5.16 presents the individual predictability curves for the height field at 1000 mb. For each case we compute the time needed to reach a constant level A of anomaly correlations. We then draw the curve $t = f(A)$ when A varies from 100% (perfect forecast) to 50% beyond which a forecast is no longer of any use. If one considers the anomaly correlation curve $A = g(t)$ it is possible to draw the curve $h(t)$ which is the upper envelope of all the curves $h_i(t)$ with $\frac{dh_i(t)}{dt} \leqslant 0$ and $h_i(t) \leqslant g(t)$. Then f is just h^{-1}. So if g is decreasing monotonously $h = g$. In practice h is very similar to g and thus f is almost a rotated g curve. We then average these curves and display the mean curve.

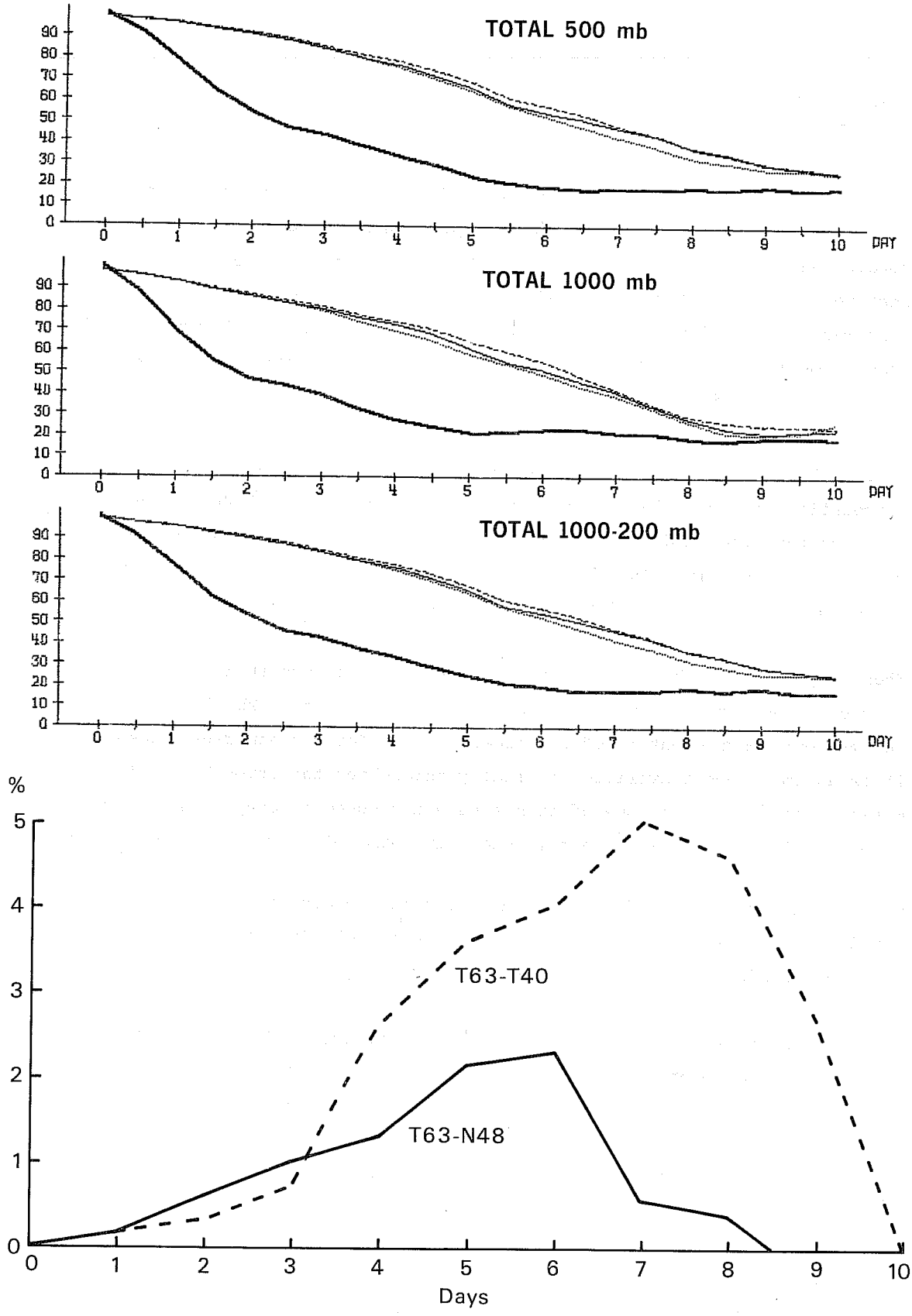

Fig. 5.15 Time evolution with respect to forecast length (day) of the ensemble mean anomaly correlations (%) of height forecasts averaged from 20°N to 82.5°N. From top to bottom: scores at 500 mb; 1000 mb; averaged between 1000 and 200 mb with —— N48 ---- T63 .... T40 and difference in scores for the averaged between 1000 and 200 mb.

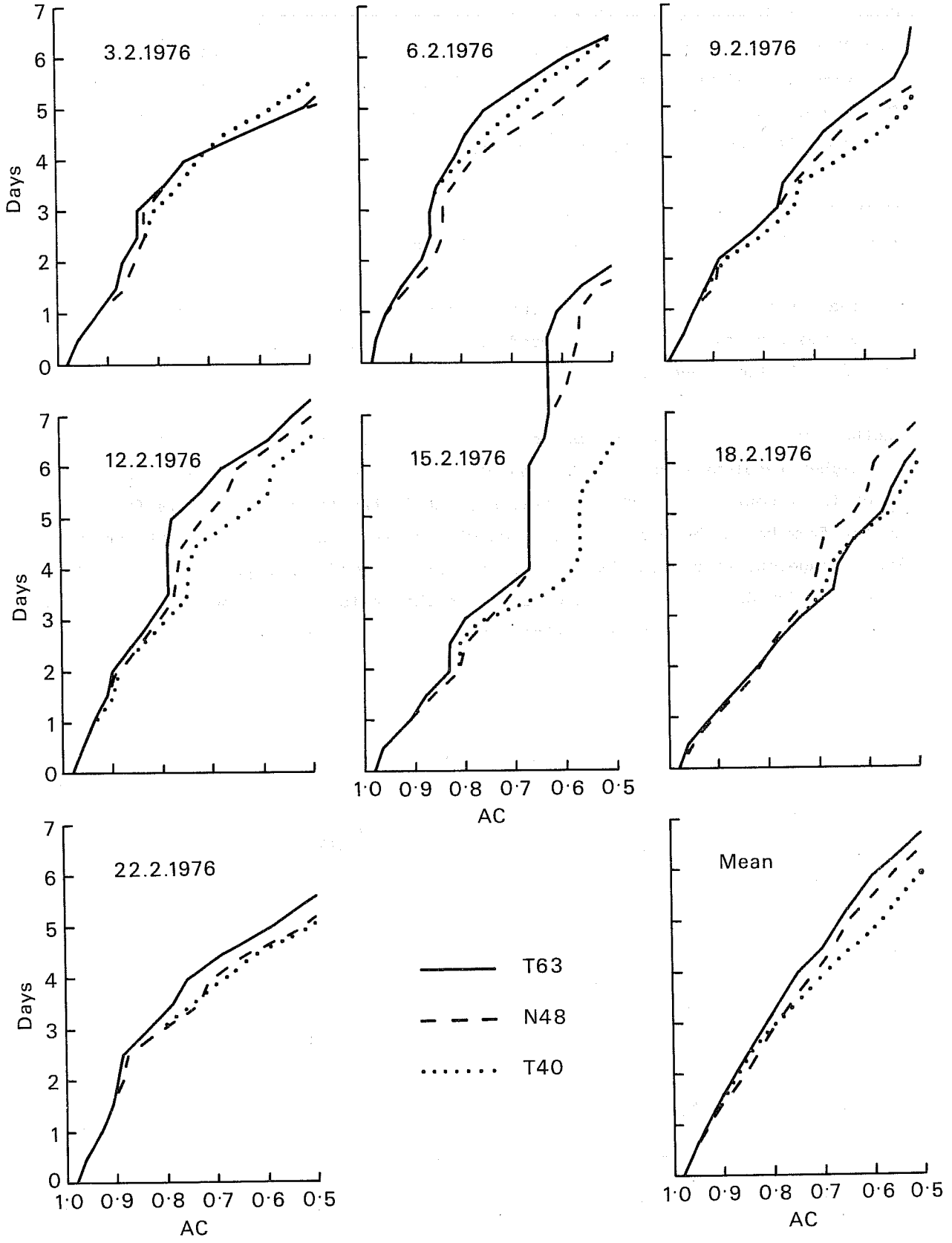

Fig. 5.16 Predictability (days) as a function of anomaly correlations of height averaged from 20°N to 82.5°N at 1000 mb for the seven individual cases and their ensemble mean.

From Fig. 5.16 one can see that in all cases but one T63 does better than N48. In four cases there is a substantial gain in predictability: forecasts from February 6th, 12th, 15th and 22nd. T40 did obviously worse than T63 in most of the cases and especially in 2 cases (forecasts from February 12th and 15th) where the difference is dramatic.

In most integrations N48 seems to give results intermediate between T63 and T40 although slightly closer to T63 than to T40.

The mean curves reflect these conclusions and show that near the surface T63 brings a mean improvement in predictability of 6 to 9 hours over N48 and 12 to 24 hours over T40.

Another important feature can be seen on Fig. 5.16. On the February 15th case the higher resolution models (T63 and N48) keep some skill for 8 to 10 days which is of course a remarkable forecast, but in the first 3 days this forecast is far from being the best of the 7 selected cases. Therefore it is at the very least dangerous to assume that a forecast will be good for days 4 to 7 if it has been good for days 1 to 3. One could argue that this is just one counter example, but as long as no more detailed study has been done it suggests caution.

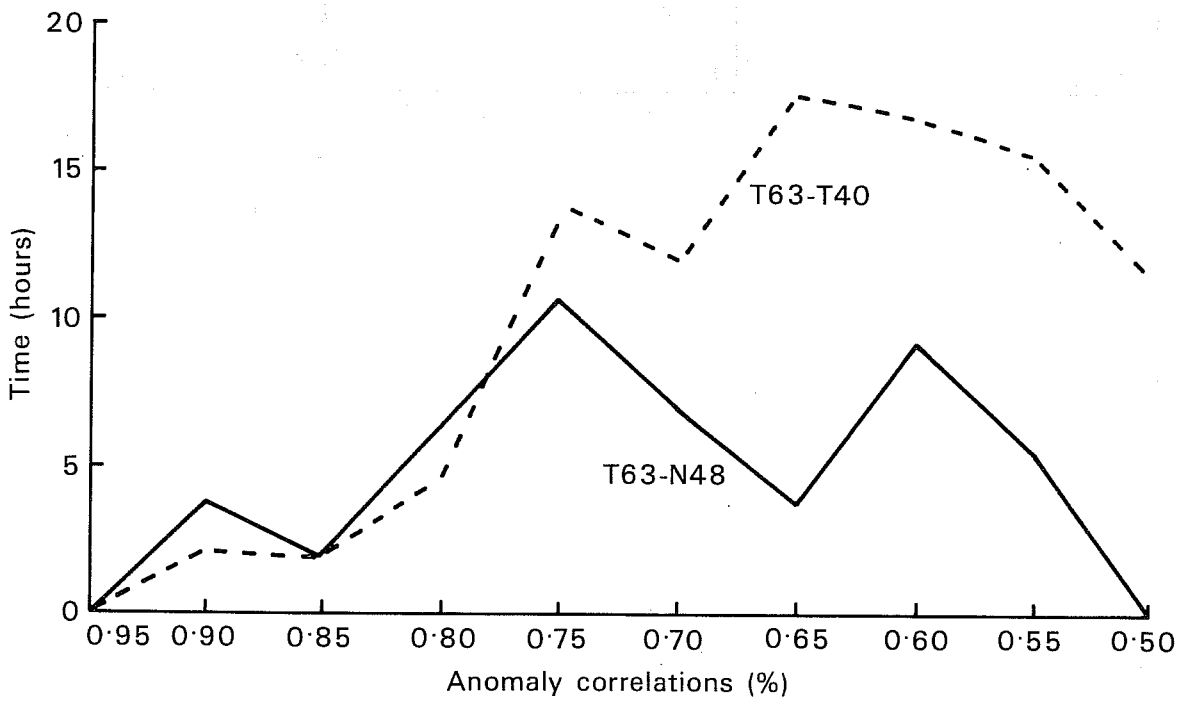

Fig. 5.17 Difference in the ensemble mean predictability (hours) as a function of anomaly correlations of height averaged from 20°N to 82.5°N and between 1000 and 200 mb.

Fig. 5.17 displays the predictability difference (hours) between T63 and N48 (full line) and between T63 and T40 (dashed line) averaged between 1000 and 200 mb. Note that it is smaller than at 1000 mb (Fig. 5.16) and again that T40 is slightly better than N48 at the beginning of the forecast. On average the 2% improvement in anomaly correlations of T63 over N48 seen in Fig. 5.14 can thus be translated in about 8 hours extended predictability, or the 5% improvement of T63 over T40 in about 14 hours increased predictability.

Fig. 5.18 to 5.20 show comparative pressure-time cross-sections of the mean anomaly correlations for the 3 models taken 2 at the time for the height field. We must put the reader on his guard against any temptation to interpret these mean curves in terms of time improvement: for example when the 70% line of anomaly correlation crosses the time axis on day $4\frac{1}{2}$ for T63 and on day 4 for T40 at 1000 mb, it does not mean that for the 70% line T63 brings an improvement of 12 h over T40 in terms of predictability. If the reader requires such information he has to refer to the predictability curves (Fig. 5.16). It means only that on day $4\frac{1}{2}$ T63 has mean anomaly correlations of 70% and T40 of less than 70%. For the total field (Fig. 5.18) one can see that the improvement of T63 over T40 and to a smaller extent over N48 is larger near the surface than near the top of the model. On the other hand, the improvement of N48 over T40 becomes clear only after $3\frac{1}{2}$ days. Up to day 2 T40 is even slightly better at all levels. It is also worth noting again that T40 is almost as good as T63 in the first 2 days.

When looking at the long wave (1-3) components (Fig. 5.19) one can see the same features amplified, but when looking at the medium wave (4-9) components (Fig. 5.20) T63 and N48 appear very close to each other and both slightly better than T40.

A question that could be asked is whether or not the spectral and grid point models behave differently in the tropics or (and) near the pole. Fig.5.21 presents a latitude-time cross-diagram of anomaly correlations for the height field at 1000 mb and one might conclude from it that T63 is superior to T40 mainly in the high middle latitudes (40 to 80°N) but it has to be pointed out that there is a very large variability from case to case and no systematic difference could be found when looking upon the individual cases. This is also valid when comparing T63 and N48.

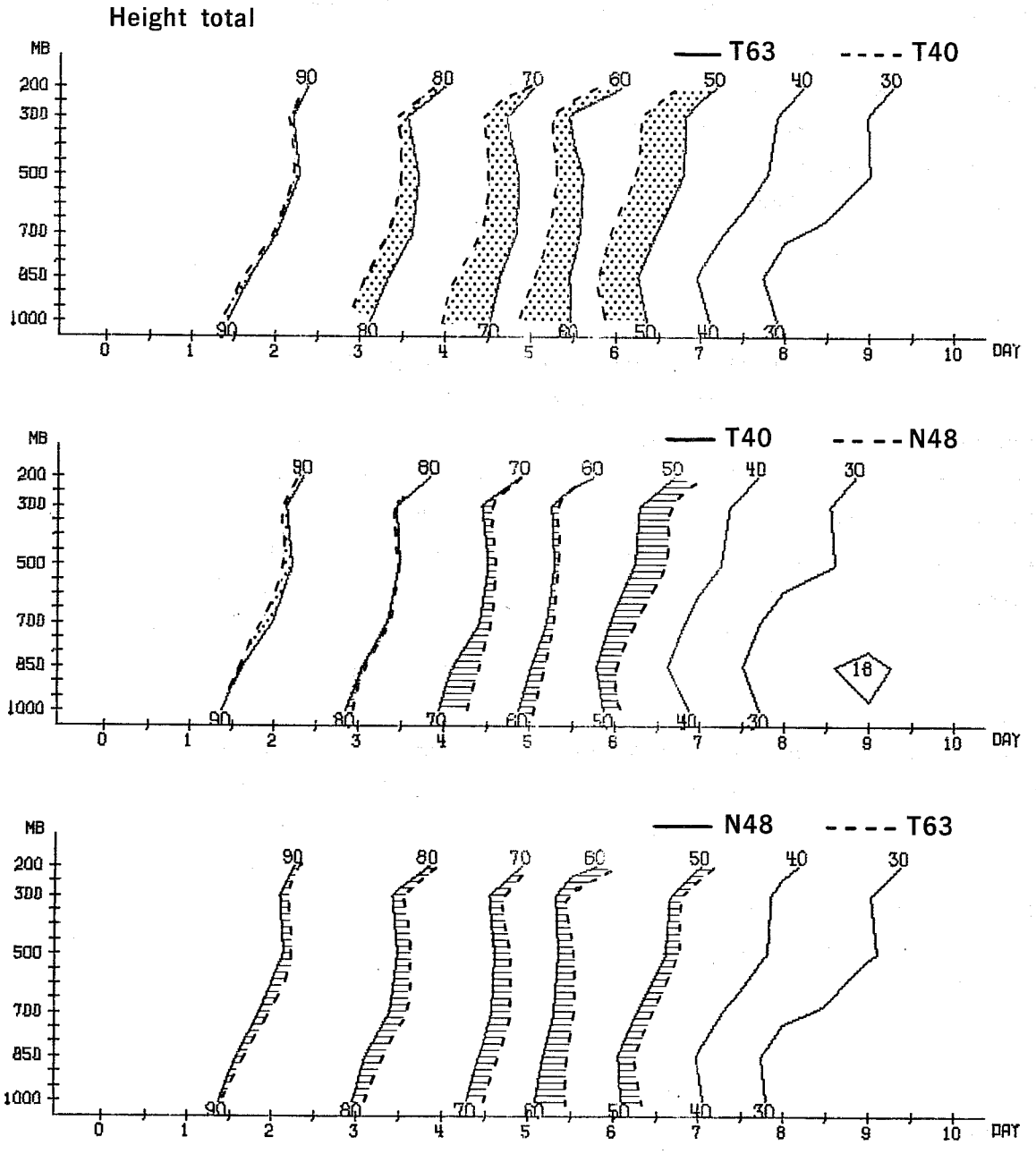

Fig. 5.18 Time-pressure cross-sections of the ensemble mean anomaly correlations of height averaged from 20°N to 82.5°N for T63, T40 and N48. For ease of comparison, the curves of each model have been represented twice. The hatched (dotted) area corresponds to an improvement of the model represented by the dashed (full) line over the model represented by the full (dashed) line.

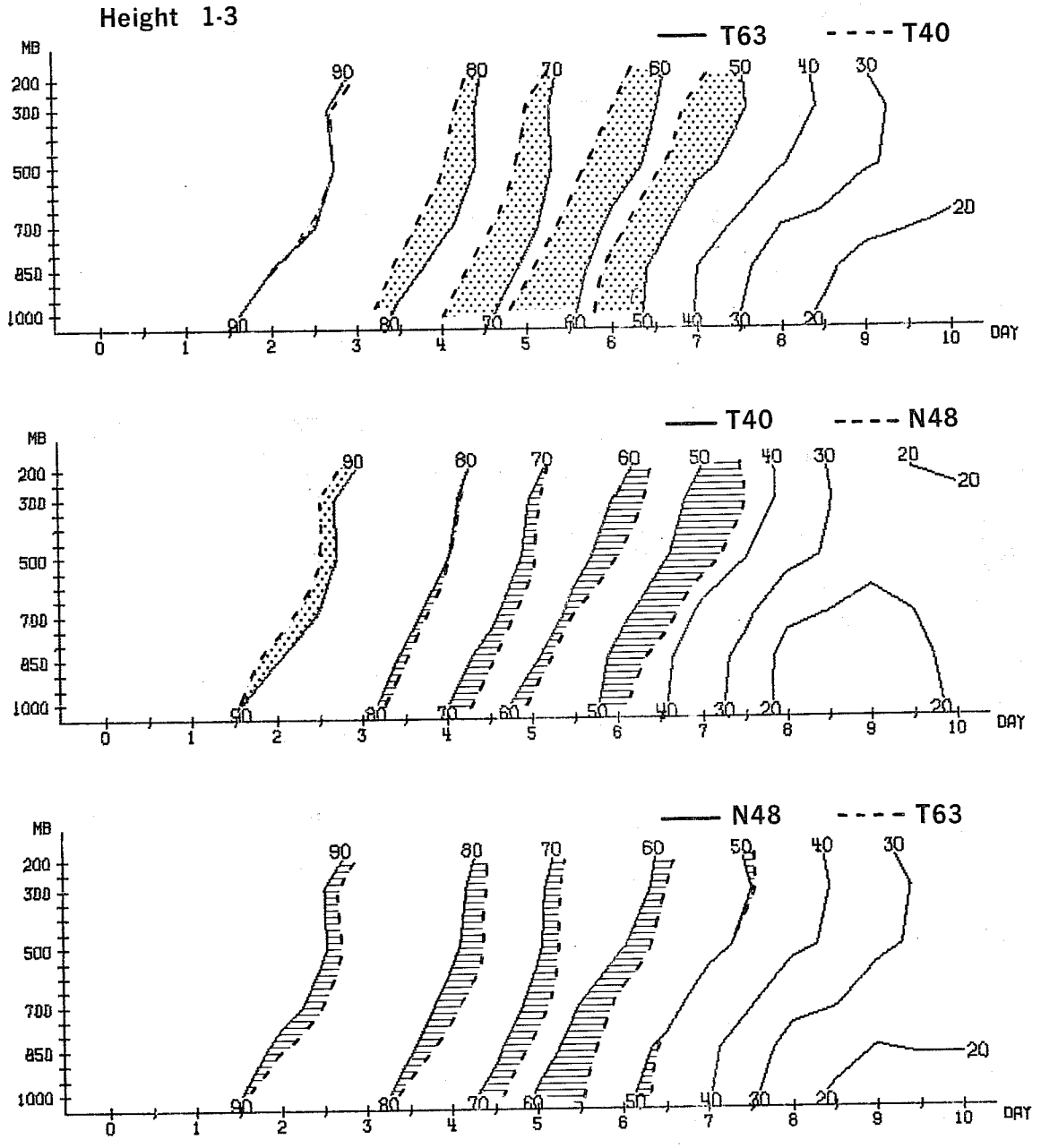

Fig. 5.19 Same as Fig. 5.18, for the planetary wavenumbers 1 to 3.

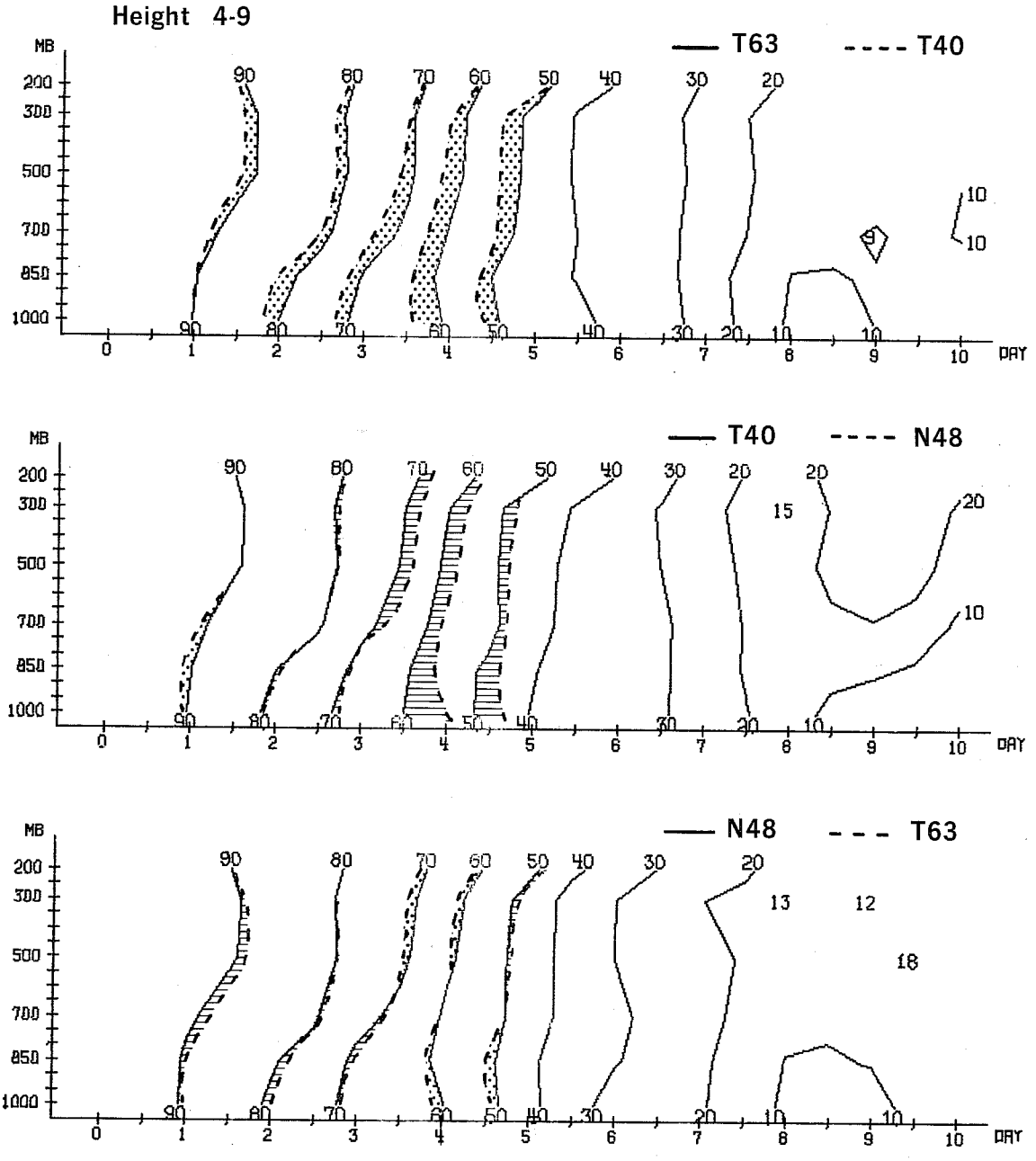

Fig. 5.20 Same as Fig. 5.18, for the planetary wavenumbers 4 to 9.

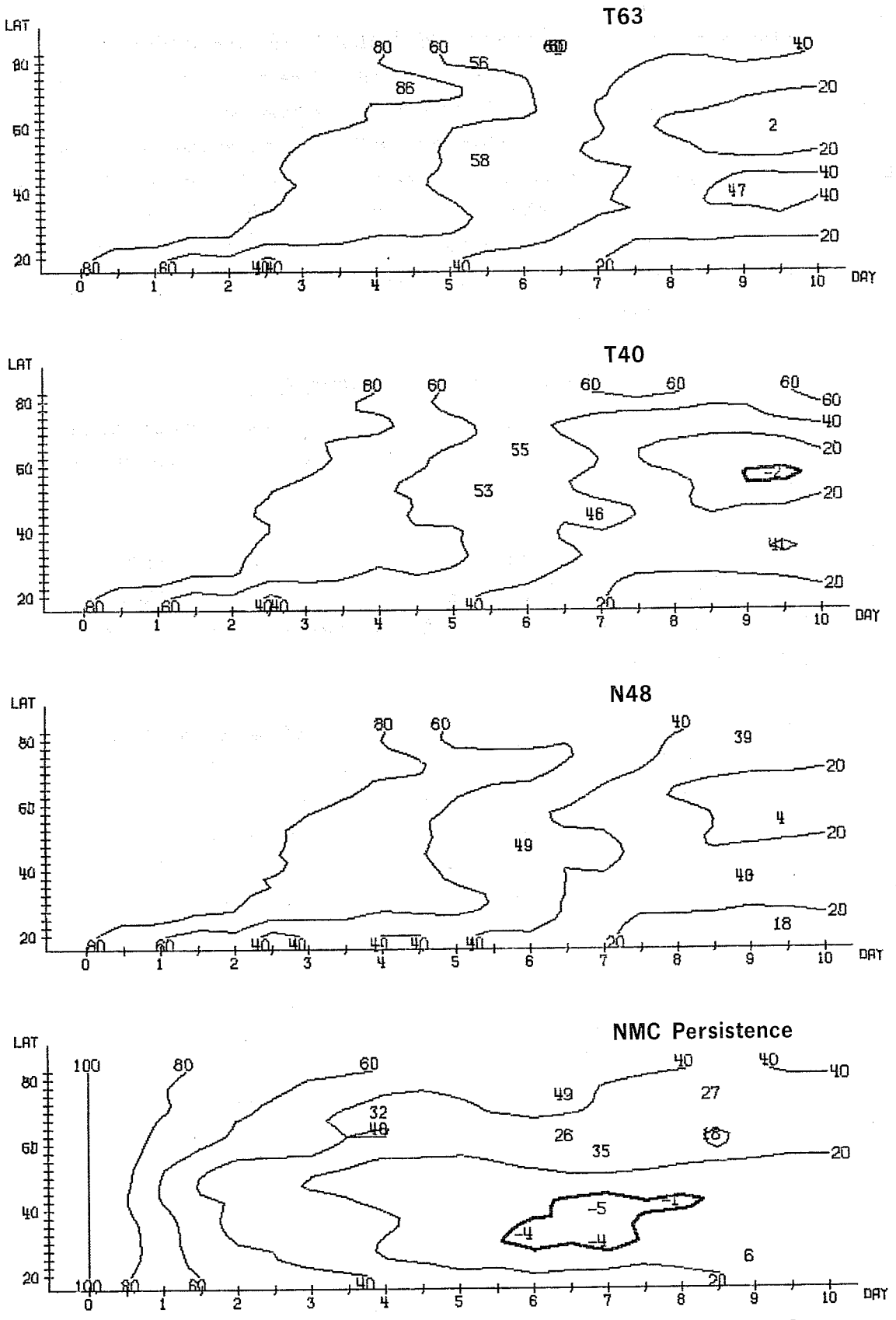

Fig. 5.21 Time-latitude cross-sections of the ensemble mean anomaly correlations of height at 1000 mb.

At this point we may draw the following conclusions: the improvement of T63 over T40 is significant only after day 2½ and is seen in both the long- and medium-wave components. On the other hand the improvement of T63 over N48 is already significant at the beginning where both T40 and T63 do better than N48, but afterwards stays smaller and mainly concentrated in the long waves. This suggests that the improvement of T63 over N48 is not perhaps entirely due to a finer equivalent horizontal resolution. One of the most probable reasons for the early advantage of the spectral models is the absence of linear phase speed errors.

5.5 Mean rms differences and correlations between models

In the previous paragraph we showed that despite the closeness in performance of the 3 models differences could be found. The purpose of this section is to look at the differences in themselves.

We first compare T63 and T40 to N48. Fig. 5.22 presents the standard deviation of the differences in the height field averaged between 1000 and 200 mb over the 7 cases evaluated between T63 and N48 on one hand and T40 and N48 on the other hand.

The differences between T63 or T40 and N48 need a long time to reach the norm, even in the short waves (10-20). In the long waves (1-3) the models are closer to each other than each of them is to climate even at the end of the 10-day period. The other point is that N48 is closer to T63 than it is to T40 in all groups of wavenumbers. The time evolution of the difference is very similar to the rate given in TR13 when comparing N48 with two different physical packages.

Fig. 5.23 shows the intercorrelations of the height anomalies between T63 or T40 and N48 similarly averaged and the conclusions drawn from Fig. 5.22 are confirmed. Fig. 5.24 shows the same between N48 or T40 and T63. Of course, the curves labelled N48 vs T63 and T63 vs N48 are identical. From these two figures it is obvious that T63 is closer to N48 than to T40 which is not surprising after what we have shown in the previous paragraphs. The interesting point is that a spectral model with high resolution can be closer to a grid point model with sufficient resolution than to another spectral model with coarse resolution pointing out to a convergence of the models with increasing horizontal resolution, independently of the discretization technique used.

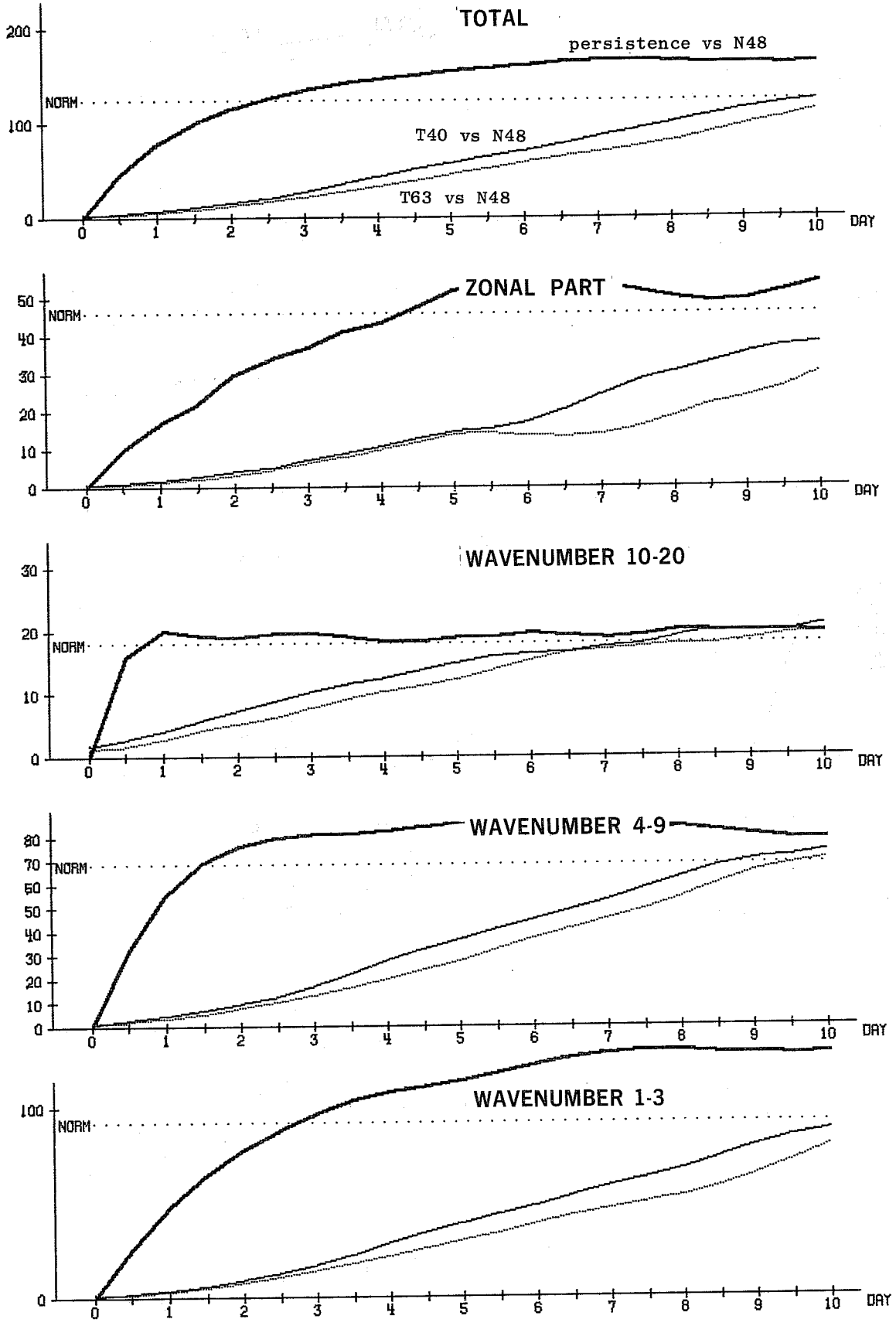

Fig. 5.22 Root mean square (rms) height differences (m) between N48 and either T40 or T63, averaged for various wavenumber bands from 20°N to 82.5°N and between 1000 and 200 mb. Ensemble mean of 7 February 1976 cases.

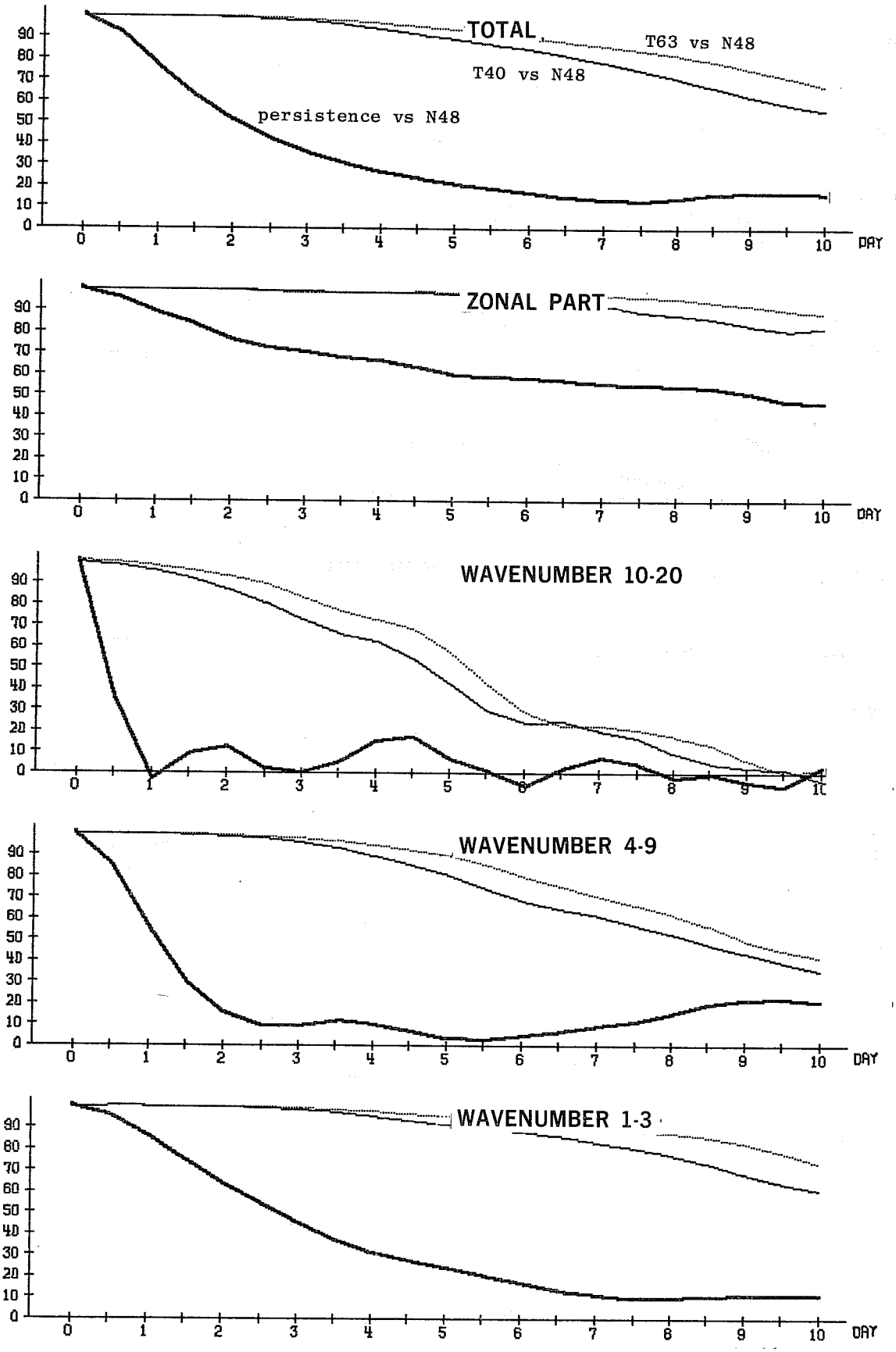

Fig. 5.23 Same as Fig. 5.22 for height intercorrelations (%) between N48 and either T40 or T63.

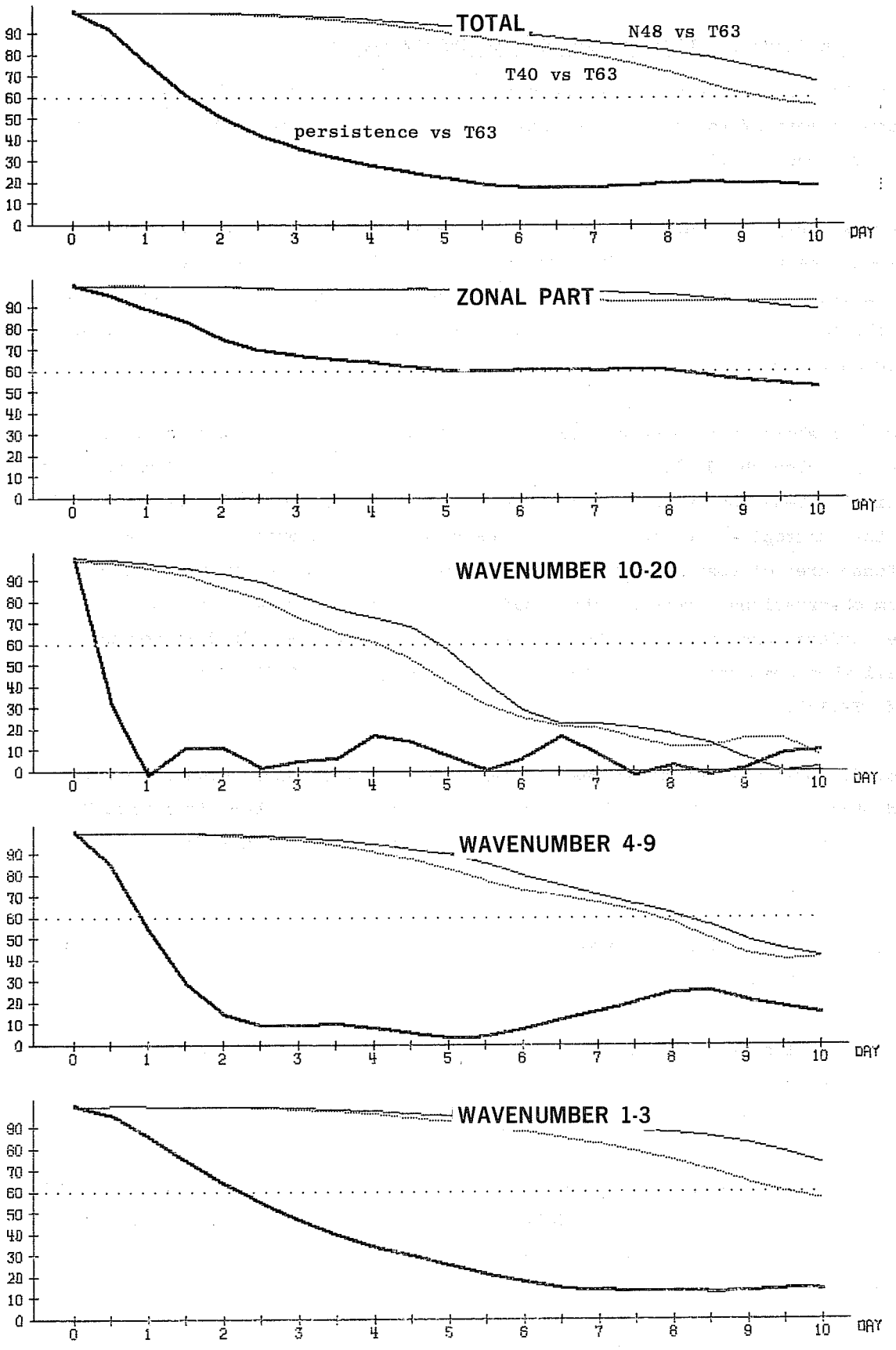

Fig. 5.24 Same as Fig. 5.22 for height intercorrelations (%) between T63 and either T40 or N48.

6. GEOGRAPHICAL DISTRIBUTION OF THE SYSTEMATIC ERRORS

By systematic errors on day N, we simply mean the differences between the ensemble mean of the day-N forecasts and the ensemble mean of the verifying observations or climatology.

Since we only considered 7 cases all of the same year, the verifying day-N ensemble mean cannot be assimilated to a climatology. However the aim of the forecasts is also to reproduce the correct departures from climatology. In the following we shall mainly try to emphasize the differences or similarities between the models.

Fig. 6.1 shows latitude-pressure cross sections of the zonal mean of zonal wind and also the deviations of forecast from observed values. All models have a similar behaviour with too strong winds near the surface and northward shift of the subtropical jet maximum. T40 appears to have a broader but less intense area of positive errors, corresponding to a smaller overall departure from observations. Both spectral models have slightly weaker errors near the surface, especially in the middle latitudes, but these differences are small when compared to the ones induced by changing physical parameterization (cf. TR.13).

Fig. 6.2 presents the zonal mean of temperature differences between forecasts and observations. The 3 models have an extremely similar behaviour with T40 doing slightly worse near the surface in the high middle latitudes (60^{o} to 80^{o}N).

Fig. 6.3 shows systematic errors (forecast minus observed) on days 4 and 7 in the 500 mb height field for N48, T40 and T63.

On day 4 all models produce already too intense lows over the Northern Pacific and Northern Europe and the differences between the 3 patterns are small both in amplitude and position.

On day 7 the pattern looks the same with larger negative errors occurring in the same areas as on day 4. The models prove to be very similar at this stage: the main difference is an even larger negative error for the two spectral models over the Northern Pacific.

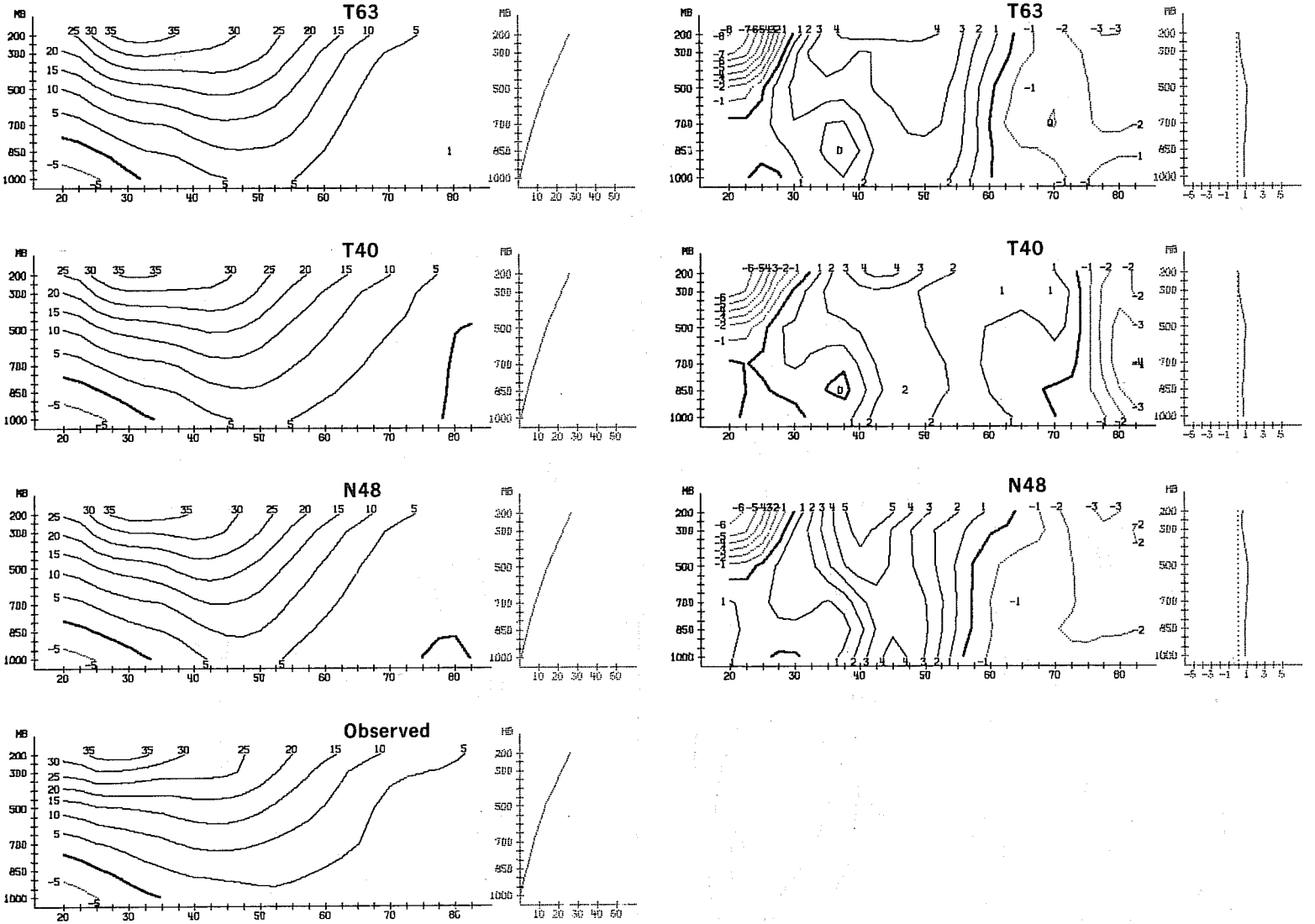

Fig. 6.1 Pressure-latitude cross-sections of zonal mean of zonal wind (left panels) forecast by T63, T40, N48 and observed and deviations of forecast from observed (right panels). Ensemble means of 7 February 1976 cases. Time average of forecast days 7 to 10.

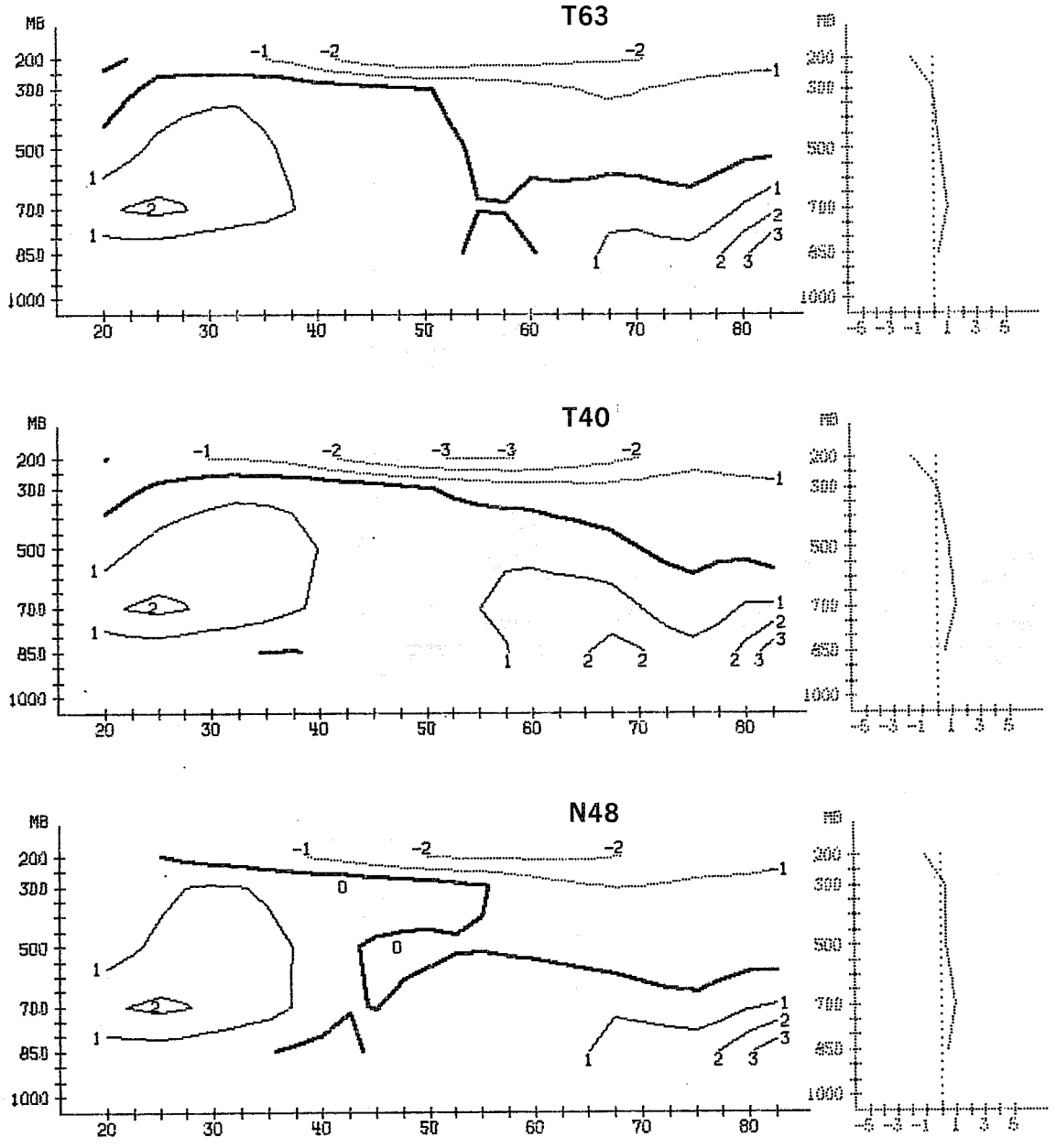

Fig. 6.2 Pressure-latitude cross-sections (left) and vertical mean profiles (right) of the deviations of zonal mean temperature between forecast and observed values for T63, T40 and N48. Ensemble mean of 7 February 1976 cases. Time averages of forecast days 7 to 10.

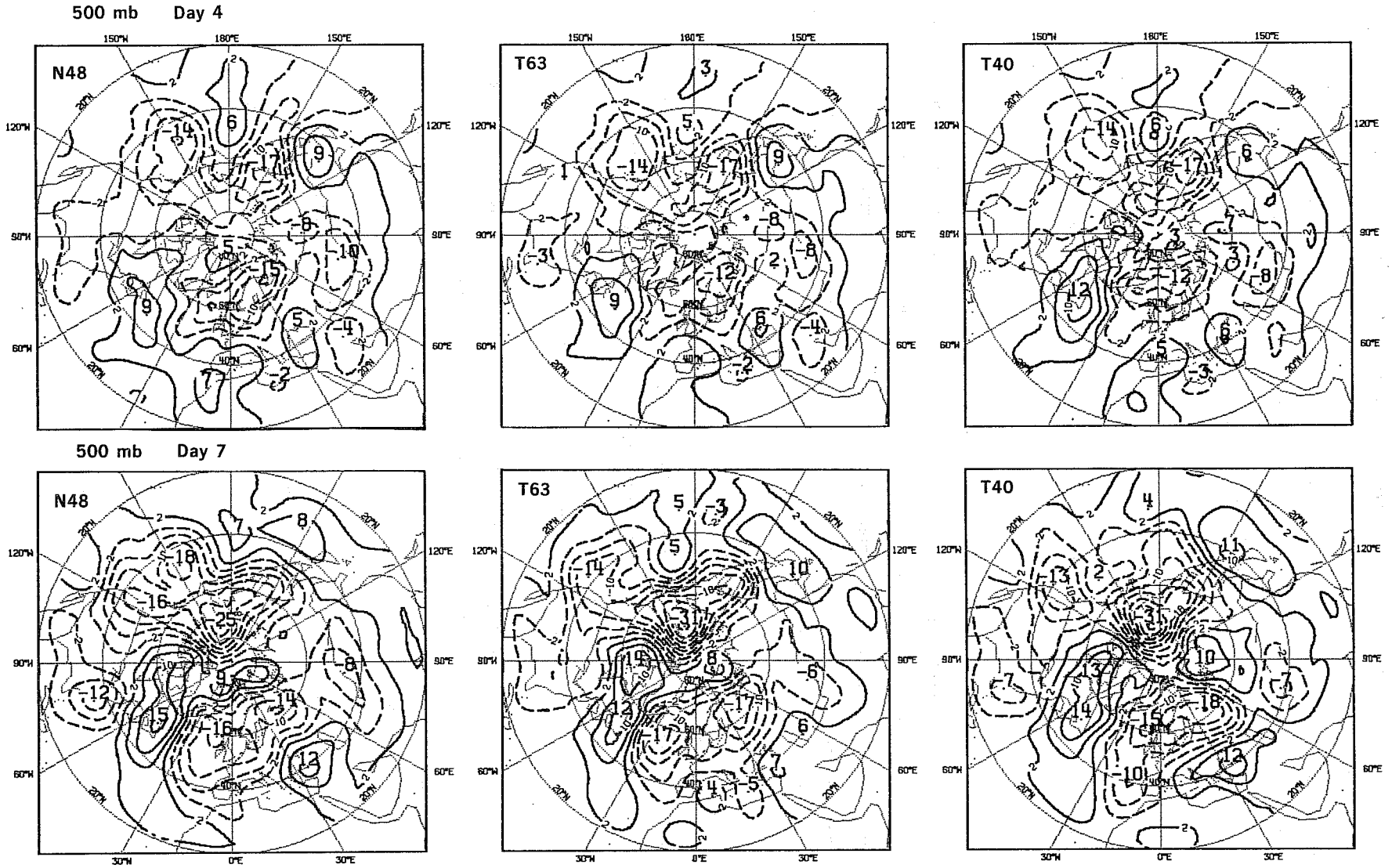

Fig. 6.3 Height error (dam) at 500 mb for N48, T63 and T40 on day 4 (top) and 7 (bottom) of the forecasts. Ensemble mean of 7 February 1976 cases.

Fig. 6.4 shows the same on day 10 in both 500 and 1000 mb height field. Although the pattern is again very similar - they all again produce too intense lows over the Northern Pacific and Europe - some noticeable differences in amplitude can be pointed out. T63 generates less intense lows at both 500 and 1000 mb over Europe while over north western Atlantic it develops more intense highs. As a mean, T63 appears better on day 10, due to the much better performance over Europe.

Fig. 6.5 shows the mean maps on day 10 of the 500 mb height field for the three models N48, T63 and T40 at the top, for N48 with a different physical package, GFD, (see TR13 for details), the NMC analysis and February climatology, at the bottom.

The models are too zonal and fail to reproduce the two intense troughs over eastern Asis and America. One can see from these maps why T63 has less intense errors over Europe on day 10: the spurious trough over the Greenwich meridian - instead of a ridge in both observed and climatological maps - is much less pronounced in T63 than in N48 maps. T40 has a trough similar to N48 but further to the west.

Fig. 6.6 presents the same maps at 1000 mb. The models are less similar at this level than they were at 500 mb and it is to be noticed that the two grid point model forecasts made with two different physical packages are indeed more alike than N48 and T63 with the same physical package. As at 500 mb, T63 deviates slightly less than T40 and N48 from reality. In particular the spurious trough over the Greenwich meridian is less intense than in N48.

Fig. 6.7 shows the systematic errors on day 10 in the 850 mb temperature field. There is little to add to what was said for the height field: once more the models are very similar. They generate in particular large positive errors over north western Europe.

Fig. 6.8 presents the results in terms of differences to climatology for the height field at 500 mb. None of the models reproduces the large negative anomaly centered over Greenland. They in turn generate too intense negative differences over the Northern Pacific. The large positive area over the Pacific is well reproduced by all the models.

As pointed out in TR13 a considerable part of the systematic errors comes from the large scales but the averaging process makes it unlikely that a significant part would be found in the very small scales.

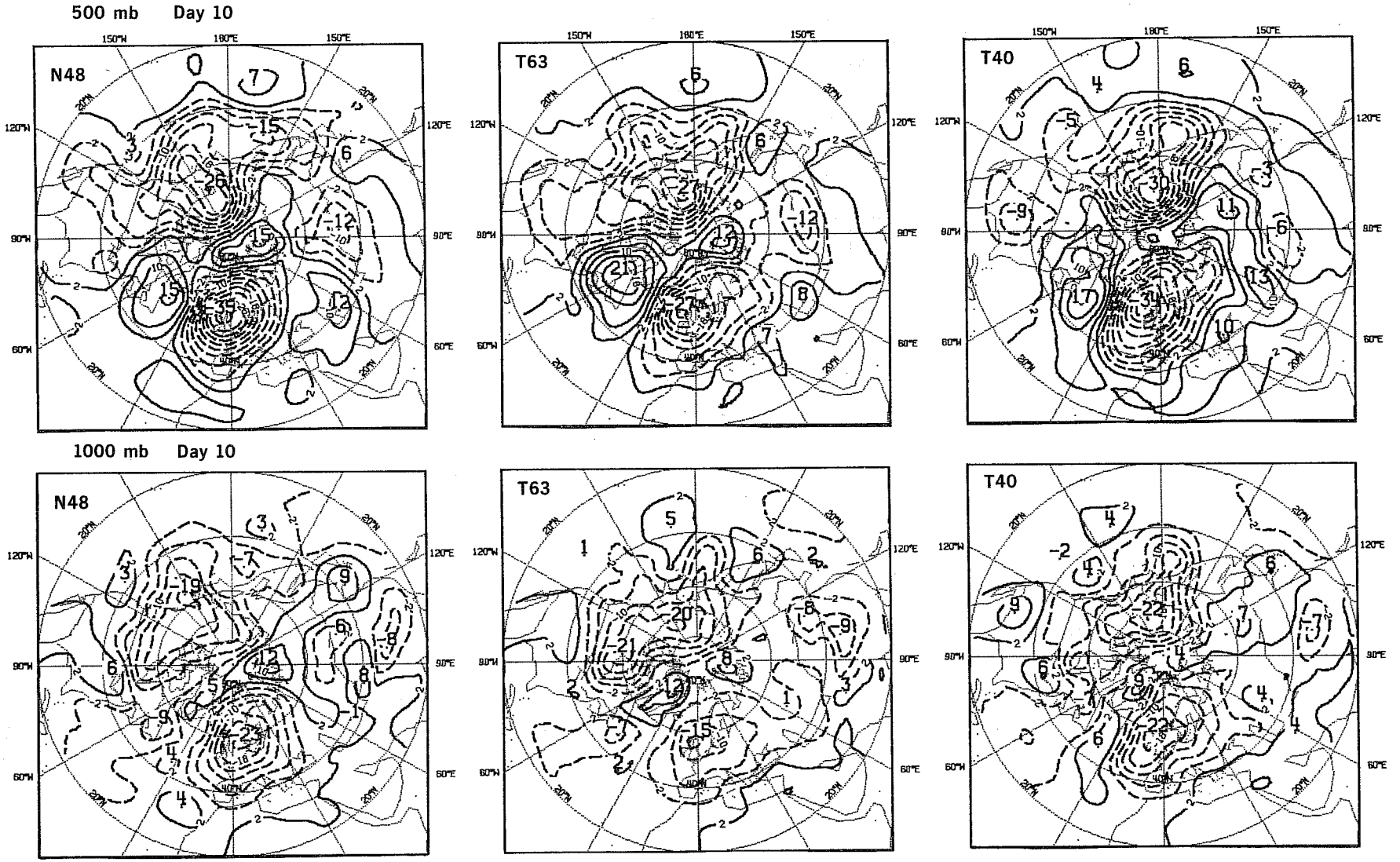

Fig. 6.4 Same as Fig. 6.3 at 500 mb (top) and 1000 mb (bottom) on day 10.

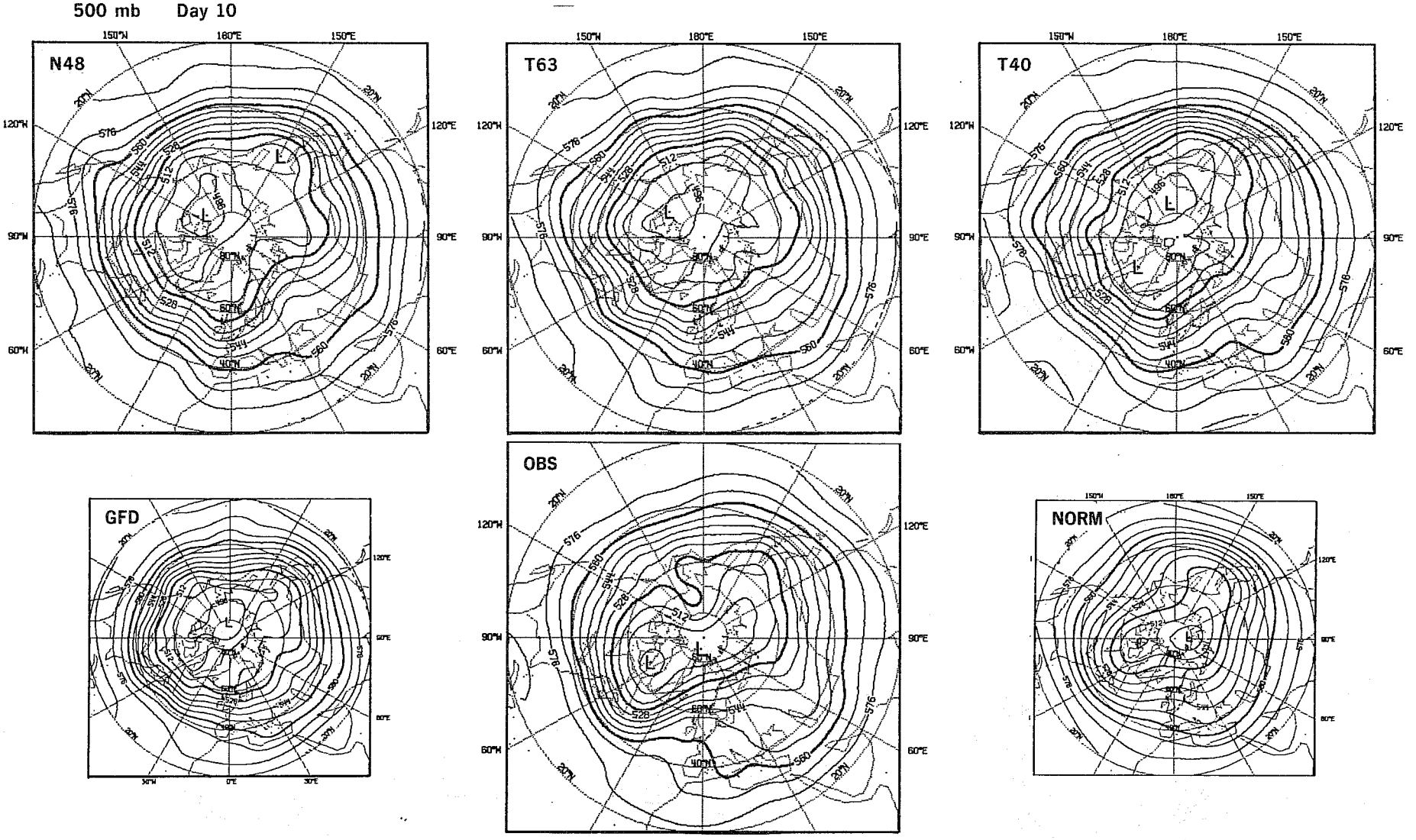

Fig. 6.5 Height (dam) at 500 mb . Top panels from left to right: N48, T63 and T40 on day 10 of the forecasts. Bottom panels from left to right: N48 with a different physical parameterization (GFD), the observations (OBS) and February climate (NORM). Ensemble mean of 7 February 1976 cases.

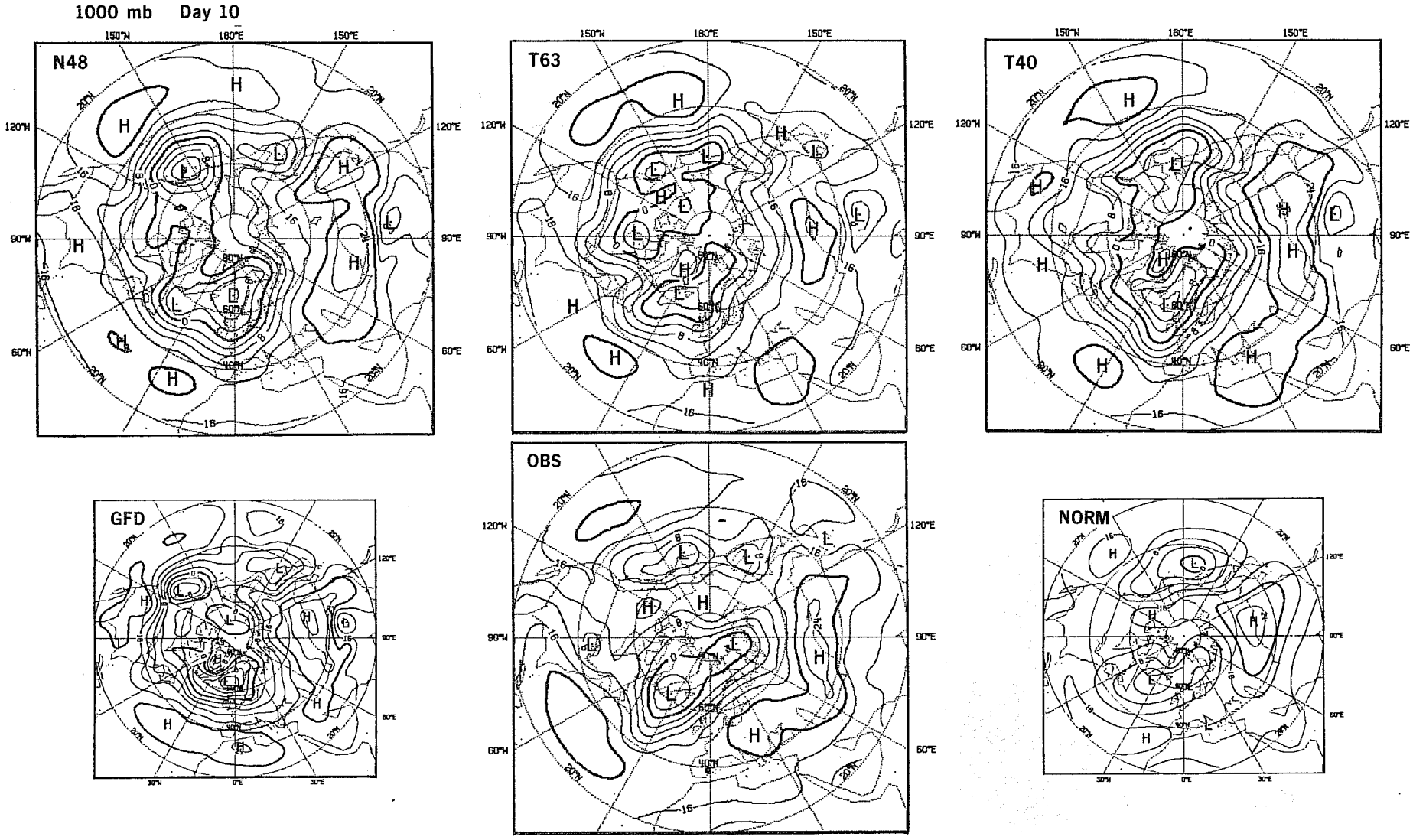

Fig. 6.6 Same as Fig. 6.5 at 1000 mb.

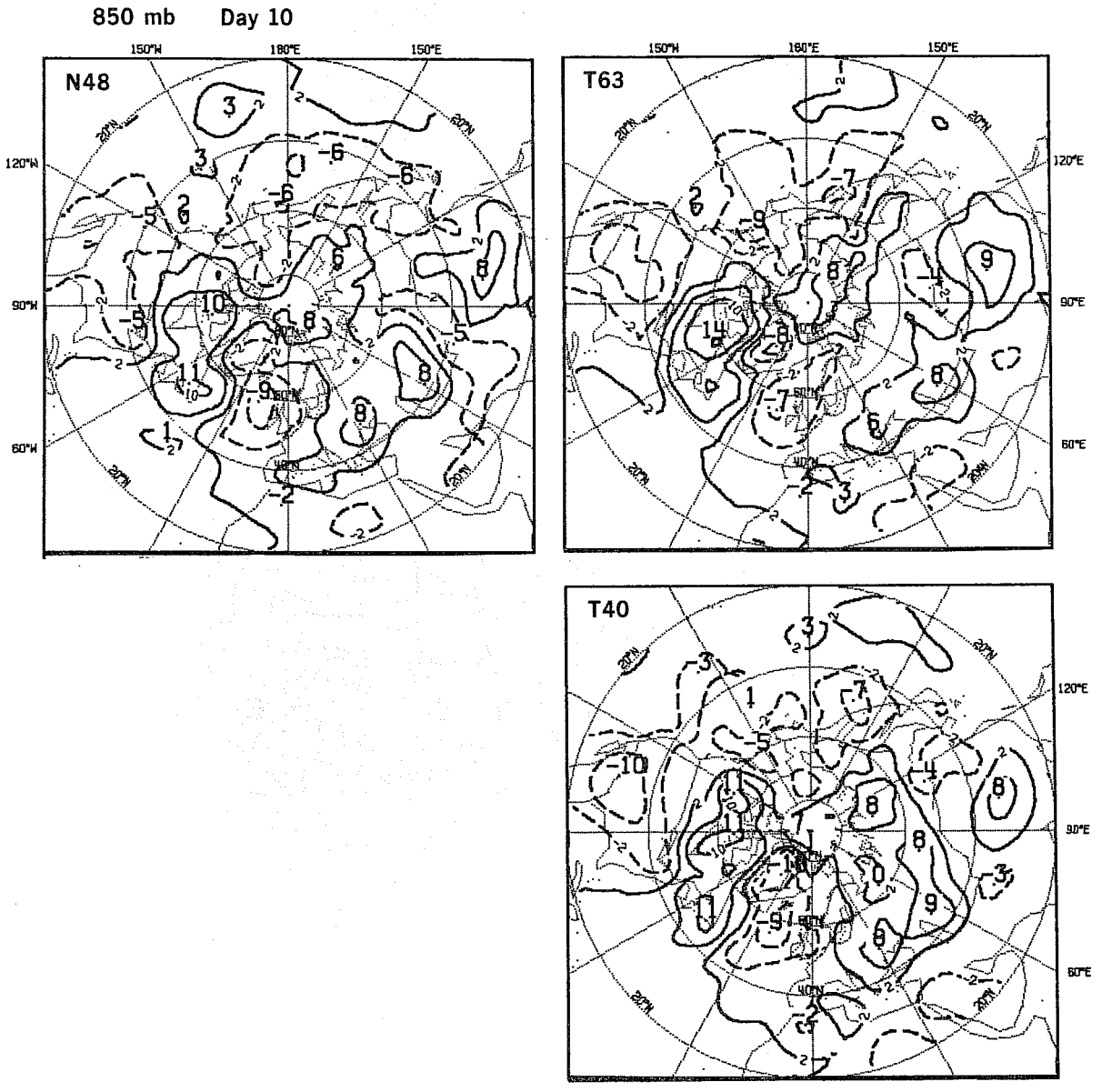

Fig. 6.7 Temperature error (^{o}K) at 850 mb for N48, T63 and T40 on day 10 of the forecasts. Ensemble mean of 7 February 1976 cases.

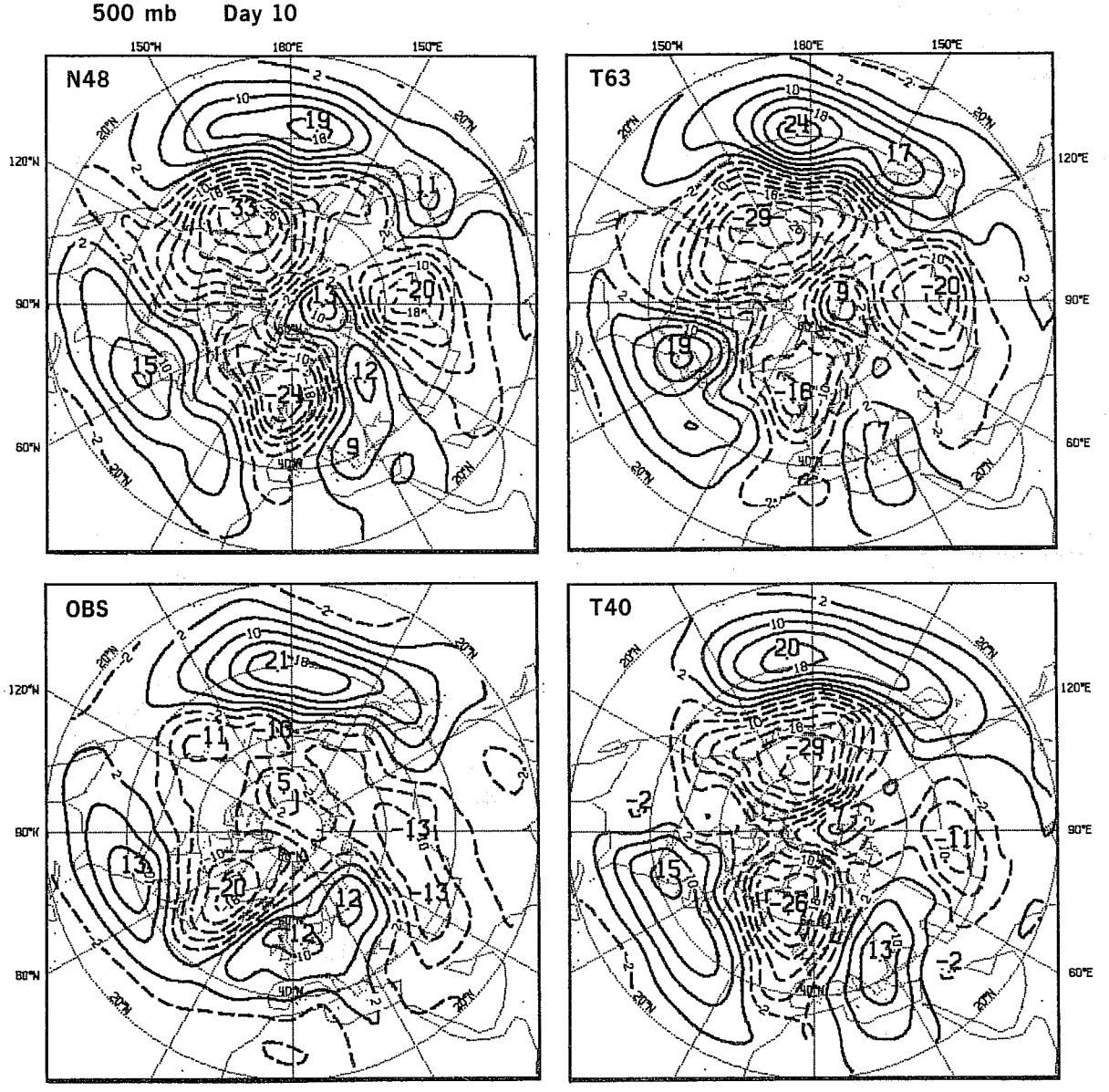

Fig. 6.8 Height anomaly (difference from climate) at 500 mb observed (OBS) and forecast by N48, T63 and T40 on day 10. Ensemble mean of 7 February 1976 cases.

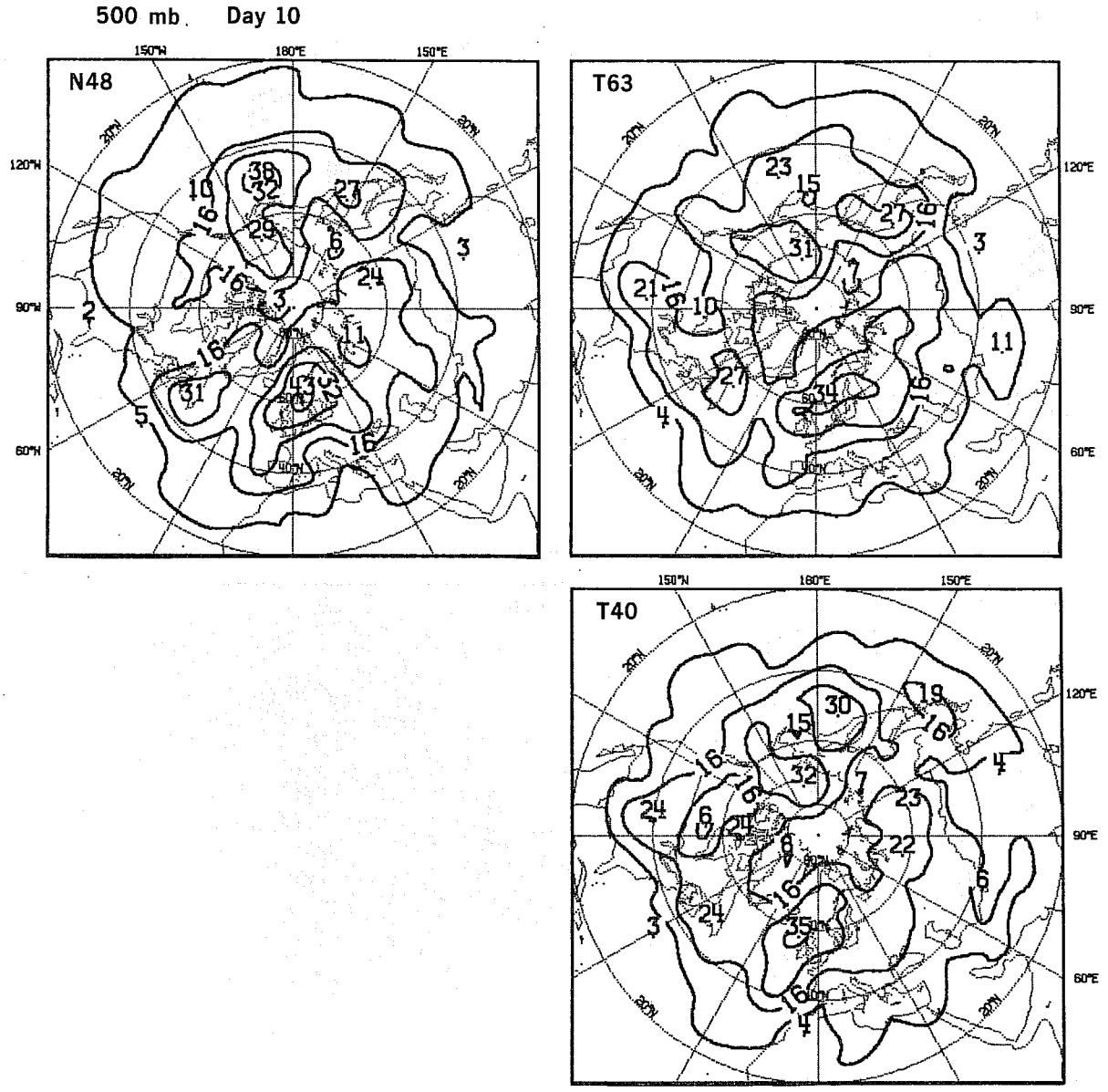

Fig. 6.9 Root mean square (rms) error of height at 500 mb for 10-day forecasts made by N48, T63 and T40. Ensemble mean of 7 February 1976 cases.

The growth of the systematic errors was found in TR13 to be fairly regular for N48 and we show here that it is almost the same for T63, T40 and N48. It means that the errors grow in a way which only weakly depends on the horizontal resolution used - at least for the resolutions used here - and on the technique used in the horizontal - spectral or grid point. This relative insensitivity must be considered when we are looking at differences between spectral and grid point technique. The intrinsic differences that are due only to the horizontal techniques used, might become partially or almost completely hidden by large mean errors induced by other problems.

Fig. 6.9 shows the rms errors of the three models for the 500 mb height field on day 10. When comparing with Fig. 6.4 the conclusion is that the largest errors occur in the same places as the large systematic errors, suggesting that the latter are an important part of the total error.

In conclusion we must emphasize the similarity of the systematic errors. All models produce the same large error pattern with only fairly small variations in intensity. Therefore the systematic errors do not seem to be strongly correlated to the horizontal resolution in the range considered (T63 to T40) nor to the technique used in the horizontal.

Other experiments (several 50 days integrations) tend to show that they are also not strongly related to the initial conditions. However, many other possibilities are still to be investigated, amongst which are the vertical scheme and resolution and the physical parameterizations.

7. ENERGETICS

In this Chapter we shall continue to concentrate our attention on the region north of 20°N in the layer between 1000 and 200 mb.

7.1 Time evolution of the total energetics

In this Section we present two types of results.

- the time evolution of the ensemble averaged energetics: kinetic energy (KE), available potential energy (AE), conversion from zonal to eddy KE (CK) and AE (CA).

- the time evolution of the kinetic energy of the ensemble averaged flow. For convenience we shall refer to the latter as the kinetic energy of the "stationary" part of the flow (KES)

All diagnostics involving the wind field have been computed using its geostrophic component.

Figs. 7.1 to 7.4 present the time evolution of KE, AE, CK and CA averaged over the Northern Hemisphere in the usual way (between 20° and 82.5°N and 1000 - 200 mb) and Fourier decomposed into total(0-20), zonal (0), long (1-3), and medium (4-9) wavenumber groups.

From Fig. 7.1 we can note the following features. Both T63 and N48 have a level of total KE which slowly deviates from the observed one with higher values (even slightly larger for N48) while T40 keeps it almost correct. The wavenumber decomposition shows however that all models, including T40, have failed to achieve the correct KE partitioning between the various scales. They all generate too much zonal KE and have too little in the low wavenumber (1-3) group. The higher resolution models - T63 and N48 - behave almost identically in these two groups (zonal and 1-3) while T40 differs from them by having a smaller excess of zonal energy and at the same time a larger deficit in the long waves, already substantial on day 2. For the medium wavenumber (4-9) group N48 stands out with an excess of KE while T40 and T63 have nearly the correct level. This better behaviour of T63 over N48 in the medium waves explains its slightly better performance in the total KE.

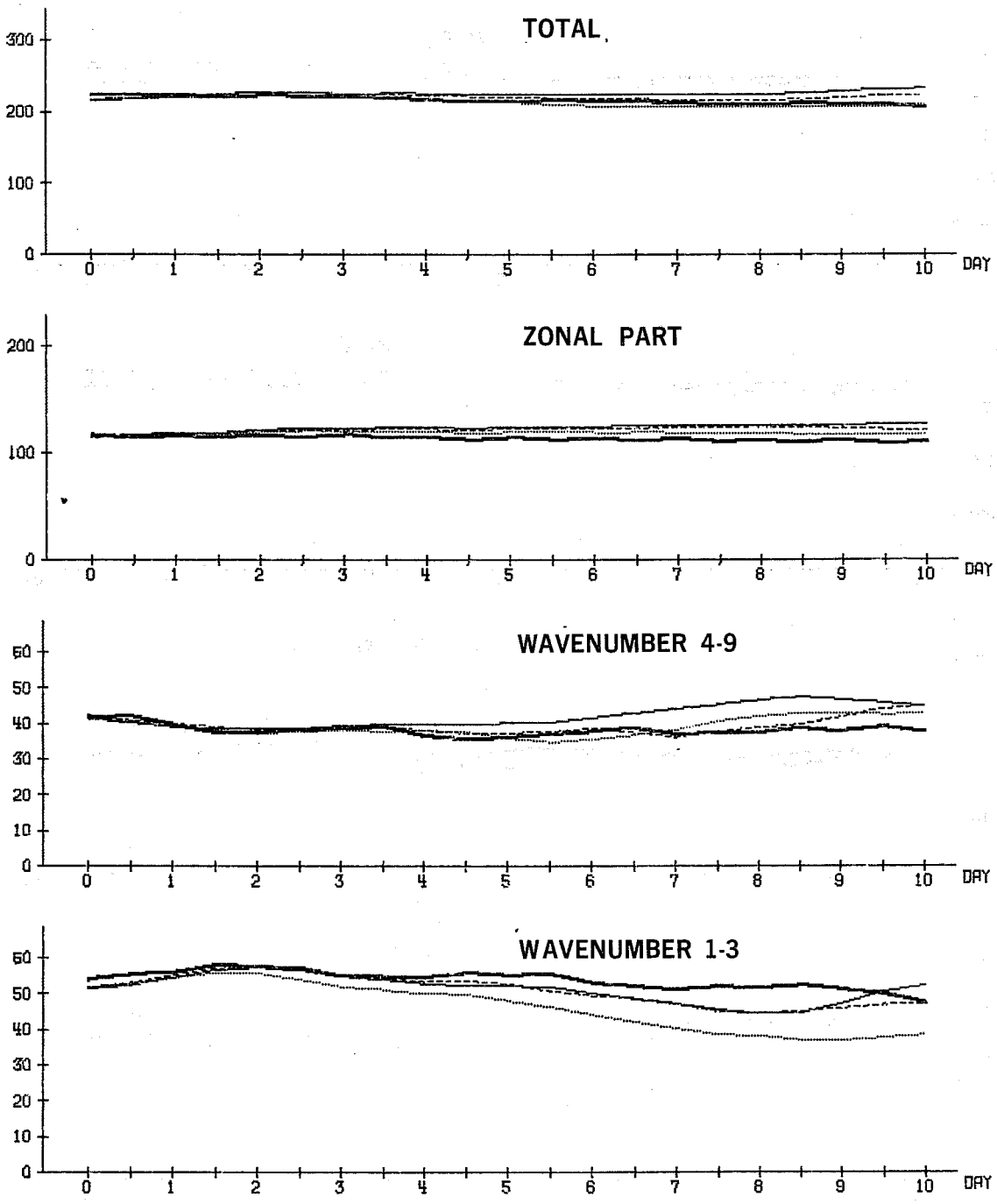

Fig. 7.1 Time evolution of kinetic energy (10 kJ/m^2) averaged from 20^{o}N to 82.5^{o}N and between 1000 and 200 mb for various wavenumber groups. Ensemble means of 7 February 1976 cases.

observed ——— N48 ------T63 .....T40

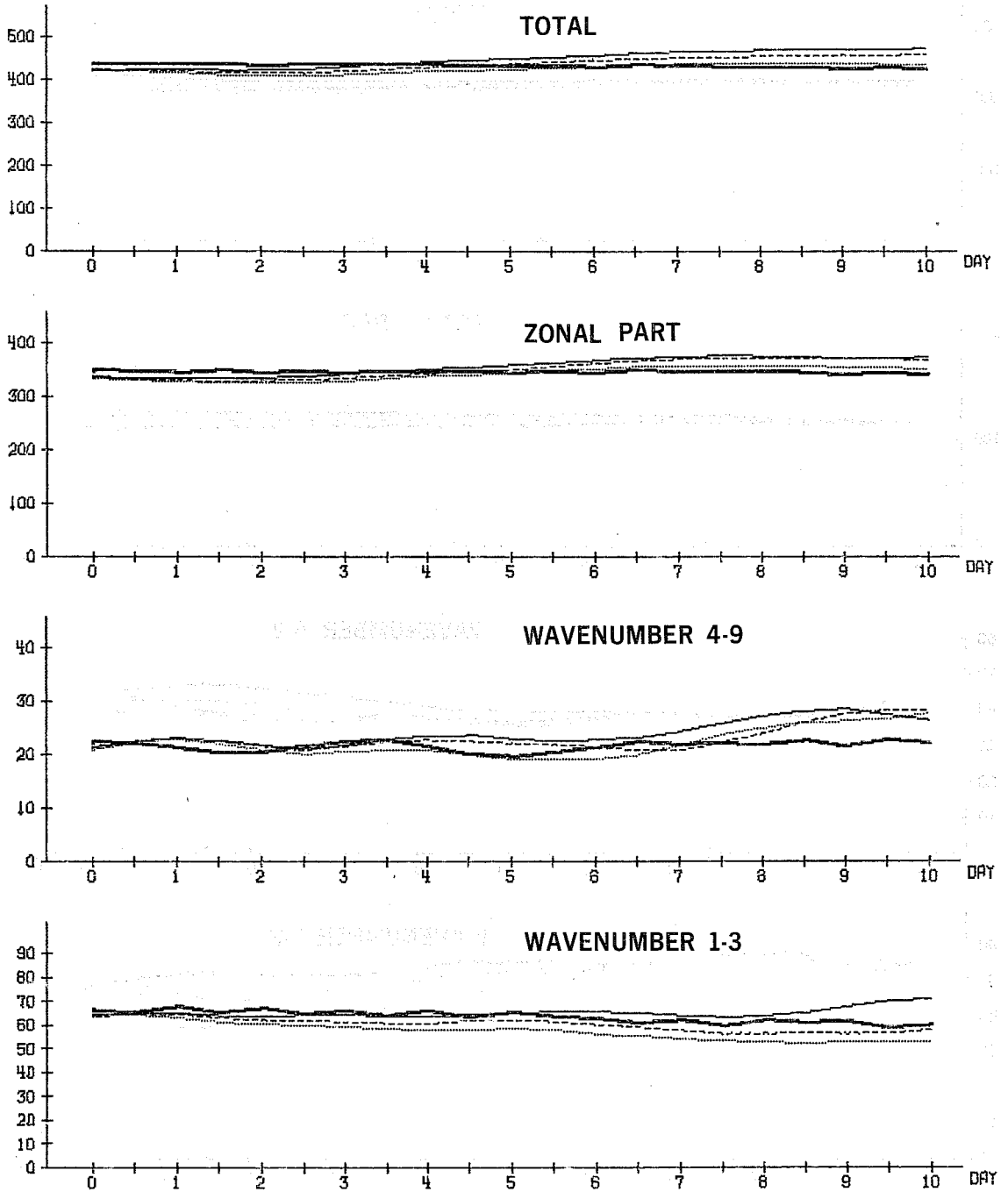

Fig. 7.2 Same as Fig. 7.1 for available potential energy (10 kJ/m^2).

observed N48 ------T63 .....T40

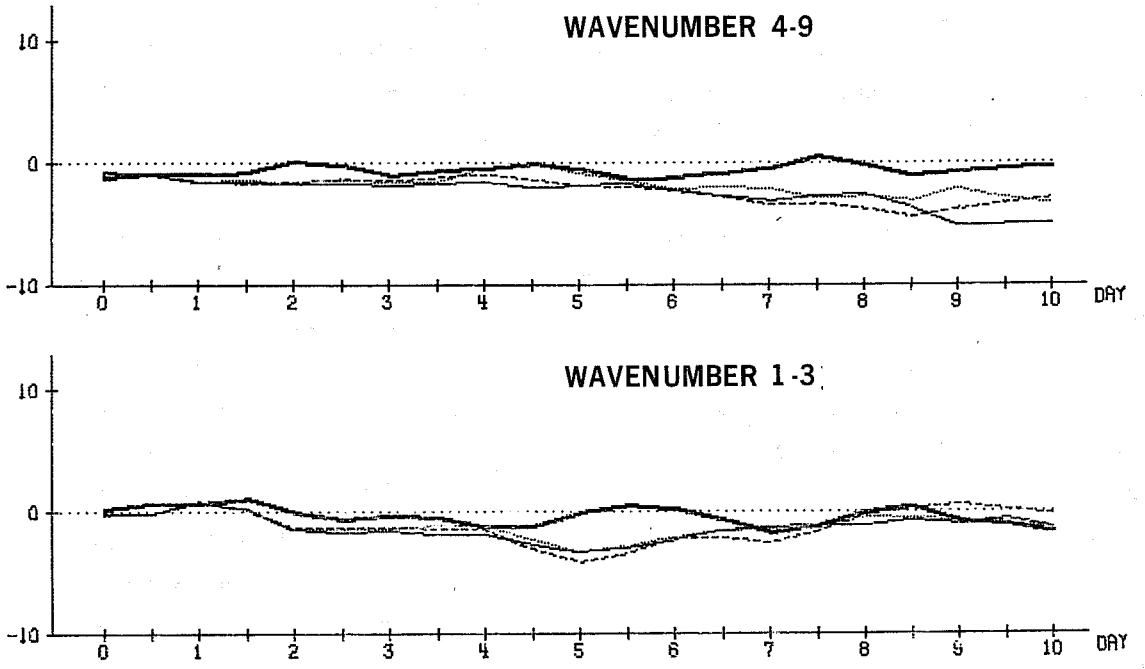

Fig. 7.3 Same as Fig. 7.1 for conversion of zonal to eddy kinetic energy (10^{-1} Watt/m^2)

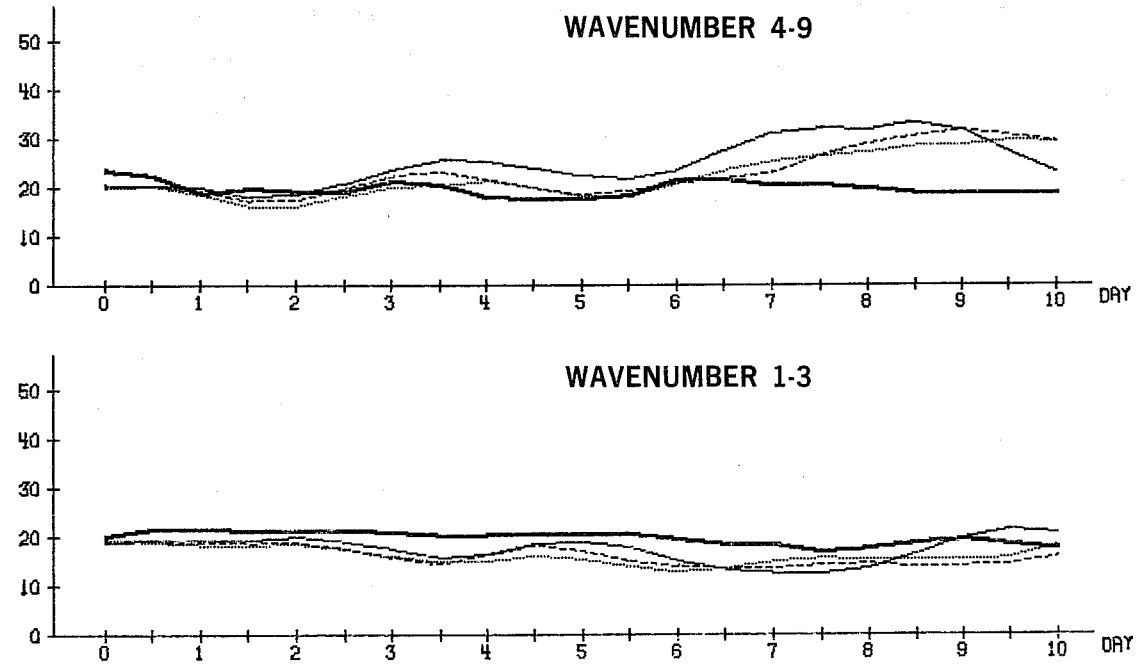

Fig. 7.4 Same as Fig. 7.1 for conversion of zonal to eddy available potential energy (10^{-1} Watt/m^2)

observed N48 ------T63 .....T40

From Fig. 7.2 one can make similar comments about the behaviour of the models for the total and zonal AE. However N48 and T63 are no longer identical in the long wave components of AE: N48 tends to overestimate it in the last 4 days while T63 shows slight underestimation throughout. T40 again shows a noticeable deficiency. This last point, i.e. less AE in wavenumber group 1-3 for T40 than for T63 is almost systematic, being observed in most of the 7 individual cases. For the medium wavenumber group we do not wish to make any comment since we noticed a very large variability from case to case. Therefore 7 cases are not enough to allow the mean curve to be considered as representative. In any case all the results concerning AE are to be interpreted with great care since other experiments not reported here suggest that AE is extremely sensitive to changes in the physical parameterization schemes. From Fig. 7.3 one can immediately see that all models differ little from each other with respect to CK in both wavenumber groups displayed: all models suffer from excessive conversion from eddy to zonal KE. From Fig. 7.4 one can observe slightly higher rates of CA for N48 than for T40 and T63. This leads to an agreement with observations better in the long-wave components and worse in the medium-wave components, with no overall advantage.

Fig. 7.5 shows the time evolution of KES averaged and spectrally decomposed as KE (Fig. 7.1) From a comparison between the total and stationary part (the difference KE-KES is called the transient part) of KE one may conclude that most of the zonal part and about half of the long-wave components of KE belong to the "stationary" part of the flow, while the medium-wave components of KE belong to the "transient" part of the flow.

One can also note the extremely similar behaviour of the models in all wavenumber groups: all models generate too much zonal KES and show a growing deficiency in the long waves. By comparing 7.1 and 7.5 it is possible to see that most of the error in the zonal and the long-wave part of KE can be attributed to KES. It is however clear that the additional loss of long-wave KE suffered by T40 is related to the transient part of the flow.

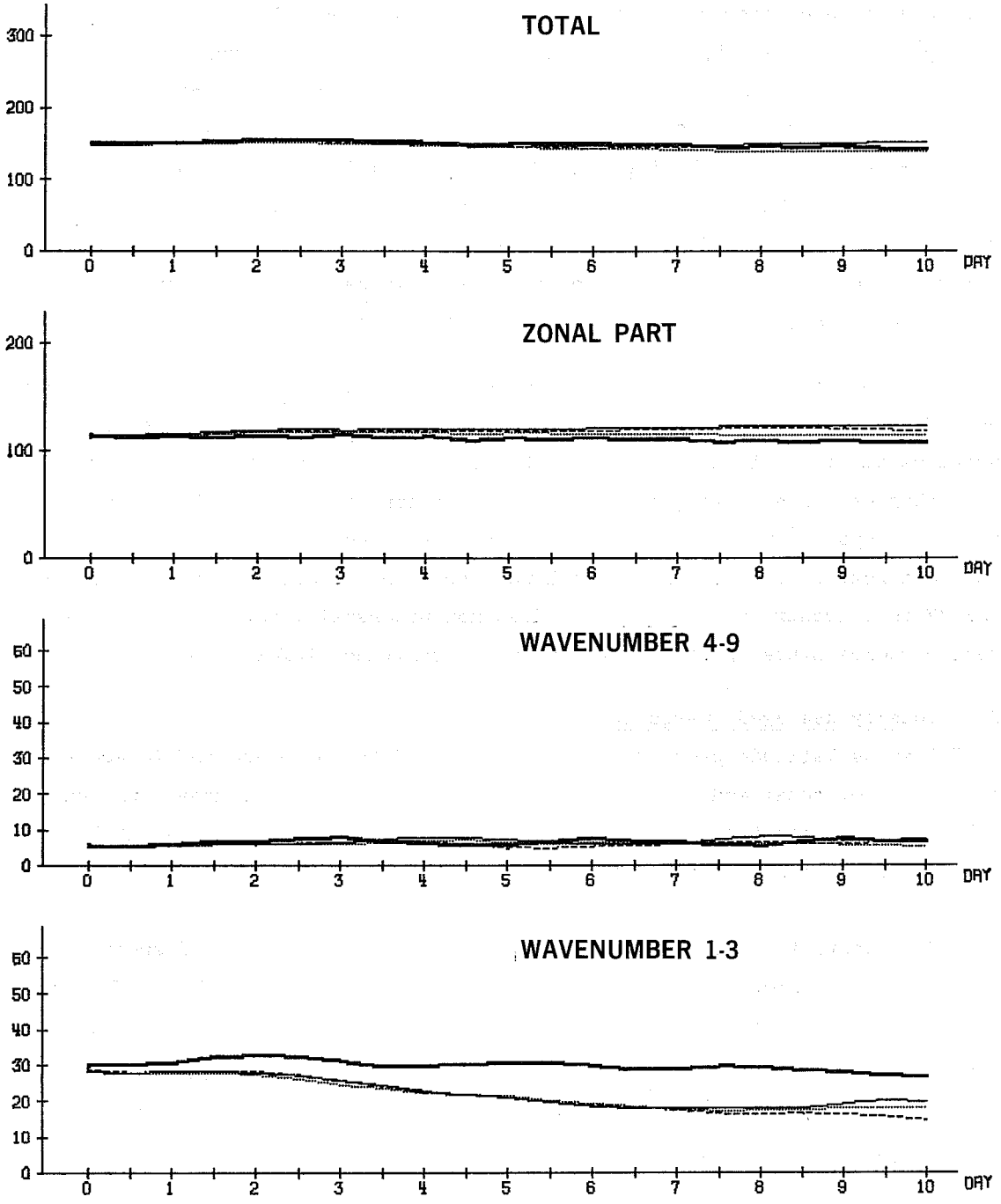

Fig. 7.5 Time evolution of kinetic energy (10 kJ/m^2) for the ensemble mean flow averaged from 20^{o}N to 82.5^{o}N and between 100 and 200 mb.

observed ——— N48 ------T63 .....T40

7.2 Spectra of KE

Fig. 7.6 displays for the 300,500,850 and 1000 mb levels the ensemble mean spectra of KE observed and forecast by the 3 models averaged over the last 3 days of the 10-day period and over the latitude band 40 to 60°N. At all levels T63 and N48 have more KE in the long-wave components (1-3) than T40 and are closer to observations in wavenumber 1. In the short-wave components (10-20) the situation is reversed with T63 and N48 having less KE than T40, mainly in the lower troposphere (850 and 1000 mb). This is again more realistic. The main difference between T63 and N48 is seen in the medium-wave components (4-9). This corroborates the results of Fig. 7.1 showing the level of KE in this part of the spectra in better agreement with reality than those of either T40 or N48.

The spectra of observed KE have a very weak slope in the long waves at high levels (300 and 500 mb) only. But this is seen at all levels in the forecasts. For the long waves at higher levels T63 agrees better with reality. There the influence of the physical effects is presumably less important than the influence of the dynamics. Comparing T40 and T63 it is tempting to conclude that higher resolution leads to a better KE spectrum in the long waves aloft where indeed, most of the total KE is concentrated. This result does not necessarily contradict the verification scores since spectra only deal with amplitude information.

7.3 Zonally averaged energetics

Fig. 7.7 shows latitude-pressure cross-sections of the observed and forecast mean distribution of total eddy KE (wavenumbers 1-20). Although the models present similar deficiencies the position and intensity of the maximum are slightly better in T63 which is again closer to N48 than to T40.

Fig. 7.8 presents the total momentum flux (wavenumbers 1-20). The 2 spectral models show a slight superiority over N48 both near the surface and in the middle atmosphere where they create a smaller negative area in the middle and high latitudes. In the higher atmosphere, T63 and T40 have spread the positive area more realistically towards the north, although the intensity of the maximum is too large for T40, too small for T63 and about correct for N48.

Finally, Fig. 7.9 displays the total sensible heat flux (wavenumbers 1-20). Near the surface T63 generates a maximum with better intensity than N48 and T40 and this is likely to be connected with more accurate surface winds. Near the top all models show a similarly wrong secondary maximum in the middle latitudes.

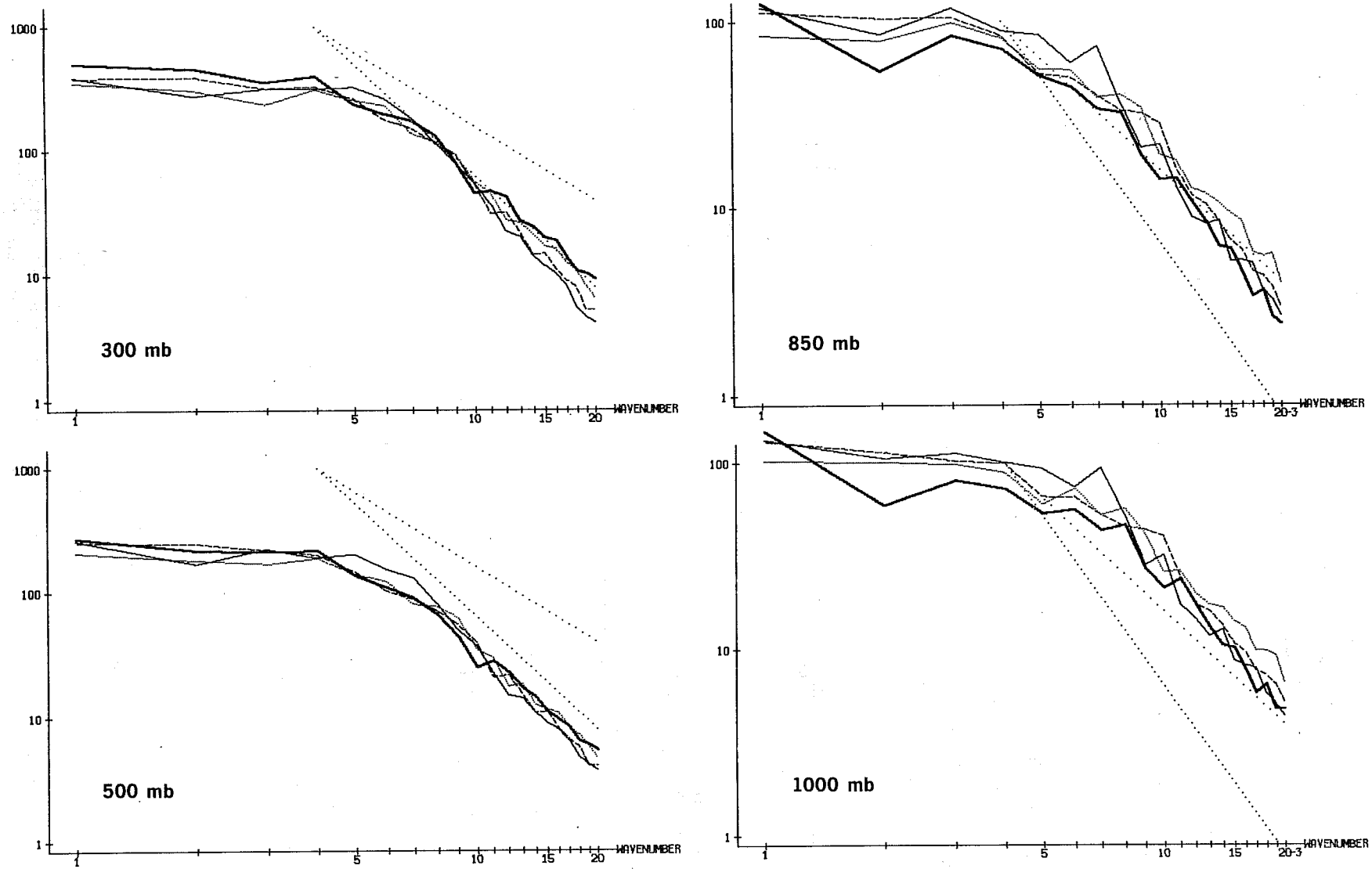

Fig. 7.6 Spectra of geostrophic kinetic energy (kJ/m^2/bar) at 300, 500, 850 and 1000 mb averaged from 40^{o}N to 60^{o}N and for the forecast days 7 to 10. Heavy solid line: observed; thin solid line: N48; dashed line: T63 and dotted line T40. Ensemble mean of 7 February 1976 cases.

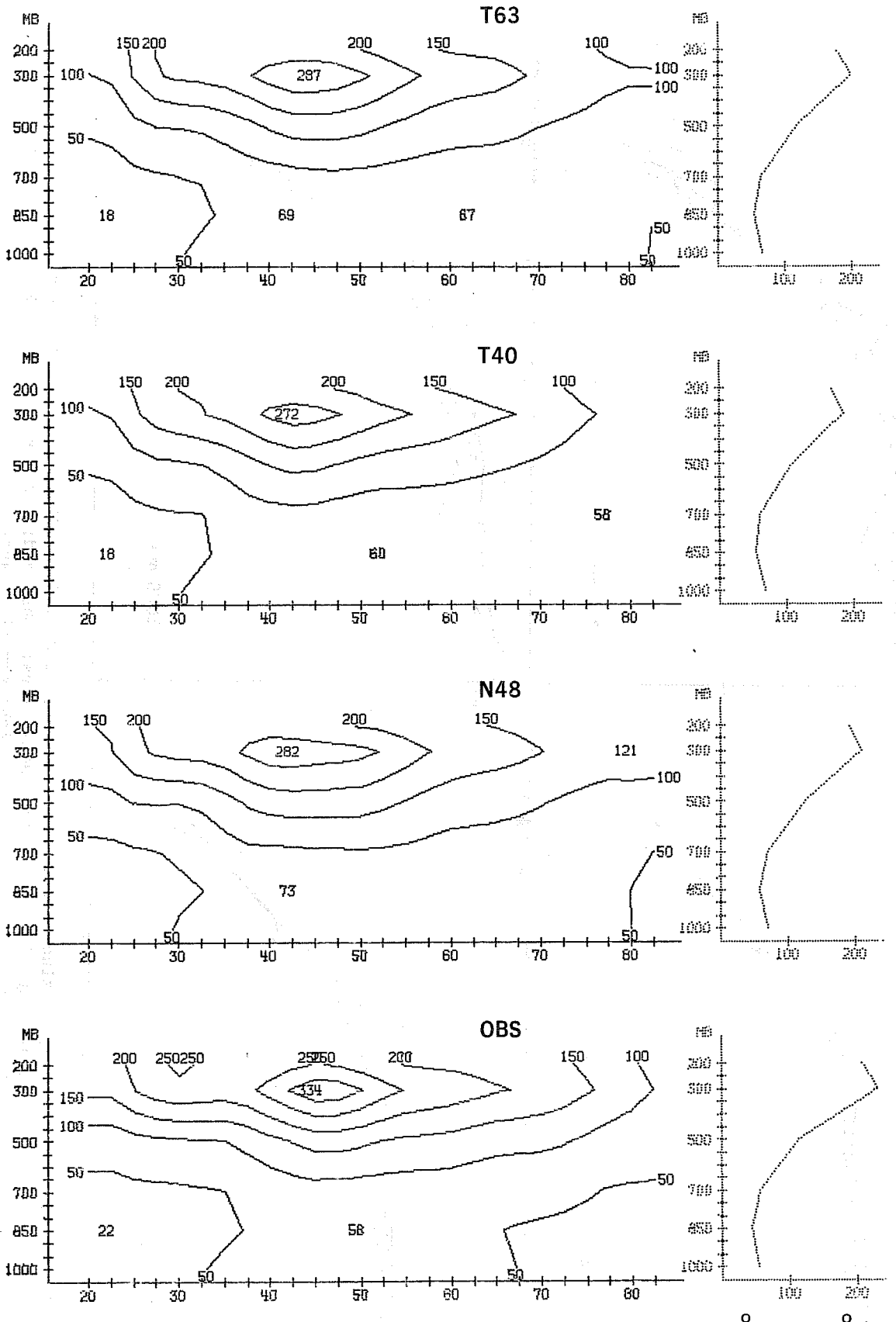

Fig. 7.7 Latitude-pressure cross-sections (left) and mean (20^{o}N - 82.5^{o}N) vertical profiles (right) of eddy kinetic energy (10 kJ/m^2/bar) observed (OBS) and forecast by T63, T40 and N48 averaged between days 7 to 10. Ensemble mean of 7 February 1976 cases.

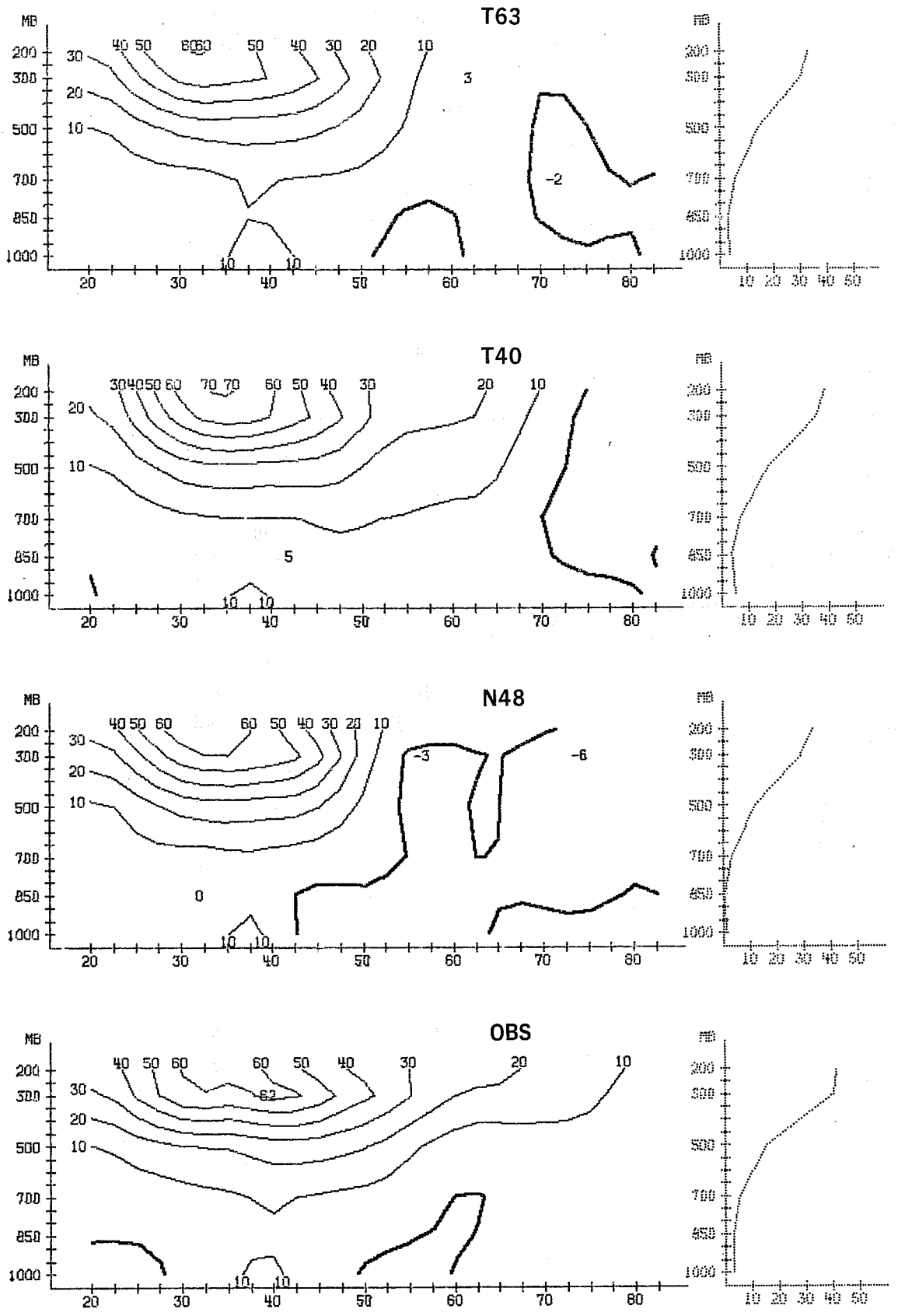

Fig. 7.8 Same as Fig. 7.7 for the momentum flux (m^2/s^2)

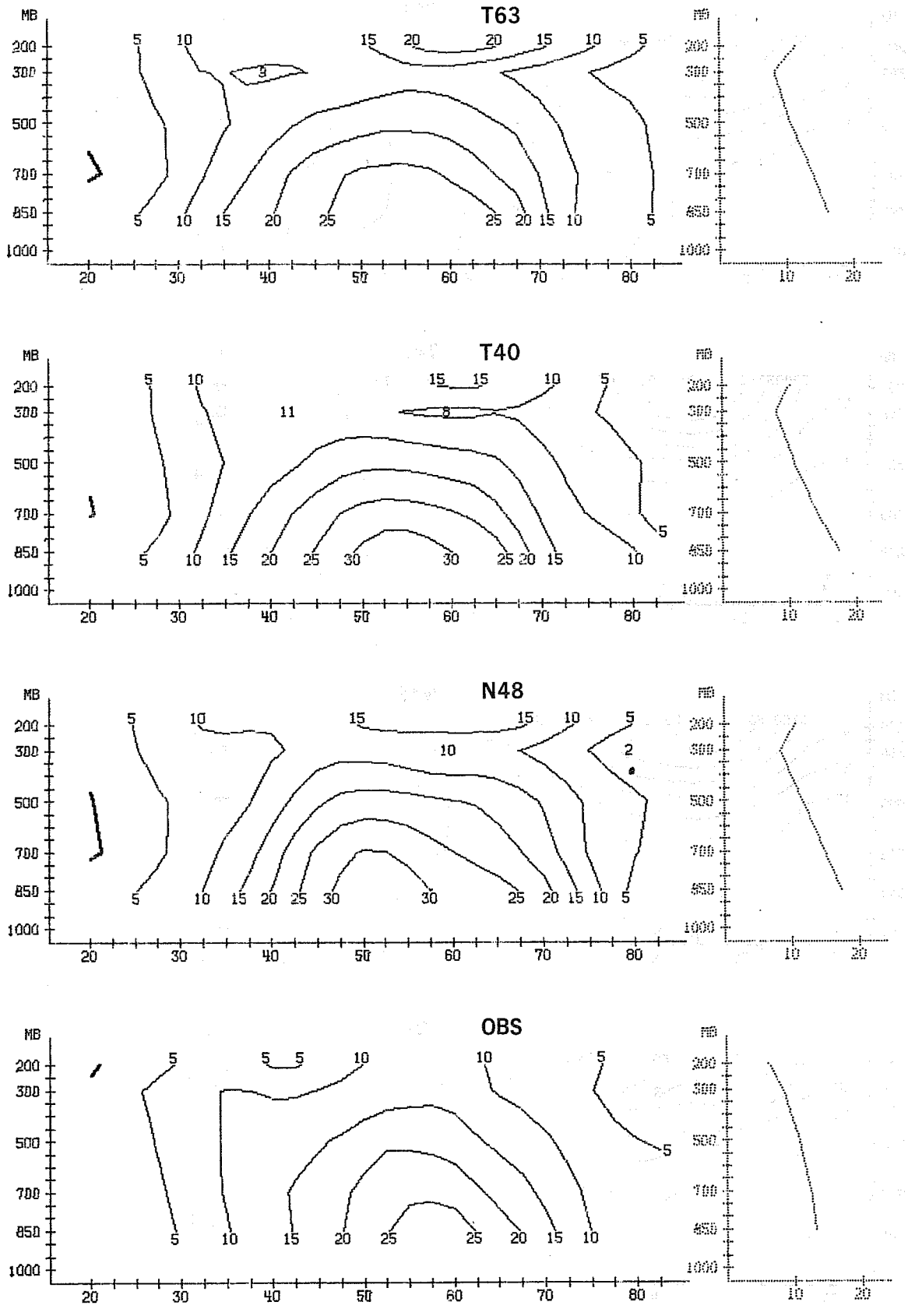

Fig. 7.9 Same as Fig. 7.7 for the sensible heat flux (^{o}K m/s)

8. SUMMARY AND CONCLUSION

An important conclusion that can be drawn from this report is without doubt that *the spectral and grid point models with the fairly high resolution used here are quite similar*. This suggests a convergence towards a solution almost independently of the method used as the horizontal resolution is increased. The high similarity appears in every part of the comparison: synoptic maps, objective scores, energetics,..... Despite the closeness some significant differences can be observed, allowing other important conclusions to be drawn.

Firstly T63 performs noticeably better than T40. The improvement is very small in the first two days but becomes larger and almost systematic at longer range. It appears in most of the individual cases and in all groups of wavenumbers. The medium as well as the long waves benefit from the increased horizontal resolution not only in terms of scores, but also in terms of energetics, especially for the long waves. In terms of predictability the mean improvement can be evaluated at 12 to 24 hours according to the level of accuracy considered and it suggests that some more improvement, although possibly smaller can be expected from an even higher resolution. As one might have guessed, a priori, *the better behaviour of T63 compared to T40 is more pronounced near the surface than near the top of the atmosphere* which suggests that the accuracy of forecasts could be improved without too large a cost by increasing the horizontal resolution more in the low levels than in the high levels.

Secondly T63 performs although less noticeably, yet *significantly better than N48. The improvement is already clear at short range where in fact T40 successfully competes with N48. Beyond day 2 or 3 N48 gives results of intermediate quality between T63 and T40, although closer to T63 than to T40 on the mean*. However cases can be found where N48 is not in between T40 and T63. This implies that a higher resolution is not totally but only partially responsible for the better performances of T63. More experiments are needed to better understand some of the differences between spectral and grid point techniques. Although the experiment described in this report includes seven cases only it is worth recalling that in the only case where T63 did worse than N48 (forecast from February 18th) T40 did at least as well as T63 and this case corresponded to a poor overall forecast for all models. On the contrary, in the case where T63 gave a very good forecast (February 15th), T63 did noticeably better than N48 and much better than T40. From a synoptic point of view, T63 did significantly better than N48 in two cases with respect to two major synoptic events: A better 4-day forecast of the storm over the North Sea on February 10th and a better 8-9 day forecast of the major circulation change over Europe on February 23 - 24th.

In terms of predictability the mean improvement of T63 over N48 is of the order of 6 to 9 hours and is more pronounced near the surface. It is mainly concentrated in the larger scales.

A quasi-operational comparison between T63 and N48 (once a week) has been performed in ECMWF for one full year, between September 1979 and August 1980, in order to select the best model for operational purposes. Preliminary examination of the results brings further support and statistical significance to the comparison T63 and N48.

The problem of finding the truncation of a spectral model giving an average result equivalent to those of the N48 grid point model is of some practical interest. The 1000 mb predictability curves of Fig. 5.16 show sensitivity to resolution. We may safely assume that predictability increases continously as resolution is increased from T40 to T63.

Furthermore we can assume in a first approach that the error in a spectral model is roughly proportional to $\frac{1}{N^2}$ where N is the maximum wavenumber of the truncation. Therefore if we also assume that the predictabity is a measure of the error, we can compute approximately from Fig. 5.16 the truncation equivalent to N48 for various levels of accuracy. We find the following table.

Level of anomaly correlation	90%	80%	75%	70%	65%	60%	55%	50%
Truncation equivalent to N48	< T40	T42	T44	T49	T54	T53	T53	T53

The values obtained in this manner at 1000 mb give only an estimate which is roughly valid at all levels.

Thus at short range and high correlation values, T40 is competetive with N48. *For medium range forecasting the ECMWF N48 grid point model is approximately equivalent to the ECMWF spectral model with a triangular truncation T53.*

A parameter often mentioned as a measure of the relative efficiency of spectral versus grid point models is the ratio of the number of degrees of freedom used, notwithstanding the fact that many more calculations per degree of freedom are required in a spectral model. *In the present situation the ratio of the number of degrees of freedom of N48 over T53 is about 6* (about 4 when comparing N48 and T63 and about 10 when comparing N48 and T40), which is well within the values (between 4 to 9) quoted by Leblanc (1977) or by Bass and Orszag (1976).

We would also like to recall that in the design of the present experiments the choice of truncation T63 was made in order to minimize the differences between the models to be compared. For example physical effects calculations are made on nearly identical grids and it has been possible to maintain comparable overall efficiency between the models (T63 and N48).

Objective scores tend to show that even then T63 is superior to N48 improving mean anomaly correlations by 2% and bringing on average an extra 6 to 9 hours of predictability to the forecast. The true and not purely statistical significance of this increased predictability is borne out by the better handling of certain synoptic situations. The energetics have confirmed but not explained these differences.

The fact that at short range (less than 3 days) T40 is statistically though marginally better than N48 is perhaps also not insignificant.

From another point of view we have shown that *the N48 performance is approximately equivalent to that of T53 which is about 40% more efficient*.

Finally, we would like to mention that the present results are in agreement with the results of other comparisons between spectral and other types of models (admittedly not always as controlled as the present one) and which have lead to the implementation of spectral models for routine numerical weather forecasting in Australia (1976), Canada (1976) and recently the United States (1980).

Acknowledgements

We are grateful to D.A. Burridge, T. Hollingsworth and A. Simmons for helpful discussions and useful comments about the manuscript, and to K. Arpe for providing most of the diagnostic tools. We acknowledge Iris Rhodes for typing the manuscript and Ms R. Shambrook for preparing the figures shown.

REFERENCES

Arpe, K., 1980 Confidence limits for verification and energetics studies. ECMWF Technical Report No.18, pp.24.

Asselin, R., 1972 Frequency filter for time integrations. Mon.Wea.Rev., 100, 487-490.

Baede, A.P.M., Hansen, A.W., 1978 A ten day high resolution nonadiabatic spectral integration; a comparative study. ECMWF Technical Report No.7, pp.82.

Baede, A.P.M., Jarraud, M., Cubasch, U., 1979 Adiabatic formulation and organisation of ECMWF's spectral model. ECMWF Technical Report No.15, pp.40.

Bass, A., Orszag, S.A., 1976 Spectral modeling of atmospheric flows and turbulent diffusion. Available from Environmental Sciences Research Laboratory. Office of Research and development. US environmental Protection Agency. Research triangle Park, North Carolina 27711, USA.

Bourke, W., Puri, K., Thurling, R., 1974 Numerical prediction for the southern hemisphere via the spectral method. GARP WGNE Report No.7 (available from WMO, Geneva, Switzerland, p.22-42).

Burridge, D.M. and Haseler, J., 1977 A model for medium range weather forecasting, adiabatic formulation. ECMWF Technical Report No.4, pp.46.

Daley, R., Girard, C., Henderson, J., Simmons, I., 1976 Short term forecasting with a multi-level spectral primitive equation model. Atmosphere, 14, 98-134.

Deron, E., Hollingsworth, A., Hoskins, B.N., Simmons, A.J., 1974 A comparison of grid point and spectral methods in a meteorological problem. Quart. J.Roy.Met.Soc., 100, 371-383.

Eliasen, E., Machenhauer, B., and Rasmussen, E., 1970 On a numerical method for integration of the hydrodynamical equations with a spectral representation of the horizontal fields. Report No.2 available from: Institut fur teoretisk meteorologi, København universitet, Copenhagen Denmark.

Girard, C., Jarraud, M., 1980 On some predictability problems. ECMWF Technical Memorandum No.17, pp.11

Hansen, A.W., 1979 A numerical study of a grid point model and a spectral model using real data. Report No. 7 available from: Institut fur teoretisk meteorologi, København universitet, Copenhagen, Denmark.

Hollingsworth, A., Arpe, K., Tiedtke, M., Capaldo, M., Savijärvi, H. Åkesson, O., Woods, J.A. 1979 Comparison of medium range forecasts made with two parameterization schemes. ECMWF Technical Report No.13, pp.214.

Leblanc, M., 1977 Sensitivity experiments with a spectral model. Publication in meteorology No. 120, pp.171. Available from McGill University, Montreal, Canada.

REFERENCES (Continued)

Machenhauer, B., and Daley, R., 1972 A baroclinic primitive equation model with a spectral representation in 3 dimensions. Report No. 4. Available from Institut fur teoretisk meteorologi Københavens universitet, Copenhagen, Denmark.

Miyakoda, K., R.F. Strickler, C.J. Nappo, P.L. Baker and G.D. Hembree, 1971 The effect of horizontal grid resolution in an atmospheric circulation Model, J.Atmos.Sci., 28, 487-499.

Orszag, S.A., 1970 Transform method for calculation of vector coupled sums. Application to the spectral form of the vorticity equation. J.Atmos.Sci., 27, 890-895.

Phillips, N.A., 1957 A coordinate system having some special advantages for numerical forecasting. J.of Met., 14, 184-185.

Puri, K., 1980 Extended range forecasts for southern hemisphere with the ANMRC spectral model. Submitted to Mon.Wea.Rev.

Puri, K., Bourke, W., 1974 Implications of horizontal resolutions in spectral model integrations. Mon.Wea.Rev., 102, 333-347.

Rasmussen, E., 1974 An investigation of the truncation errors in a barotropic primitive equations model on spectral form. Report No.5. Available from Institut fur teoretisk meteorologi Københavens universitet, Copenhagen, Denmark.

Simmons, A.J., Hoskins, B.J., 1975 A comparison of spectral and finite difference simulations of a growing baroclinic wave. Quart.J.Roy.Met.Soc., 101, p.551-565.

Temperton, C., Williamson, D.L., 1979 Normal mode initialisation for a multi-level grid point model. ECMWF Technical Report No.11, pp.91.

Tiedtke, M., Geleyn, J.-F., Hollingsowrth, A., Louis, J.-F., 1979. ECMWF model parameterisation of sub grid scale processes. ECMWF Technical Report No.10, pp.46.

ECMWF PUBLISHED TECHNICAL REPORTS

No. 1 A Case Study of a Ten Day Prediction

No. 2 The Effect of Arithmetic Precisions on some Meteorological Integrations

No. 3 Mixed-Radix Fast Fourier Transforms without Reordering

No. 4 A Model for Medium-Range Weather Forecasting - Adiabatic Formulation

No. 5 A Study of some Parameterizations of Sub-Grid Processes in a Baroclinic Wave in a Two-Dimensional Model

No. 6 The ECMWF Analysis and Data Assimilation Scheme - Analysis of Mass and Wind Fields

No. 7 A Ten Day High Resolution Non-Adiabatic Spectral Integration: A Comparative Study

No. 8 On the Asymptotic Behaviour of simple Stochastic-Dynamic Systems

No. 9 On Balance Requirements as Initial Conditions

No.10 ECMWF Model - Parameterization of Sub-Grid Processes

No.11 Normal Mode Initialization for a multi-level Gridpoint Model

No.12 Data Assimilation Experiments

No.13 Comparison of Medium Range Forecasts made with two Parameterization Schemes

No.14 On Initial Conditions for Non-Hydrostatic Models

No.15 Adiabatic Formulation and Organization of ECMWF's Spectral Model

No.16 Model Studies of a Developing Boundary Layer over the Ocean

No.17 The Response of a Global Barotropic Model to Forcing by Large-Scale Orography

No.18 Confidence Limits for Verification and Energetics Studies

No.19 A Low Order Barotropic Model on the Sphere with the Orographic and Newtonian Forcing

No.20 A Review of the Normal Mode Initialization Method

No.21 The Adjoint Equation Technique Applied to Meteorological Problems

No.22 The Use of Empirical Methods for Mesoscale Pressure Forecasts

No.23 Comparison of Medium Range Forecasts made with Models using Spectral or Finite Difference Techniques in the Horizontal